UNIVERSITY OF NAPLES FEDERICO II

PhD THESIS IN MATERIALS AND STRUCTURES
ENGINEERING

XXVI CYCLE

"Rational design of nanoparticles to improve anticancer drug delivery"

Tutor: Candidate:
Prof. Paolo Antonio Netti   Valentina Belli
Dr. Daniela Guarnieri

Coordinator:
Prof. Giuseppe Mensitieri

April 2011-April 2014

ACKNOWLEDGEMENTS

First of all, I would like to thank my supervisor, Professor Paolo Antonio Netti, for welcoming me into his group five years ago when I was still a Master student and for giving me the opportunity to pursue a Ph.D. His help, guidance and constant enthusiasm have been very much appreciated during all these years. I am also very grateful to Dr. Daniela Guarnieri for her constant supervision, availability, teachings and feedback. It was always a great pleasure to discuss the projects with her and planning our experiments. I owe a thousand thanks to her.

I would like to thank mainly my wonderful and loving family for their tremendous support and encouragement. I have been blessed with the greatest parents, the best family one could ever wish for! Mom, Dad, and Andrea thank you for believing in me. Your unconditional love has made everything possible. I am truly lucky.

Heartiest thanks to the most ideal person in my life, my fiancé Giuseppe for always being there for me. I owe a very special thanks to all his patience, encouragement and love that only you can give me.

Lastly, it gives me pleasure to thank Alessandra, Lucio, Federica and all my friends for strengthening and guiding me whenever I needed it.

Table of Contents

Rational design of nanoparticles to improve anticancer drug delivery

By

Belli Valentina

ABSTRACT

The need to improve current cancer therapies is a pivotal point in the drug delivery systems. A major challenge is to disclose new strategies that can combine the use of targeted nanoparticles (NPs) to the efficient delivery of chemotherapeutic agents in the vicinity of tumor masses, minimizing the side effects on healthy cells. To this purpose, a preliminary step is that of defining the optimal NP characteristics able to improve drug delivery at target tissues. However, these aspects need to be defined in suitable models that can actually mimic the main cell activities, including adhesion, migration and differentiation. These features are instead missed when cells are grown on flat plastic dishes, as it occurs in traditional two dimensional (2D) systems; thus, the 2D unnatural environment can provide inaccurate data, failing to predict the *in vivo* real cell response to NP treatments.

In this context, the main goal of this thesis has been that of identifying the key parameters useful for a rational design of anticancer drug delivery systems. To this aim, the following issues have been addressed:

- the effect of three dimensional (3D) extracellular matrix, made up of collagen type I, in controlling the diffusion and cellular uptake of NPs with variable size and surface charge;

- the cytotoxic efficacy of biodegradable NPs to deliver the Doxorubicin (Dox) anticancer drug in three dimensional matrices, as a function of size;

- the possibility to control "on demand" Dox release, in order to reach a more efficient tumor-specific targeting.

Results indicate that, in 3D environment, size, surface charge and functionalization are all crucial NP features that can modulate their ability to diffuse through the ECM and finally reach the cells. In parallel, the same properties also influence the cytotoxic effects and the cellular responses, with smaller sizes facilitating diffusion through the collagen matrix and increasing the efficiency of NP treatments.

Finally, the covalent conjugation of Dox to NPs through cleavable linkers allowed obtaining a more controlled drug release. This type of nanocarrier was made specifically responsive to matrix metalloproteinase-2 (MMP2), which is known to be over-expressed in the tumor extracellular matrix, so that the drug release from NPs, as the relative cytotoxic effect, were specifically triggered by MMP2 cleavage.

Altogether, the results obtained indicate that the physical-chemical characteristics of NPs and their behaviour in a 3D environment, that better mimics *in vivo* growth conditions, are crucial parameters that need to be taken into consideration for a more rational design of nanocarriers finalized to drug delivery in tumor tissues.

CHAPTER 1

1.1. INTRODUCTION

1.1.1. Nanoparticles in cancer therapy

Conventional chemotherapeutic agents distribute non-specifically into the body, and thus can target both cancerous and normal cells. This non-specific drug distribution has two adverse effects: limits the therapeutic dose within target cells, and provides excessive toxicity to healthy cells, tissue and organs, thereby causing several unwanted side effects. These effects include hairloss, weakness and organ dysfunction and, altogether, lower the quality of the life of patients. Due to their versatility in targeting tissues, ability to access deep molecular targets and control drug release, the use of nanoparticles (NPs) is a promising approach to improve the modern drug delivery systems [1-7]. Over the last years, a large number of NP delivery systems has been developed for cancer treatment, including lipids (e.g. solid/lipid NPs, liposomes), polymers (e.g. biodegradable polymeric particles, dendrimers), inorganic materials (e.g. metal NPs, quantum dots), and biological materials (e.g. viral and albumin nanoparticles) [8-16] (**Fig. 1**). In addition, NPs can be tailored to carry both drugs and imaging probes simultaneously, and can be designed to specifically target molecules of diseased tissues [3, 17]. Therefore, their advantages include enhanced solubility and stability of hydrophobic drugs, prolongation of circulation time, minimization of non-specific uptake, prevention of undesirable off-target and side effects, improvement of intracellular penetration, and targeting of specific cancer markers [18]. In addition, encapsulated molecules can be released from NPs in a controlled manner over time to maintain a drug concentration within a therapeutic window, or drug release can be triggered by a stimulus unique to the delivery site [19, 20]. Several studies underlined the great potentiality of these NP systems. For example, Xie and colleagues established that NPs made up of poly lactic-co-glycolic acid (PLGA)-loaded with curcumin can represent a promising approach for obtain a sustained and controlled drug delivery [21]. In

another study, Acharya and co-workers demonstrated the synergistic effect of dual drugs entrapped in polymeric NPs. The combined formulation resulted in enhanced cytotoxicity against leukemic K562 cells compared with the free drugs at a lower dose [22].
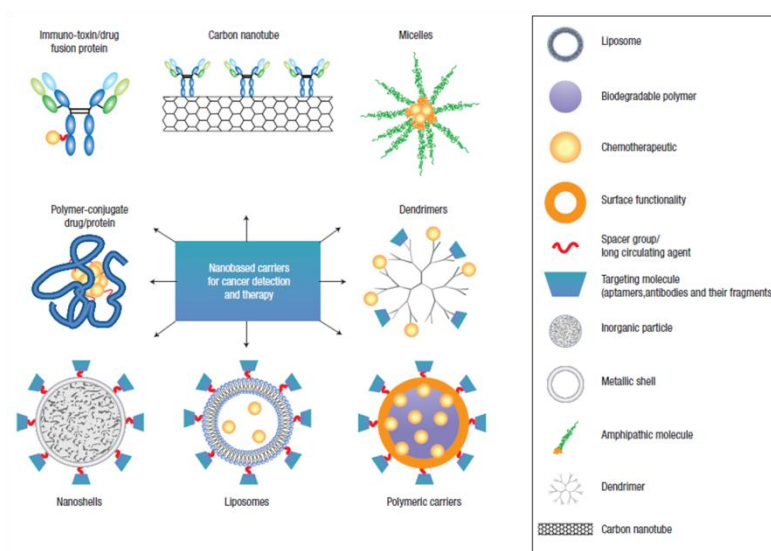
Figura 1. *Example of different kind of nanocarriers for cancer detection [7].*

Despite these advancements on drug delivery, the efficiency of chemotherapy remains substantially limited by the resistance of cancer cells to anticancer drugs, a parameter that fluctuates significantly in different patients. This phenomenon, called multidrug resistance (MDR), is one of the major causes of treatment failure in cancer therapy, and is attributed to the decreased accumulation of drug in the tumor site and possibly to the role of the membrane P-glycoprotein in accelerating the drug efflux [23-25] (**Fig. 2-C**). To overcome the problem of efflux action of P-glycoprotein and sustain the drug effect, various drug delivery systems have been developed [26-28]. For instance, PLGA NP formulations capable of delivering the cytotoxic drug vincristine or the chemosensitizer verapamil, or their combination, were prepared by Song *et al* [29]. The results obtained showed that PLGA NPs simultaneously loaded with the anticancer drug and the chemosensitizer might provide a potentially favorable formulation for *in vivo* treatment of drug-resistant cancers, since this simultaneous administration

resulted highly efficient even on MCF-7/ADR cells resistant to vincristine. In other studies, an efficient and targeted delivery of antisense oligodeoxynucleotides using folic acid-conjugated hydroxypropyl-chitosan NPs was developed to reduce production of P-glycoprotein and overcome tumor drug resistance [30].

Beside the control of drug efflux, another important aspect for improving the efficiency of drug delivery systems consists in controlling the relationships and the possible interactions that can be established between NPs and biological compounds after administration. Indeed, the physical and chemical properties of NPs, such as size, shape, surface charge and composition, can affect their interactions with several components of the blood flow and exert a strong effect on their extravasation and diffusion in tumor environment [2, 31-33]. Firstly, the surface of NPs can be designed either to attach specific ligands that can enhance their uptake by target tissues, or to increase the blood circulation half-life that consequently influences their distribution [34, 35]. Indeed, it is well known that NPs, when administered into the blood, are rapidly cleared and taken up within few time by the cells of the reticulo-endothelial system (RES)/mononuclear phagocyte system (MPS) present in the body, and remain particularly distributed in liver, lungs, spleen, and bone marrow [35-37]. NP uptake can be optimized also by functionalization of NP surface that is by addition of chemical functional groups. This approach is often used to add modifications that can improve the new NP formulations with drug controllable release, a parameter that in turn can optimize the concentration of the active drug at the sites of action. For instance, to extend the circulation time of NPs *in vivo*, uncharged hydrophilic polymers such as polyethylene glycol (PEG) are often conjugated to the surface of particles for "stealthing" [25, 38, 39]. By preventing opsonisation, the addition of PEG drastically increases the blood half-life of all NPs, regardless of their surface charge. Furthermore, the shape, density and length of the PEG chains can be modified and exert various effects on the rate of clearance. For example, it has

been shown that increasing the molecular weight of PEG chains above 2 kDa increases the half-life of the PEGylated particles [36].

In addition to surface functionalization, blood half-life and cellular uptake also depends on NP shape and size. For instant, Chithrani *et al* demonstrated the important role of particle shape and potentially curvature on NP cellular internalization [40]. These authors reported that 14 and 75 nm spherical nanoparticles were up-taken by cells 3.75–5 times more efficiently than 74-by-14 nm rod-shaped particles. It was hypothesized that this significant difference could be due to the different particle curvature that can affect the contact area with receptors on cell membrane and the distribution of targeting ligands on NP surface. Together with NP surface conjugations and shape, NP diameter is an additional important determinant for NP diffusion and drug release [41]. Particles with small diameter allow overcoming the biological barriers and can achieve a better cellular uptake than bigger ones [42, 43]. Indeed, NPs larger than 400 nm can not be simply unable to diffuse through the tumor interstitium in sufficient quantities to have any clinical or therapeutic effect [37, 44].

Hence, all physical and chemical features of NPs have a profound influence also on their extravasation from blood vessels. In this view, it is possible to exploit passive accumulation of NPs in tumor tissues, due to morphological differences existing between healthy and sick tissues. In this regard, an overview of the extracellular matrix focussing on tumor microenvironment is needed to understand the basis of the new strategies that are currently designed to improve the effects of NPs in cancer therapy.

1.1.2. The effects of tumor extracellular matrix on NP diffusion

In a living organism, all cell types are in contact with the extracellular matrix (ECM), a complex and dynamic network of macromolecules with different physical and chemical properties. The ECM consists of numerous molecules classified traditionally as collagens, elastin, microfibrillar proteins, proteoglycans (including hyaluronan), and non-collagenous glycoproteins. The ECM is a dynamic and versatile compartment and, by modulating the production, degradation and remodelling of its components, it supports organ development, function, repairing and consequent tissue homeostasis [45, 46]. On the basis of the organization of different components, the ECM molecular network is detailed for each tissue and reflects the specific functions required for those cell types. Moreover, the diversity and sophistication of ECM components confers specific and diverse physical, biochemical and biomechanical characteristics. Physical properties such as porosity, rigidity and insolubility are essential for the scaffolding role in supporting tissue structure and integrity, and also contribute to cell division and migration [45]. The ECM cleavage and remodelling can promote cell movement through the formation of guidelines on which cells can migrate. In addition, the orientation of ECM components, such as collagen fibers, can profoundly influence the directed migration of cells, by potentiating growth factor receptor signalling. Indeed, the ECM can bind to a myriad of growth factor and, in so doing, it limits the diffuse range and accessibility of ligands to their cognate receptors. A key concept regarding the ECM environment concerns how its bio-chemical and bio-mechanical properties can influence NP passage into cancer cells and consequently their effects on these cells [47, 48]. This aspect becomes even more evident when considering that cell–ECM connection is a reciprocal interaction in which cells continually remodel the ECM present in their microenvironment, and these dynamic modifications affect NP crossing. Despite multiple regulatory mechanisms, ECM dynamics can go skew when activities of ECM remodelling proteins are uncontrolled and deregulated, resulting in devastating consequences manifested in various human diseases [49].

For example, various collagens, including collagen I, II, III, V, and IX, show increased deposition during tumor formation [50]. As consequence of the changes in its composition, the architecture of tumor-associated ECM is fundamentally different from that typical of the normal tissue. Indeed, consistent with the changes in ECM composition and topography, expression of many ECM remodelling enzymes is often deregulated in human cancers, making advantageous the use of these molecules as targeting moieties. For example, heparanases, sulfatases, permeability mediators, such as vascular endothelial growth factor (VEGF), bradykinin (BK), prostaglandins (PGs), nitric oxide (NO) and, most notably, many metalloproteases (MMPs), are frequently overexpressed in various cancers [51-53] (**Fig. 2-A**). Among others, one of the earlier events in tumor progression is the generation of activated fibroblasts, which contributes to abnormal ECM build-up and deregulated expression of ECM remodelling enzymes. Continuing, in late-stage, immune cells are often recruited to tumor sites to promote tumor-associated angiogenesis (formation of new blood vessels from existing ones). Hence, the abnormal ECM dynamics promote cancer cell proliferation, loss of cell differentiation and invasion, playing essential role in cancer progression (**Fig. 2**). This irregular condition promotes a unique anatomical and pathophysiological architecture. For instance, the blood vessels in a solid tumor are irregular in shape, dilated, leaky or defective, and the endothelial cells are poorly aligned or disorganized with large fenestrations (**Fig. 2-D**). These large gaps facilitate selective extravasation of NPs from the surrounding vessels into the tumor [54, 55].
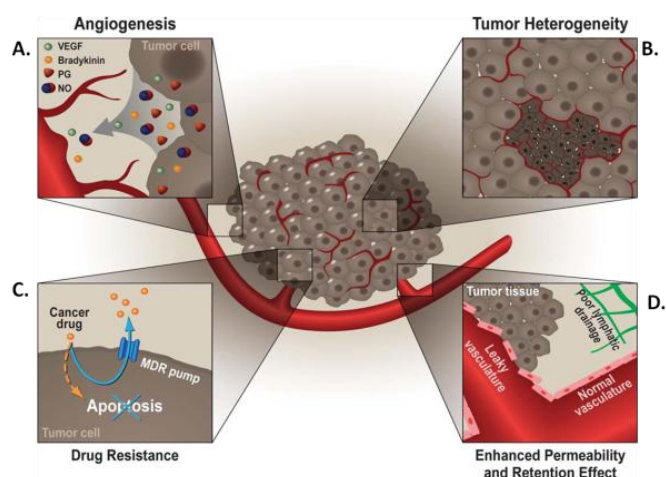
Figure 2. *The tumor environment. A) Angiogenesis due to tumor cells releasing factors, such as VEGF, BK, PK and NO that stimulate the production of new blood vessels. B) Tumor bulk C) Multidrug resistence effect, probably due to the role of the membrane P-glycoprotein in accelerating the drug efflux. D) Enhanced permeability and retection effect due to the combined effect of "leaky" defective vascular architecture and poor tumor lymphatic drainage [3].*

Furthermore, the impaired lymphatic drainage of solid tumor tissue facilitates the retention of the accumulated NPs, allowing them to release drugs in the vicinity of the target site [55]. This phenomenon is well-known as "Enhanced Permeability and Retention (EPR)" effect (**Fig. 3**). This passive targeting is widely utilized in biomedical applications, since tumor morphology facilitate the accumulation of NPs in sick tissues [56, 57]. Generally, NP-based carriers with diameter less than 200 nm are effective for passive targeted drug delivery to a solid tumor [9].

However, although passive targeting is at the basis of clinical cancer therapy, it displays several limitations. For instance, the exploitation of EPR effect is not feasible in all tumors, because the degree of vascularization and porosity of tumor vessels can vary with the tumor type and status [57]. Moreover, tumors have a negative interstitium pressure gradient, which can substantially limits the convection of NPs from the intravascular to the extravascular space within the cancerous cell mass. One way to address these challenges is to program new formulations of smart NPs with active binding ability to specific ligands after extravasation. It is well know, in fact, that solid tumors often overexpress specific antigens on cancer cell surface or within the ECM [58, 59]. Finally, the

EPR effect is found to be pronounced when the nanocarrier delivery systems are designed to evade the MPS system, so that their circulation half-life in the blood is extended.
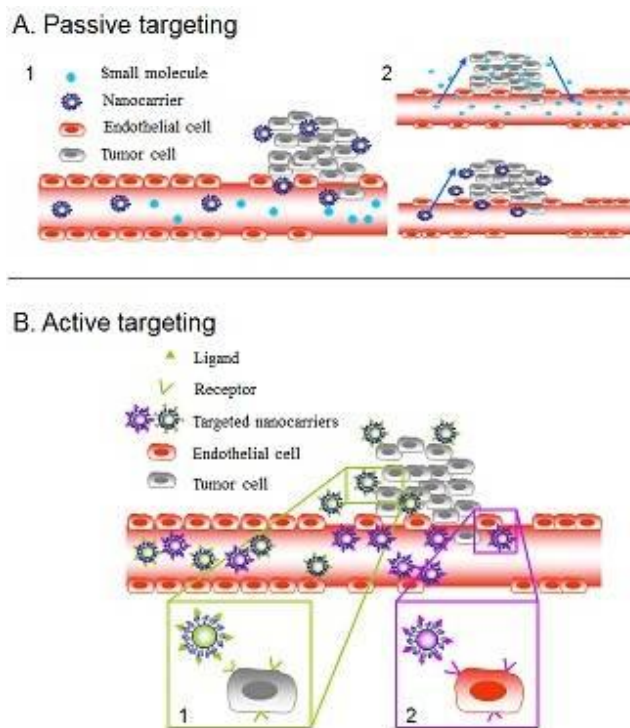
Figure 3. *Enhanced Permeability and Retection (EPR) effect: passive (A) and active targeting (B). The EPR effect ermitting accumulation of nanometer-sized particles in cancer cells. Blood vessels in tumor tissue have defective architecture with gaps as large as 200–1000 nm allowing nanoparticles to extravasate and accumulate inside the tumor tissue.*

1.1.3. Active targeting: cellular and extracellular marks

To guide the NPs to the target site, the most common strategy is to conjugate on the NP surface selective markers that enable to interact with specific active components of tumor environment, such as the membrane of cancer cells or specific organelles inside these cells [60]. Many targeting moieties include antibodies or their fragments, peptides, nucleic acids (aptamers), polysaccharides (hyaluronic acid, HA), glycoproteins (transferrin) and small molecules (folate acid) [17, 61-66]. Although monoclonal antibodies (mAbs) have widely used as escort molecules for targeted delivery, several restrictions, as their large size and difficulty in conjugation to NPs, have hampered their uses. Thus, other smaller

ligands, such as peptides, have attracted greater attention in the last years. Generally, screening of potential protein ligands is typically performed using a combinatorial phage library, and this approach selects ligands that range from 10–15 amino acids in length for their ability to selectively bind to tumor targets with high affinity [67-69]. Moreover, the capacity to link two or more markers upon NP surface can generate multivalent systems with the purpose of significantly increase the binding affinity of a particle toward a target cell, and optimize the accumulation of chemotherapics specifically in the tumor site, leaving healthy organs intact [70] (**Fig. 4**).
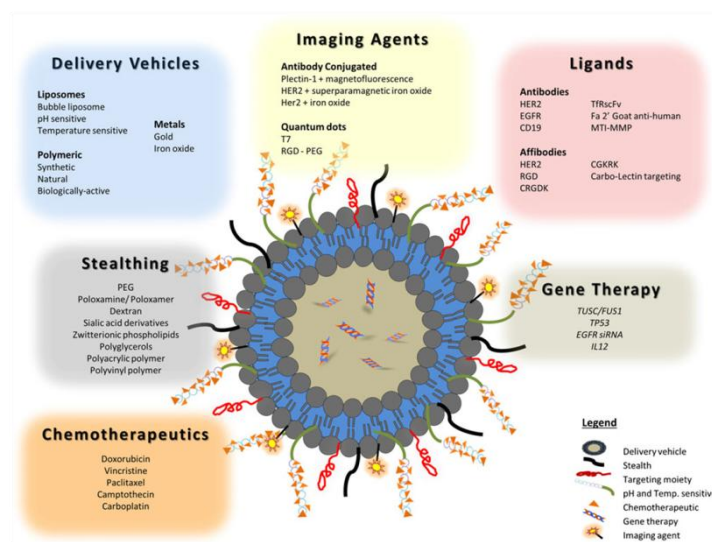
Figura 4. *Example of multifunctional nanoparticles can be designed with a choice of drug delivery, tumor targeting ligands, molecular imaging with stealth properties for several applications [71].*

A good example of this strategy was provided by Sun *et al*, who demonstrated that doxorubicin-linked to gold NPs via a poly (ethylene glycol) spacer and an acidabile hydrazone bond can potently be delivered to breast CSCs, drastically reducing their capacity of mammosphere formation and cancer initiation activity, and eliciting marked enhancement of tumor growth inhibition in murine models [72]. In addition, Yoo and Park designed model micelles formed by a copolymer of poly (D, L-lactic-co-glycolic acid) (PLGA) and PEG, where the doxorubicin

(DOX) was conjugates via chemical linkage to the PLGA, and the folate acid was added to the PEG chain. These particles exhibited increased cellular uptake, circulation time, and decreased cardiotoxicity. This last parameter indicated that the targeting moiety was able to differentiate between healthy and tumor tissue with greater specificity than untargeted DOX, while the increased cytotoxicity and cellular uptake showed that the folate-receptor actively internalized the conjugated particle into the cytoplasm [73]. Noteworthy, also transferrin-conjugated NPs have been shown to inhibit cellular proliferation and tumor growth and to display sustained release profiles and increased cellular uptake. The effectiveness of the conjugated NPs is most likely due to their ability to be taken up by receptor-mediated endocytosis, which enhances the amount of drug delivered to tumor cells and limits the amount delivered to healthy cells [74, 75]. However, despite the functionalization of NP surface with specific ligands for membrane cancer cells can have extreme potentiality, in some cases it suffers several limitations. In fact, in some tumor types where the extracellular matrix is too dense, deep penetration of NPs is hampered [76]. Functionalized NPs are often much larger than conventional drugs used for cancer treatments, so that their penetration is adversed by the high tumor cell density and the high interstitial fluid pressure (IFP), and they often do not cross more than one or two layers [77]. This feature has been recently documented also by Popovic and co-workers who, by using intravital microscopy, showed that upon injection of quantum dots with three different sizes (12, 60, 125 nm), only the smaller ones had the ability to penetrate, while the larger particles clustered in peri-vascular regions [78]. Similar findings have been reported by Dreher and colleagues who, by using dextran NPs with different diameter, demonstrated that both extravasation and penetration were efficient only for particles of small size [79]. These data strongly suggest that further attempts should be made to find an optimal NP size that can couple long-circulation properties with proper extravasation and penetration. To this goal, it is worth noting that designing ligands targeted to extracellular matrix or system with drug release "on demand"

could be helpful to overcome the penetration barrier. For example, the use of stimuli-sensitive nanocarriers, which allow release their contents in the vicinity of tumor, can keep low the molecular weight and permit the drug to penetrate deeply into the tumor (**Fig. 5**). These stimuli-responsive drug delivery systems have been designed for program drug release upon external or internal stimuli, including ultrasound, magnetic fields, heat, light, pH and specific enzyme activity [80-88]. For instance, in the case of drug delivery carriers containing magnetic NPs, Gang *et al* showed that magnetic (Fe(3)O(4)) poly epsilon-caprolactone (PCL) NPs containing the anticancer drug gemcitabine can exert high therapeutic effects by delivering efficiently the drug to magnetically targeted tumor [89]. In addition, magnetic resonance probes were used to detect cancer, so that this system provides an optimal example for designing multistage NPs for targeted therapy and cancer detection. Karthik *et al* also furnished an excellent example of photo-responsive multifunctional magnetic nanoparticles (MNPs) based on the use of coumarin-based phototrigger for cell imaging and photo-controlled delivery of anticancer drugs [90]. Another important strategy includes the design a new formulations of NPs focussed to distinguish the acidic environment of solid tumors respect to that of normal tissues [91, 92]. The pH value of highly proliferating tissues is in fact generally comprised between 6.5 to 7.2, due to the increased glycolysis and plasma membrane proton-pump activity of cancer cells [93, 94]. In addition, insufficient blood supply and poor lymphatic drainage also contribute to the acidity of the tumor microenvironment. Compared with the targeting of molecular biomarkers, the targeting of tumor extracellular pH value is insensitive to protein heterogeneity and is also not limited by the numbers of biomarkers present on the cell surface [95].
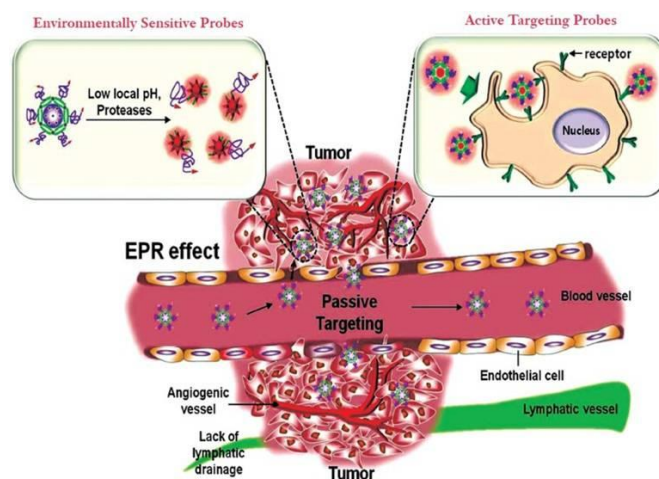
Figure 5. *Approaches of drug release due to stimuli-sensitive nanocarriers (on left) and active targeting (on right) in cancer diagnosis [96].*

Typical examples of this strategy are polymeric NP systems that change their physical and chemical properties, such as their charges or TAT peptide exposure, in response to cleavage of pH-labile groups under the stimulus of local tumor pH value [95]. One example of pH-triggered drug delivery system was provided by the group of Bae, that developed a smart system made up of poly (L-histidine)/PEG based polymeric micelles-loaded with doxorubicin. These mixed micelles were stable at pH above 7.4, while gradually destabilized below 7.0 due to the ionization of the polyHis block in the micelle core. The authors reported that this system retarded tumor growth and caused minimal weight loss in mice [97, 98]. An alternative strategy consists in functionalizing NP surface with specific components present at higher concentrations in the tumor extracellular environment respect to that of normal tissues. To this regard, particularly useful targets are some proteinases, such as heparanase and MMPs, nitric oxide (NO) and hyaluronic acid, that concentrated within and around the tumor mass [99-102]. The heparanase activity, which degrades heparin sulphate (HS) chains covalently attached of heparan sulphate proteoglycans (HSPGs), had been reported in many metastatic tumors, and its expression was observed in a variety of malignant tumors to be correlated to the malignant phenotype [59, 103].

  MMPs, family of zinc-dependent endopeptidases, also may play important roles in tumorigenesis and cancer cell progression, because they are able to digest all

the main components of basement membrane and ECM [104, 105]. Various MMP-sensitive substrates have been designed and showed stimulus responsiveness when used in drug delivery systems [106-108]. For example, Zhu *et al* used paclitaxel (PTX) as a model therapeutic, and synthesized a self-assembling drug-polymer conjugate/prodrug, PEG2000-peptide-PTX, which contained the MMP2-cleavable octapeptide between PEG and PTX. This system demonstrated high potential for effective intracellular delivery of PTX into cancer cells [108].

These new strategies could shift the paradigm of the traditional approach based on targeting markers specific to cancer cells surface (that can be highly variable among different tumor types) to a new one, that can be based on targeting specific extracellulary markers of ECM that are generally present around a tumor mass. This shift could put the fundaments for a new targeting strategy that can be more generally advantageous for biomedical applications.

1.2. AIM OF THE PROJECT

On the basis of this complex panorama, understanding the NP interactions with biological systems is a necessary step for developing NPs that can act more effectively as imaging and drug delivery agents. In this view, my work has been focused on pivotal aspects that determine the NP optimal features, that are: how physical-chemical properties, such as size, shape, functional groups and surface charge could affect the cellular response, in term of NP cellular uptake; and how the cytotoxic effects triggered by NPs-loaded with a widely chemotherapeutic drug, as doxorubicin (DOX), can vary according to different human cell lines. The traditional way to study NP-cell interactions is generally still based on following cell growth on flat dishes of polystyrene plastic in two-dimensional (2D) *in vitro* systems [40, 109-112], although 2D cultures impose highly unnatural behaviour and impose geometric and mechanical constraints to growing cells. However, within the body, the cells grow in a three dimensional (3D) ECM environment rich in type I collagen, fibrin, laminin, elastin, proteoglycans etc. Cells cultured in 3D matrices can thus better reflect the *in vivo* physiology than those cultured in 2D systems. For these reasons, several experiments were focussed to define NP uptake and cytotoxicity in different cell lines and to compare the results obtained in conventional 2D system to those obtained when cells were embedded in 3D collagen matrix.

This thesis is organized in three sections, where each chapter focussed the attention on crucial aspects that overall put the groundwork for ameliorate the current strategies in cancer treatments:

✓ The first chapter collects the experiments aimed to understand how NP features, such as size and surface charge, can affect NP diffusion and crossing through a 3D collagen matrix (the major component of ECM), where two different cell lines were embedded in. Possible interactions between NP properties and several components of ECM could, in fact, produce in the living organism a cellular response quite different from that showed in an *in vitro* 2D culture system. In particular, I investigated the

influence of (a) particle size, and (b) surface functionalization, on diffusion and cellular internalization of four different polystyrene NPs on primary human dermal fibroblasts (HDF), taken as a model of an healthy tissue, and human fibrosarcoma (HT1080), taken as a model of a tumor tissue.

✓ The second chapter discusses the suitability of biodegradable NPs loaded with a widely used chemotherapeutic agent, such as DOX, as a possible nanocarriers in drug delivery. Three NP formulations with different sizes, made up of two biodegradable co-polymers, such as poly (D, L-lactic-co-glycolic acid) (PLGA) and poly (ethylene glycol) (PEG) were loaded with DOX, and accurately characterized. The effect of these NP preparations on cell uptake and toxicity was investigated in standard 2D cell cultures on HeLa and IGROV-1 cells, which were used as *in vitro* models of human cervix carcinoma and ovarian adenocarcinoma, respectively. The cytotoxicity of Dox-loaded PELGA NPs towards HeLa cells was also assessed in 3D collagen matrices, in which the NPs were confined in a region separated from the cells by a porous membrane, thus creating an initial Dox step-wise gradient [113].

✓ Finally, the last chapter is focused to a rationale design of a novel nanocarrier able to safely carry DOX in tumor tissues in response to matrix metalloprotease-2 (MMP2) enzyme, which is over-expressed in ECM of tumors. Specifically, two MMP2 sensitive peptides were used as cleavable linkers between Dox and polyethylene glycol (PEG) to form a polymer-peptide-drug conjugate, working as a tumor-activated prodrug (TAP). The obtained TAP was then attached to the surface of 200 nm carboxyl-modified polystyrene model nanoparticles (NPs). The resulting TAP conjugated NPs were characterized *in vitro* for their release features at different MMP2 concentrations, in order to identify the minimum bioactive enzyme dose-response, and for their cytotoxic effect on three different human cell types, namely fibrosarcoma cell line (HT1080),

primary dermal fibroblasts (HDF) and umbilical vein endothelial cells (HUVECs), as models of tumor and healthy tissue, respectively.

1.3. REFERENCES

1. Wang, E.C. and A.Z. Wang, *Nanoparticles and their applications in cell and molecular biology.* Integrative Biology, 2014. **6**(1): p. 9-26.
2. Davis, M.E., Z. Chen, and D.M. Shin, *Nanoparticle therapeutics: an emerging treatment modality for cancer.* Nature Reviews Drug Discovery, 2008. **7**(9): p. 771-782.
3. Thakor, A.S. and S.S. Gambhir, *Nanooncology: The Future of Cancer Diagnosis and Therapy.* Ca-a Cancer Journal for Clinicians, 2013. **63**(6): p. 395-418.
4. Subbiah, R., M. Veerapandian, and K.S. Yun, *Nanoparticles: Functionalization and Multifunctional Applications in Biomedical Sciences.* Current Medicinal Chemistry, 2010. **17**(36): p. 4559-4577.
5. Parhi, P., C. Mohanty, and S.K. Sahoo, *Nanotechnology-based combinational drug delivery: an emerging approach for cancer therapy.* Drug Discovery Today, 2012. **17**(17-18): p. 1044-1052.
6. Zhang, L., et al., *Nanoparticles in medicine: Therapeutic applications and developments.* Clinical Pharmacology & Therapeutics, 2008. **83**(5): p. 761-769.
7. Peer, D., et al., *Nanocarriers as an emerging platform for cancer therapy.* Nature Nanotechnology, 2007. **2**(12): p. 751-760.
8. Blasi, P., et al., *Solid lipid nanoparticles for targeted brain drug delivery.* Advanced Drug Delivery Reviews, 2007. **59**(6): p. 454-477.
9. Torchilin, V.P., *Recent advances with liposomes as pharmaceutical carriers.* Nature Reviews Drug Discovery, 2005. **4**(2): p. 145-160.
10. Allen, T.M. and P.R. Cullis, *Liposomal drug delivery systems: From concept to clinical applications.* Advanced Drug Delivery Reviews, 2013. **65**(1): p. 36-48.
11. Chan, J.M., et al., *Polymeric Nanoparticles for Drug Delivery*, in *Cancer Nanotechnology: Methods and Protocols*, S.R. Grobmyer and B.M. Moudgil, Editors. 2010. p. 163-175.
12. Zhang, L., et al., *Self-assembled lipid-polymer hybrid nanoparticles: A robust drug delivery platform.* Acs Nano, 2008. **2**(8): p. 1696-1702.
13. Canfarotta, F. and S.A. Piletsky, *Engineered Magnetic Nanoparticles for Biomedical Applications.* Advanced Healthcare Materials, 2014. **3**(2): p. 160-175.
14. Hu, C.-M.J., S. Aryal, and L. Zhang, *Nanoparticle-assisted combination therapies for effective cancer treatment.* Therapeutic Delivery, 2010. **1**(2): p. 323-334.
15. Zhang, L., et al., *Co-delivery of hydrophobic and hydrophilic drugs from nanoparticle-aptamer bioconjugates.* Chemmedchem, 2007. **2**(9): p. 1268-1271.
16. MaHam, A., et al., *Protein-Based Nanomedicine Platforms for Drug Delivery.* Small, 2009. **5**(15): p. 1706-1721.
17. Ruoslahti, E., S.N. Bhatia, and M.J. Sailor, *Targeting of drugs and nanoparticles to tumors.* Journal of Cell Biology, 2010. **188**(6): p. 759-768.
18. Wilczewska, A.Z., et al., *Nanoparticles as drug delivery systems.* Pharmacological Reports, 2012. **64**(5): p. 1020-1037.
19. Moghimi, S.M., *Recent developments in polymeric nanoparticle engineering and their applications in experimental and clinical oncology.* Anti-cancer agents in medicinal chemistry, 2006. **6**(6): p. 553-561.

20.   Liu, J., et al., *pH-Sensitive nano-systems for drug delivery in cancer therapy.* Biotechnology Advances, (0).

21.   Xie, X., et al., *PLGA Nanoparticles Improve the Oral Bioavailability of Curcumin in Rats: Characterizations and Mechanisms.* Journal of Agricultural and Food Chemistry, 2011. **59**(17): p. 9280-9289.

22.   Acharya, S. and S.K. Sahoo, *Sustained targeting of Bcr-Abl plus leukemia cells by synergistic action of dual drug loaded nanoparticles and its implication for leukemia therapy.* Biomaterials, 2011. **32**(24): p. 5643-5662.

23.   Vauthier, C., et al., *Drug delivery to resistant tumors: the potential of poly(alkyl cyanoacrylate) nanoparticles.* Journal of Controlled Release, 2003. **93**(2): p. 151-160.

24.   Minko, T., L. Rodriguez-Rodriguez, and V. Pozharov, *Nanotechnology approaches for personalized treatment of multidrug resistant cancers.* Advanced Drug Delivery Reviews, 2013. **65**(13-14): p. 1880-1895.

25.   Iyer, A.K., et al., *Role of integrated cancer nanomedicine in overcoming drug resistance.* Advanced Drug Delivery Reviews, 2013. **65**(13-14): p. 1784-1802.

26.   Xiang, Q., et al., *Cabozantinib reverses multidrug resistance of human hepatoma HepG2/adr cells by modulating the function of P-glycoprotein.* Liver International, 2014: p. n/a-n/a.

27.   Sharom, F.J., *Complex interplay between the P-glycoprotein multidrug efflux pump and the membrane: its role in modulating protein function.* Frontiers in Oncology, 2014. **4**.

28.   Roy, A., et al., *Carboxymethylcellulose-Based and Docetaxel-Loaded Nanoparticles Circumvent P-Glycoprotein-Mediated Multidrug Resistance.* Molecular Pharmaceutics, 2014.

29.   Song, X.R., et al., *Reversion of multidrug resistance by co-encapsulation of vincristine and verapamil in PLGA nanoparticles.* European Journal of Pharmaceutical Sciences, 2009. **37**(3-4): p. 300-305.

30.   Wang, J., et al., *Reversion of multidrug resistance by tumor targeted delivery of antisense oligodeoxynucleotides in hydroxypropyl-chitosan nanoparticles.* Biomaterials, 2010. **31**(15): p. 4426-4433.

31.   Lundqvist, M., et al., *Nanoparticle size and surface properties determine the protein corona with possible implications for biological impacts.* Proceedings of the National Academy of Sciences of the United States of America, 2008. **105**(38): p. 14265-14270.

32.   Monopoli, M.P., et al., *Physical-Chemical Aspects of Protein Corona: Relevance to in Vitro and in Vivo Biological Impacts of Nanoparticles.* Journal of the American Chemical Society, 2011. **133**(8): p. 2525-2534.

33.   Nel, A.E., et al., *Understanding biophysicochemical interactions at the nano-bio interface.* Nature Materials, 2009. **8**(7): p. 543-557.

34.   Nativo, P., I.A. Prior, and M. Brust, *Uptake and intracellular fate of surface-modified gold nanoparticles.* Acs Nano, 2008. **2**(8): p. 1639-1644.

35.   Moghimi, S.M., A.C. Hunter, and J.C. Murray, *Long-circulating and target-specific nanoparticles: Theory to practice.* Pharmacological Reviews, 2001. **53**(2): p. 283-318.

36.   Owens, D.E. and N.A. Peppas, *Opsonization, biodistribution, and pharmacokinetics of polymeric nanoparticles.* International Journal of Pharmaceutics, 2006. **307**(1): p. 93-102.

37. Alexis, F., et al., *Factors affecting the clearance and biodistribution of polymeric nanoparticles.* Molecular Pharmaceutics, 2008. **5**(4): p. 505-515.

38. Veronese, F.M. and G. Pasut, *PEGylation, successful approach to drug delivery.* Drug Discovery Today, 2005. **10**(21): p. 1451-1458.

39. Dobrovolskaia, M.A. and S.E. McNeil, *Immunological properties of engineered nanomaterials.* Nature Nanotechnology, 2007. **2**(8): p. 469-478.

40. Chithrani, B.D., A.A. Ghazani, and W.C.W. Chan, *Determining the size and shape dependence of gold nanoparticle uptake into mammalian cells.* Nano Letters, 2006. **6**(4): p. 662-668.

41. Steichen, S.D., M. Caldorera-Moore, and N.A. Peppas, *A review of current nanoparticle and targeting moieties for the delivery of cancer therapeutics.* European Journal of Pharmaceutical Sciences, 2013. **48**(3): p. 416-427.

42. Brigger, I., C. Dubernet, and P. Couvreur, *Nanoparticles in cancer therapy and diagnosis.* Advanced Drug Delivery Reviews, 2002. **54**(5): p. 631-651.

43. Goodman, T.T., P.L. Olive, and S.H. Pun, *Increased nanoparticle penetration in collagenase-treated multicellullar spheroids.* International Journal of Nanomedicine, 2007. **2**(2): p. 265-274.

44. Gullotti, E. and Y. Yeo, *Extracellularly Activated Nanocarriers: A New Paradigm of Tumor Targeted Drug Delivery.* Molecular Pharmaceutics, 2009. **6**(4): p. 1041-1051.

45. Lu, P., et al., *Extracellular Matrix Degradation and Remodeling in Development and Disease.* Cold Spring Harbor Perspectives in Biology, 2011. **3**(12).

46. Muiznieks, L.D. and F.W. Keeley, *Molecular assembly and mechanical properties of the extracellular matrix: A fibrous protein perspective.* Biochimica Et Biophysica Acta-Molecular Basis of Disease, 2013. **1832**(7): p. 866-875.

47. Stylianopoulos, T., et al., *Diffusion Anisotropy in Collagen Gels and Tumors: The Effect of Fiber Network Orientation.* Biophysical Journal, 2010. **99**(10): p. 3119-3128.

48. Lieleg, O., R.M. Baumgaertel, and A.R. Bausch, *Selective Filtering of Particles by the Extracellular Matrix: An Electrostatic Bandpass.* Biophysical Journal, 2009. **97**(6): p. 1569-1577.

49. Muschler, J. and C.H. Streuli, *Cell-Matrix Interactions in Mammary Gland Development and Breast Cancer.* Cold Spring Harbor Perspectives in Biology, 2010. **2**(10).

50. Egeblad, M., M.G. Rasch, and V.M. Weaver, *Dynamic interplay between the collagen scaffold and tumor evolution.* Current Opinion in Cell Biology, 2010. **22**(5): p. 697-706.

51. Ilan, N., M. Elkin, and I. Vlodavsky, *Regulation, function and clinical significance of heparanase in cancer metastasis and angiogenesis.* International Journal of Biochemistry & Cell Biology, 2006. **38**(12): p. 2018-2039.

52. Page-McCaw, A., A.J. Ewald, and Z. Werb, *Matrix metalloproteinases and the regulation of tissue remodelling.* Nature Reviews Molecular Cell Biology, 2007. **8**(3): p. 221-233.

53. Kessenbrock, K., V. Plaks, and Z. Werb, *Matrix Metalloproteinases: Regulators of the Tumor Microenvironment.* Cell, 2010. **141**(1): p. 52-67.

54. Fang, J., H. Nakamura, and H. Maeda, *The EPR effect: Unique features of tumor blood vessels for drug delivery, factors involved, and limitations and*

augmentation of the effect. Advanced Drug Delivery Reviews, 2011. **63**(3): p. 136-151.

55.   Greish, K., et al., *Enhanced Permeability and Retention (EPR) Effect and Tumor-Selective Delivery of Anticancer Drugs.* Delivery of Protein and Peptide Drugs in Cancer. 2006. 37-52.

56.   Danhier, F., O. Feron, and V. Preat, *To exploit the tumor microenvironment: Passive and active tumor targeting of nanocarriers for anti-cancer drug delivery.* Journal of Controlled Release, 2010. **148**(2): p. 135-146.

57.   Maeda, H., *Macromolecular therapeutics in cancer treatment: The EPR effect and beyond.* Journal of Controlled Release, 2012. **164**(2): p. 138-144.

58.   Li, M.-H., et al., *Dendrimer-based multivalent methotrexates as dual acting nanoconjugates for cancer cell targeting.* European Journal of Medicinal Chemistry, 2012. **47**: p. 560-572.

59.   Vlodavsky, I., et al., *Mammalian heparanase: involvement in cancer metastasis, angiogenesis and normal development.* Seminars in Cancer Biology, 2002. **12**(2): p. 121-129.

60.   Haley, B. and E. Frenkel, *Nanoparticles for drug delivery in cancer treatment.* Urologic Oncology-Seminars and Original Investigations, 2008. **26**(1): p. 57-64.

61.   Chung, Y.-I., et al., *The effect of surface functionalization of PLGA nanoparticles by heparin- or chitosan-conjugated Pluronic on tumor targeting.* Journal of Controlled Release, 2010. **143**(3): p. 374-382.

62.   Kim, E., et al., *Prostate cancer cell death produced by the co-delivery of Bcl-xL shRNA and doxorubicin using an aptamer-conjugated polyplex.* Biomaterials, 2010. **31**(16): p. 4592-4599.

63.   Jiang, S., et al., *Preparation, characterization, and antitumor activities of folate-decorated docetaxel-loaded human serum albumin nanoparticles.* Drug Delivery. **0**(0): p. 1-8.

64.   Dassie, J.P. and P.H. Giangrande, *Current progress on aptamer-targeted oligonucleotide therapeutics.* Therapeutic Delivery, 2013. **4**(12): p. 1527-1546.

65.   Pang, J., et al., *Folate-conjugated hybrid SBA-15 particles for targeted anticancer drug delivery.* Journal of Colloid and Interface Science, 2013. **395**: p. 31-39.

66.   Hong, G.-b., J.-x. Zhou, and R.-x. Yuan, *Folate-targeted polymeric micelles loaded with ultrasmall superparamagnetic iron oxide: combined small size and high MRI sensitivity.* International Journal of Nanomedicine, 2012. **7**: p. 2863-2872.

67.   Brissette, R., J.K.A. Prendergast, and N.I. Goldstein, *Identification of cancer targets and therapeutics using phage display.* Current Opinion in Drug Discovery & Development, 2006. **9**(3): p. 363-369.

68.   Krag, D.N., et al., *Selection of tumor-binding ligands in cancer patients with phage display libraries (vol 66, pg 7724, 2006).* Cancer Research, 2006. **66**(17): p. 8925-8925.

69.   Fang, B., et al., *A novel cell-penetrating peptide TAT-A1 delivers siRNA into tumor cells selectively.* Biochimie, 2013. **95**(2): p. 251-257.

70.   Montet, X., et al., *Multivalent effects of RGD peptides obtained by nanoparticle display.* Journal of Medicinal Chemistry, 2006. **49**(20): p. 6087-6093.

71.   Babu, A., et al., *Nanodrug Delivery Systems: A Promising Technology for Detection, Diagnosis, and Treatment of Cancer.* AAPS PharmSciTech, 2014: p. 1-13.

72.   Sun, T.-M., et al., *Cancer stem cell therapy using doxorubicin conjugated to gold nanoparticles via hydrazone bonds.* Biomaterials, 2014. **35**(2): p. 836-845.

73.   Yoo, H.S. and T.G. Park, *Folate receptor targeted biodegradable polymeric doxorubicin micelles.* Journal of Controlled Release, 2004. **96**(2): p. 273-283.

74.   Sahoo, S.K. and V. Labhasetwar, *Enhanced Antiproliferative Activity of Transferrin-Conjugated Paclitaxel-Loaded Nanoparticles Is Mediated via Sustained Intracellular Drug Retention.* Molecular Pharmaceutics, 2005. **2**(5): p. 373-383.

75.   Sahoo, S.K., W. Ma, and V. Labhasetwar, *Efficacy of transferrin-conjugated paclitaxel-loaded nanoparticles in a murine model of prostate cancer.* International Journal of Cancer, 2004. **112**(2): p. 335-340.

76.   Wong, C., et al., *Multistage nanoparticle delivery system for deep penetration into tumor tissue.* Proceedings of the National Academy of Sciences of the United States of America, 2011. **108**(6): p. 2426-2431.

77.   Lammers, T., et al., *Drug targeting to tumors: Principles, pitfalls and (pre-) clinical progress.* Journal of Controlled Release, 2012. **161**(2): p. 175-187.

78.   Popovic, Z., et al., *A Nanoparticle Size Series for In Vivo Fluorescence Imaging.* Angewandte Chemie-International Edition, 2010. **49**(46): p. 8649-8652.

79.   Dreher, M.R., et al., *Tumor vascular permeability, accumulation, and penetration of macromolecular drug carriers.* Journal of the National Cancer Institute, 2006. **98**(5): p. 335-344.

80.   Lim, E.-K., et al., *Delivery of Cancer Therapeutics Using Nanotechnology.* Pharmaceutics, 2013. **5**(2): p. 294-317.

81.   Vivero-Escoto, J.L., et al., *Photoinduced Intracellular Controlled Release Drug Delivery in Human Cells by Gold-Capped Mesoporous Silica Nanosphere.* Journal of the American Chemical Society, 2009. **131**(10): p. 3462-+.

82.   Gary-Bobo, M., et al., *Multifunctionalized mesoporous silica nanoparticles for the in vitro treatment of retinoblastoma: Drug delivery, one and two-photon photodynamic therapy.* International Journal of Pharmaceutics, 2012. **432**(1-2): p. 99-104.

83.   Lee, J.-H., et al., *On-Demand Drug Release System for InVivo Cancer Treatment through Self-Assembled Magnetic Nanoparticles.* Angewandte Chemie-International Edition, 2013. **52**(16): p. 4384-4388.

84.   Katagiri, K., et al., *Magnetoresponsive On-Demand Release of Hybrid Liposomes Formed from Fe3O4 Nanoparticles and Thermosensitive Block Copolymers.* Small, 2011. **7**(12): p. 1683-1689.

85.   Tachibana, K. and S. Tachibana, *The use of ultrasound for drug delivery.* Echocardiography-a Journal of Cardiovascular Ultrasound and Allied Techniques, 2001. **18**(4): p. 323-328.

86.   Felber, A.E., M.-H. Dufresne, and J.-C. Leroux, *pH-sensitive vesicles, polymeric micelles, and nanospheres prepared with polycarboxylates.* Advanced Drug Delivery Reviews, 2012. **64**(11): p. 979-992.

87.   Makhof, A., Y. Tozuka, and H. Takeuchi, *pH-Sensitive nanospheres for colon-specific drug delivery in experimentally induced colitis rat model.* European Journal of Pharmaceutics and Biopharmaceutics, 2009. **72**(1): p. 1-8.

88. Soppimath, K.S., et al., *Multifunctional core/shell nanoparticles self-assembled from pH-induced thermosensitive polymers for targeted intracellular anticancer drug delivery.* Advanced Functional Materials, 2007. **17**(3): p. 355-362.

89. Gang, J., et al., *Magnetic poly ε-caprolactone nanoparticles containing Fe3O4 and gemcitabine enhance anti-tumor effect in pancreatic cancer xenograft mouse model.* Journal of Drug Targeting, 2007. **15**(6): p. 445-453.

90. Karthik, S., et al., *Photoresponsive Coumarin-Tethered Multifunctional Magnetic Nanoparticles for Release of Anticancer Drug.* Acs Applied Materials & Interfaces, 2013. **5**(11): p. 5232-5238.

91. Callahan, D.J., et al., *Triple Stimulus-Responsive Polypeptide Nanoparticles That Enhance Intratumoral Spatial Distribution.* Nano Letters, 2012. **12**(4): p. 2165-2170.

92. Manzoor, A.A., et al., *Overcoming Limitations in Nanoparticle Drug Delivery: Triggered, Intravascular Release to Improve Drug Penetration into Tumors.* Cancer Research, 2012. **72**(21): p. 5566-5575.

93. Barar, J. and Y. Omidi, *Dysregulated pH in Tumor Microenvironment Checkmates Cancer Therapy.* BioImpacts: BI, 2013. **3**(4): p. 149.

94. Kato, Y., et al., *Acidic extracellular microenvironment and cancer.* Cancer Cell International, 2013. **13**.

95. Zhao, Z., et al., *A Controlled-Release Nanocarrier with Extracellular pH Value Driven Tumor Targeting and Translocation for Drug Delivery.* Angewandte Chemie-International Edition, 2013. **52**(29): p. 7487-7491.

96. Park, K., *Polysaccharide-based near-infrared fluorescence nanoprobes for cancer diagnosis.* Quantitative imaging in medicine and surgery, 2012. **2**(2): p. 106-13.

97. Kim, K.S., et al., *A cancer-recognizable MRI contrast agents using pH-responsive polymeric micelle.* Biomaterials, 2014. **35**(1): p. 337-343.

98. Lee, Y.J., et al., *pH-Sensitive Polymeric Micelle-Based pH Probe for Detecting and Imaging Acidic Biological Environments.* Biomacromolecules, 2012. **13**(9): p. 2945-2951.

99. Egeblad, M. and Z. Werb, *New functions for the matrix metalloproteinases in cancer progression.* Nature Reviews Cancer, 2002. **2**(3): p. 161-174.

100. McKenzie, E.A., *Heparanase: a target for drug discovery in cancer and inflammation.* British Journal of Pharmacology, 2007. **151**(1): p. 1-14.

101. Gialeli, C., A.D. Theocharis, and N.K. Karamanos, *Roles of matrix metalloproteinases in cancer progression and their pharmacological targeting.* Febs Journal, 2011. **278**(1): p. 16-27.

102. Arpicco, S., et al., *Hyaluronic Acid Conjugates as Vectors for the Active Targeting of Drugs, Genes and Nanocomposites in Cancer Treatment.* Molecules, 2014. **19**(3): p. 3193-3230.

103. Vlodavsky, I., et al., *Significance of heparanase in cancer and inflammation.* Cancer microenvironment : official journal of the International Cancer Microenvironment Society, 2012. **5**(2): p. 115-32.

104. Curran, S. and G.I. Murray, *Matrix metalloproteinases: molecular aspects of their roles in tumour invasion and metastasis.* European Journal of Cancer, 2000. **36**(13): p. 1621-1630.

105. Vihinen, P., R. Ala-aho, and V.M. Kahari, *Matrix metalloproteinases as therapeutic targets in cancer.* Current Cancer Drug Targets, 2005. **5**(3): p. 203-220.

106. Zhu, L., P. Kate, and V.P. Torchilin, *Matrix Metalloprotease 2-Responsive Multifunctional Liposomal Nanocarrier for Enhanced Tumor Targeting.* Acs Nano, 2012. **6**(4): p. 3491-3498.

107. Rizzi, L., et al., *Novel biotinylated bile acid amphiphiles: Micellar aggregates formation and interaction with hepatocytes.* Organic & Biomolecular Chemistry, 2011. **9**(8): p. 2899-2905.

108. Zhu, L., et al., *Enhanced anticancer activity of nanopreparation containing an MMP2-sensitive PEG-drug conjugate and cell-penetrating moiety.* Proceedings of the National Academy of Sciences of the United States of America, 2013. **110**(42): p. 17047-17052.

109. Jiang, W., et al., *Nanoparticle-mediated cellular response is size-dependent.* Nature Nanotechnology, 2008. **3**(3): p. 145-150.

110. Cartiera, M.S., et al., *The uptake and intracellular fate of PLGA nanoparticles in epithelial cells.* Biomaterials, 2009. **30**(14): p. 2790-2798.

111. Lunov, O., et al., *Differential Uptake of Functionalized Polystyrene Nanoparticles by Human Macrophages and a Monocytic Cell Line.* Acs Nano, 2011. **5**(3): p. 1657-1669.

112. Rancan, F., et al., *Skin Penetration and Cellular Uptake of Amorphous Silica Nanoparticles with Variable Size, Surface Functionalization, and Colloidal Stability.* Acs Nano, 2012. **6**(8): p. 6829-6842.

113. Biondi, M., et al., *Sub-100 nm biodegradable nanoparticles: in vitro release features and toxicity testing in 2D and 3D cell cultures.* Nanotechnology, 2013. **24**(4).

CHAPTER 2

Nanoparticle size and surface charge as key factors in 3D matrix cellular uptake

2.1. ABSTRACT

Until recently, basic research, developed for testing the performance of nanoparticles (NPs) and the efficiency of novel anti-cancer drug, was generally performed on cells grown on two dimensional (2D) substrates, such as plastic or glass. However, this unnatural condition likely forces cells to adjust to artificially flat and rigid surfaces, generating data misleading that could be interpreted in a wrong way. Hence, the need to develop a new type of *in vitro* model that better mimics the three dimensional (3D) environment in which *in vivo* cells reside. This context is essential either for better understanding how NPs diffuse in a more complex environment, namely the extracellular matrix (ECM), and for predicting the particle properties that drive their delivery to cells. Indeed, the diffusion of NPs depends not only on their physico-chemical properties, including size, surface charge and functionalization as well as from the features typical of ECM. To shed light on this context, we investigated the effects of NP size and surface charge on their diffusion and cellular uptake in 3D scaffold, made up of a major component of ECM, as collagen type I. Two different cell types, primary human dermal fibroblast (HDF) and human fibrosarcoma (HT1080) were embedded in this dense network of fibers, in order to mimic the natural environment of healthy and tumor tissues, respectively. Cell behaviour in the 3D collagen gel was investigated and compared to cells grown on 2D glass coverslips. Moreover, cell response to polystyrene nanoparticles (PS-NPs) was also evaluated as a function of NP size (44 and 100 nm), surface functionalization ($-NH_2$ and $-COOH$) and diffusion through the 3D collagen matrix. Results were compared among cell types and with 2D cell culture

conditions. Furthermore, experimental data were used to develop a descriptive mathematical model able to explain NP uptake kinetics in 3D matrices.

In summary, results showed that PS-NPs with small size and positive surface charge had a greater ability to diffuse in a complex matrix and higher capacity to be internalized by cells, suggesting that these two features should be considered in the rational design of NP for biomedical applications.

2.2. INTRODUCTION

Recent advances in nanotechnology have led to the development of nanosized particles with controlled size and surface charge, which are promising in cancer detection and treatment [1-4]. To this aim, the diffusion of nanoparticles (NPs) in the extracellular matrix (ECM) is crucial to recognize the target cell population and release the therapeutic agent(s) locally, or mainly, in tumor tissues. The ECM is mainly composed of collagen, elastin, proteoglycans (e.g., hyaluronic acid) and non-collagenous glycoproteins, which form a three-dimensional (3D) network enclosing cells according to an organ-specific manner [5-7]. Furthermore, these molecules contribute either to control cellular activities such as adhesion, migration, proliferation, differentiation and survival, but also can have an effect on NP diffusion [8-11]. Nevertheless, the traditional way to study NP-cell interactions still consists in cellular adhesion on flat dishes of polystyrene plastic in two-dimensional (2D) *in vitro* system [12-16], although 2D cultures impose highly unnatural geometric and mechanical constraints to growing cells. Indeed, the most cells reside *in vivo* in a three-dimensional (3D) environment surrounded by ECM and other neighbouring cells, conditions that are different from those found by cells cultured *in vitro* on 2D substrata. As consequence, the latter condition fails to provide an accurate representation of *in vivo* growing cells, as they lack the contextual cues found in the native 3D tissue. For these reasons, 3D cell cultures are expected to provide a tool bridging the gap between the *in vitro* and the *in vivo* optimal conditions for cell culture. Thus, 3D systems can mirror *in vivo* conditions more closely than conventional 2D models and can be more predictive platforms to assess *in vivo* delivery efficiencies. In this more complex environment, the cellular response to NP diffusion and uptake could be so different from what it is expected. Therefore, there is now an emerging need to understand how NPs diffuse in the ECM and how cells respond to internalized NPs in a more native and complex environment to finally define the particle properties which can enhance and optimize their transport/uptake to cancer cells. As regarding, the transport of NPs in ECM/tissues depends on the

physico-chemical properties of both devices (i.e. shape, size and surface chemistry) and ECM [17, 18]. In general, NPs diffuse in ECM network by Brownian random walks, and their transport is (indirectly) influenced by steric interactions (i.e. collisions with collagen fibers), which depend on NP size, and (directly) by the electrostatic interactions between NP surfaces, charged ECM components and cells [11]. For these reasons, a major issue in this context is the overcoming of the manifold extracellular barriers hampering the reaching of the target cells, which are often present within internal regions of tissues. In this view, a key concept is to understand how NP size and surface charge influence their transport through ECM towards specific cells. Indeed, NP size and surface charge are crucial technological features which strongly influence NP interactions with the ECM and the cell membranes, and so doing also cellular uptake [19-21]. In this way, few studies have been performed to understand how cell behaviour and interactions with NPs can change in a 3D environment [22]. Other works, instead, are focused on NP diffusion involved in drug delivery within dense tumor ECMs that restricted particle penetration. For this issue, the most common model was represented by multicellular spheroid [23-25]. For instance, Goodman and co-workers studied the effect of polystyrene NPs of various sizes (20-40-100 and 200 nm in diameter), combined with collagenase treatment, on the uptake by human cervical carcinoma spheroids [26]. The results showed that penetration of particles into the spheroid core was limited to NPs smaller than 100 nm. However, collagenase-coated 100 nm NPs demonstrated a 4-fold increase in the number of particles delivered to the spheroid core compared to the control NPs, revealing that particles delivery to tumor may be substantially imporved by incorporation of ECM-modulating enzymes in the delivery formulations. Although the use of spheroids as model of tumor mass was helpful, the usefulness of these techniques is limited, due to the spheroid structure. Indeed, the spheroids are composed by multicellular layers, made up of proliferating cells on the outside, quiescent cells on the inside and necrotic cells at the center, due to nutrient and oxygen transport limitations [27]. This complex

structure hampers a clear understanding of the mechanisms involved in NP internalization by cells. In this panorama, the aim of this work is to understand how NP features and 3D environment can affect cellular uptake. In particular, we have investigated the influence of particle size and surface functionalization of polystyrene (PS) NPs, with two diameters and different surface functionalization (-COOH and -NH$_2$ groups), on the transport within collagen and on internalization by two cell lines, namely primary human dermal fibroblasts (HDF) and human fibrosarcoma (HT1080), entrapped in a 3D collagen matrix, using 2D cultures as a reference. The choose of these cell lines underlined the need to reproduce the *in vitro* model of healthy and tumor tissues, HDF and HT1080 respectively. On the other hand, the collagen was chosen since is the most abundant protein in mammalian organisms and the major component of ECM of the connective tissue, which provides tissue mechanical properties [28-31] and the natural environment for cell growth, adhesion, proliferation, and migration [32]. In this work, NP diffusion within collagen matrix and cellular uptake kinetics were investigated as a function of NP size and surface charge through spectrofluorimetric and confocal microscopy techniques. Moreover, starting from experimental data, a mathematical model was developed. The model considers NP uptake is envisaged as a process driven by adsorption/desorption, followed by NP internalisation via energy-dependent pathways. NP internalisation was taken into account starting from a pseudo-chemical equilibrium, and the numerical simulations were used to predict/elucidate the effect of size and surface charge in NP uptake in 3D matrices.

2.3. MATERIALS AND METHODS

2.3.1. Polystyrene nanoparticles

Green dye-loaded (fluorescence: $\lambda_{ex} \sim 468$ nm; $\lambda_{em} \sim 508$, 0.04 and 0.1 µm, Duke Scientific Corporation), yellow-green dye-loaded carboxylate-modified microspheres COOH-PS NPs (fluorescence: $\lambda_{ex} \sim 505$ nm; $\lambda_{em} \sim 515$, 0.1 µm, Invitrogen) and orange amine-modified beads NH_2-PS NPs (fluorescence: $\lambda_{ex} \sim 481$ nm; $\lambda_{em} \sim 644$ nm, 0.1 µm, Sigma Aldrich) were used without further modification or purification. NP dispersions were prepared by diluting the concentrated stock solutions into the complete medium, Eagle's minimal essential medium (EMEM, Lonza) used for cell culture at room temperature (RT) immediately prior to the experiments on cells, with an identical time delay between diluting and introducing to the cells for all experiments. Before sampling, NPs were vigorously mixed by vortexing, as recommended by the company. Measurement of size and ζ-potential of NPs were made with ZetaSizer Nano ZS (Malvern Instruments, Malvern, UK).

2.3.2. Three-dimensional collagen matrix

The collagen solution was purchased from Sigma Aldrich. The collagen gel were prepared by diluting stock solution with 10 X Dulbecco's phosphate saline buffer (D-PBS, Gibco) (8:1 volume ratio) and adjusting the pH to 7.2 by dropwise addition of NaOH and HCl. The final concentration obtained was 2.4 mg ml^{-1}. The solution was then poured in right cell culture dish, dependent of kind of experiments, and incubated at 37 °C for about 1 h to allow the fibrillogenesis process. Afterwards, fresh cell culture medium added to the gel.

2.3.3. Cell culture

To test the biological effect of the NPs, Human Dermal Fibroblast (HDF) and Human Fibrosarcoma cell lines (HT1080) were used. The latter were cultured with complete medium, composed of EMEM supplemented with 10 % fetal bovin serum (FBS, Gibco), 100 U/ml penicillin, 100 mg ml^{-1} streptomycin. The HDF cell lines were cultured with the same medium but supplemented with 20 %

FBS, 100 U/ml penicillin, 100 mg ml^{-1} streptomycin and 2 X non essential amino-acids. Cells were incubated in a humidified controlled atmosphere with 95 % to 5 % ratio of air/CO_2, at 37 °C. Medium was changed every 2 days. All experiments were performed in triplicate.

2.3.4. Cell viability and proliferation

The increment of DNA content was used to estimate cell proliferation within 3D collagen matrices. To quantify DNA contents, Pico Green assay (Invitrogen) was carried out. After 1, 2, 5 and 7 days of culture, collagen gels were degraded by collagenase solution (Roche Applied Science) for about 40 min at 37 °C, at final concentration of 2.5 mg ml^{-1}. After matrix digestion, cells were recovered by centrifugation at 1000 rpm for 5 min and lysated with 0.1 % Triton X 100 solution in PBS. PicoGreen reagent was added to cell lysates and fluorescence was read by a plate reader at 260 nm wavelength. DNA content was evaluated by interpolating raw data with the calibration curve.

2.3.5. Confocal microscopy for nanoparticle uptake in 2D and in 3D systems

For 2D cell culture conditions, 4 * 10^4 cells were seeded in 1 ml of medium on cover glass. Cells were incubated with all kinds of NPs, at the same concentrations used for NP uptake experiments (see below: *nanoparticles uptake* sections), for 24 hours at 37 °C in 5 % CO_2. Instead, for the 3D conditions, cells were grown in 0.3 ml of collagen at final concentration of 2.4 mg ml^{-1}. The day after, samples were rinsed with PBS to remove non internalized NPs and fixed with 4 % paraformaldehyde for 20 min under chemical fume hood. Then, cells were permeabilized with 0.1 % Triton 100 X in PBS for 10 min and the actin microfilament were stained with TRITC-phalloidin (Sigma) for 30 min at RT. Cell nuclei were stained with DAPI. Samples were observed by confocal and multiphoton microscope system (Leica TCS SP5 MP). Images acquired with a resolution of 1024X1024 pixels.

2.3.6. Nanoparticle uptake in conventional 2D culture

To evaluate the intracellular uptake of all kind of NPs, 4×10^4 cells were seeded in 1 ml of medium for each cell lines, in 24 well. NPs were dispersed in cell culture medium at final concentration of $2.1 * 10^{11}$ and $1.8 * 10^{10}$ NP ml^{-1}, for 0.04 and 0.1 µm PS NPs, $1.8 * 10^{10}$ and $1.83 * 10^{10}$ NP ml^{-1}, for -COOH and -NH$_2$ PS-NPs, respectively. Cells were incubated with NP suspension for 1, 3, 6, 9, 15 and 24 hours. After incubation, cells were rinsed two times with PBS and lysed with 0.1 ml of buffer composed of 4 % CHAPS, 7 M Urea, 2 M Thiourea and 30 nM Trizma, purchased by Sigma Aldrich, and 0.4 ml of PBS. Cell lysates were analyzed by a spectrofluorometer (Enspire 2300, Perkin-Elmer), to measure the amount of internalized NPs.

2.3.7. Nanoparticles uptake in 3D collagen matrix

For the uptake of PS NPs in 3D matrix, 4×10^4 cells were seeded in 0.5 ml of collagen in each well of 24 well. After fibrillogenesis, cells were exposed to $4.2 * 10^{11}$ and $3.6 * 10^{10}$ NP ml^{-1} for 0.04 and 0.1 µm PS-NPs, and $3.6 * 10^{10}$ and $3.66 * 10^{10}$, for -COOH and -NH$_2$ PS-NPs, respectively. Cells were incubated with NP suspension at the same times reported for NPs uptake in 2D. After each time, the collagen gels were digested by collagenase A (see above: *cell viability and proliferation* section). Cell lysates were analyzed by a spectrofluorometer (Enspire 2300, Perkin-Elmer).

2.3.8. Kinetics of nanoparticle uptake

In this work, NP uptake is viewed as a two-step process consisting of the non-specific binding (i.e. adsorption) of the NPs onto the cell surface and the subsequent cell internalisation. In particular, we consider that cells are initially free from NPs and, once at the cell surface, NPs can either be internalised or undergo de-binding (i.e. desorption). Therefore, NP uptake can be envisaged as a process driven by adsorption/desorption, followed by NP internalisation via energy-dependent pathways, and can be modelled by a modified second order binding equation, taking into account NP internalisation by a pseudo-chemical

equilibrium relation [33], described by the stoichiometric exchange between NPs and cell membrane, as follows:

$$NP + cell\ surface \xleftrightarrow{k_B, k_D} NP - cell\ surface \xrightarrow{k_i} NP\ internalis\,ation \tag{1}$$
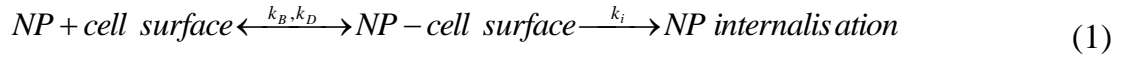
Equation (1) describes the overall NP uptake process consisting of NP binding to the cell surface followed either by NP de-binding or internalization. Here we assume that for each cell population and NP diameter, there exists a limiting capacity of binding and another, independent limiting capacity to internalise a cell surface on which NPs are attached. The binding capacity is a measure of the fraction of the cell membrane able to adsorb NPs (namely the reactive surface) [34-36], and was considered constant in time. This means that after each internalisation event, the reactive surface is continuously and instantaneously regenerated. In particular, the internalisation step occurs by creating an intracellular endosome after each NP is internalised.

Thus, the rate of overall NP uptake is defined by the balance between the rates of NP binding/de-binding and of cell internalisation, which are defined by the three corresponding kinetic rate coefficients, i.e. k_D [mg•mL^{-1}•h^{-1}], k_B [h^{-1}] and k_i [h^{-1}]. A modified version of the single cell model of particle interaction was used. The following equations describe the interactions of NPs with a single cell in terms of the number of particles bound/internalized *per* cell, and of the total number of particles (bound and internalised) as a function of time. The number of NPs bound on a cell *per* unit time is proportional to the concentration of NPs in the reservoir (culture medium in 2D or collagen in 3D). De-bound and internalised NPs, in turn, are proportional to the number of bound particles. Hence, the following equations can be written:

$$\frac{dN_B}{dt} = k_B C_{NP}^{medium}(N_{MAX} - N_B) - k_D N_B - \frac{dN_i}{dt} \tag{2}$$

$$\frac{dN_i}{dt} = k_i N_B \tag{3}$$

$$N_T = N_B + N_i \tag{4}$$

In each experiment 4 x 104 cells have been used, and 1 mL of culture medium or collagen employed. Under these conditions, experimental results showed that the C_{NP}^{medium} term could not be considered constant in all cases, due to extensive NP uptake. Therefore, in model equations the time variation of NP concentration within the culture medium, i.e. an important driving force of the process, was taken into account. In particular, NP concentration within the culture medium was modeled considering that the rate of NP disappearance in the culture medium was the opposite of the rate of the overall uptaken NPs (i.e. N_T).

$$\frac{dC_{NP}^{medium}}{dt} = -\frac{\pi d^3}{6} n_{cell} V_{medium} \rho_{NP} \left(\frac{dN_B}{dt} + \frac{dN_i}{dt} \right) \tag{5}$$

2.3.9. Scanning Electron Microscopy (SEM)
After 24 hours of incubation, with all type of PS-NPs at the same concentrations used for uptake experiments, 3D collagen matrix was rinsed two times with PBS and fixed with 2.5 % glutaraldehyde + 0.1 M cacodylate for 3 hours and dehydrated in increasing ethanol series (70 %, 80 %, 90 % and 100 %), then the samples were submitted for critical point (LEICA EM CPD300). The samples were platinum/palladium–sputtered and analyzed by SEM (Leica S400).

2.3.10. PS-NPs diffusion in collagen matrix
Permeability experiments of NPs were performed using transwell permeable inserts (6.5 mm in diameter, 3 μm pores size; Corning Incorporated, Corning, NY). The times of kinetics were the same used for NP uptake. For 2D experiments, 0.1 ml of cell culture medium w/o phenol red containing the right

NP concentrations were added to donor chamber; while the acceptor chamber was filled with 0.4 ml fresh cell culture medium. For 3D experiments, the medium with NPs were added after collagen fibrillation. After each time, the donor chamber was shifted to new acceptor chamber with the same amount of fresh medium. The fluorescence tracer concentration in the samples was determined by a spectrophotometric analysis (Enspire 2300, Perkin-Elmer). The results were reported as percentage of transported NPs.

2.4. RESULTS AND DISCUSSION

2.4.1. Cell viability and proliferation

To assess cell viability and proliferation within 3D collagen matrix, Pico Green assay was carried out (**Fig. 1A**). The equal number of cancer and non-cancer cells was embedded and grown within the matrix until one week. It was observed that, for both cell lines, the proliferation rate was not in any way hindered in our 3D environment. Conversely, the cells were grown in optimal condition for all biological activities, such as in traditional 2D cell culture. In particular, the HDF proliferation rate was slower compared to HT1080 proliferation rate already from 24 hours in both conditions.
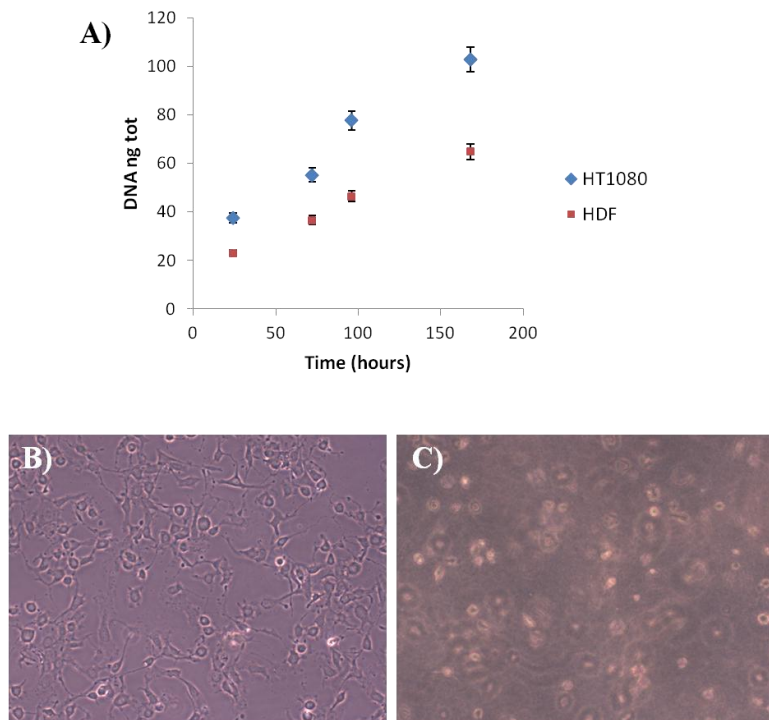
Figure 5. *Cell behaviour and morphology in 3D collagen matrix. A) Proliferation rate of HDF and HT1080 cell lines followed for 7 days, in 3D collagen matrix obtained by DNA quantification (PicoGreen assay); Optical microscope images of HT1080 cells after 24 h of growth in 2D culture dish (B) and 3D collagen matrix (C). Objective 10X.*

Indeed, the cancer cells were distinguished from normal cells by abnormal activities, such as unlimited replication, proliferation and reproducing follow by tissue invasion and related metastasis, sustained angiogenesis, insensitivity to antigrowth signals [37, 38]. Furthermore, it is important to underline that cell

morphology changed when cells were grown in a more natural environment. In particular, HT1080 adopted more rounded shaped within collagen matrix compared to flat morphology typical of conventional systems (**Fig. 1B-C**). This change in cell morphology can reflect a different cytoskeleton organization between 2D and 3D systems [39, 40].

2.4.2. Nanoparticle characterization

Fluorescently PS-NPs were dispersed in phosphate buffer saline in order to determine nanoparticle size, polydispersivity and ζ-potential by dynamic light scattering (DLS). The DLS measurements showed that PS-NPs had a good stability and monodispersion in PBS solution, while the ζ-potential reflected the positive surface charge related to the presence of amine groups, and the negative charge due to the carboxyl groups (**Table 1**). All properties of PS-NPs, measured by DLS analysis, were consistent with their theoretical features.

	44 PS-NPs	100 PS-NPs	NH$_2$ PS-NPs	COOH PS-NPs
Size [nm ± SD]*	43.67 ± 1.08	106.70 ± 5.35	102.46 ± 0.13	110.32 ± 0.12
ζ-potential [mV ± SD]	-25.25 ± 5.26	-21.97 ± 2.11	+41.72 ± 2.18	-40.42 ± 1.39

*PDI < 0.1

Table 1. *Measurements of size and ζ-potential of all PS-NPs by dynamic light scattering.*

2.4.3. Nanoparticles uptake

To investigate NPs internalization, HDF and HT1080 cell lines were exposed to all PS-NPs in both 2D and 3D culture conditions. The confocal images of HT1080 cells, in traditional 2D system, showed that NPs entered the cells and their number increased in time, as indicated by fluorescence intensity enhancement (**Fig. 2**).
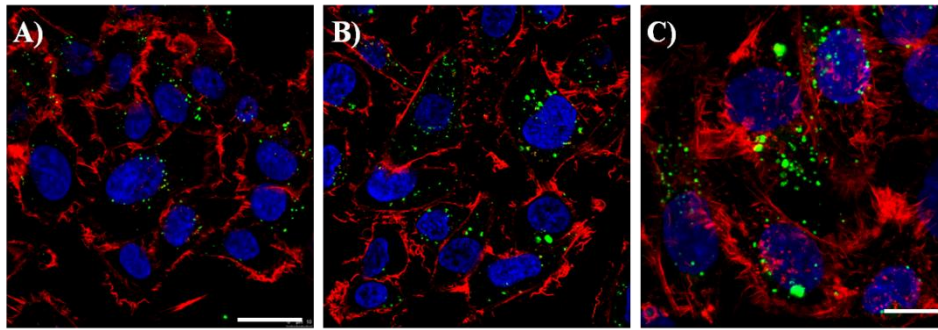
Figure 2. *Confocal image of HT1080 cells incubated at 37 °C with 44-NPs for 1 h (a), 6 h (b) and 24 h (c). Different colors are applied to improve visualization: nuclei (DAPI) are shown in blue; actin filaments (phalloidin) in red; nanoparticles in green. Scale bar: 10 μm.*

In addition, as shown in **Fig. 3**, all PS-NPs were efficiently internalized by cancer cells after 24 hours of incubation.
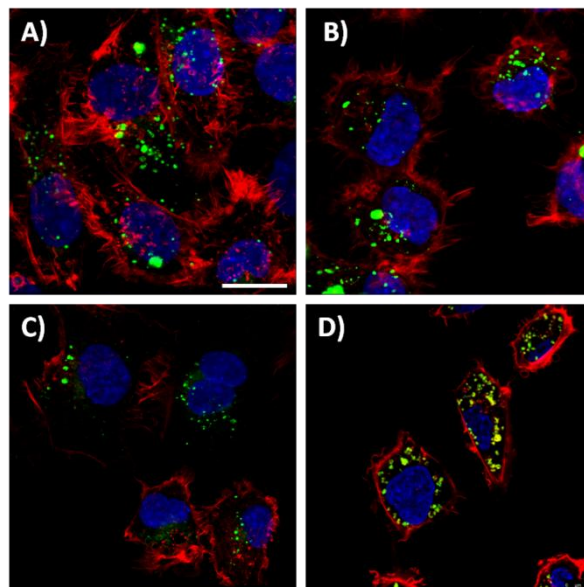
Figure 3. *Confocal image of HT1080 cells incubated for 24 h with 44-NPs (a), 100-NPs (b), COOH-NPs (c) and NH$_2$-NPs. Different colors are applied to improve visualization: nuclei (DAPI) are shown in blue; actin filaments (phalloidin) in red; nanoparticles in green. Scale bar: 10 μm.*

On the other hand, confocal images of HDF cell line also confirmed the presence of all kind of particles, used in this work, within fibroblats after 24 hours of incubation (**Fig. 4**).
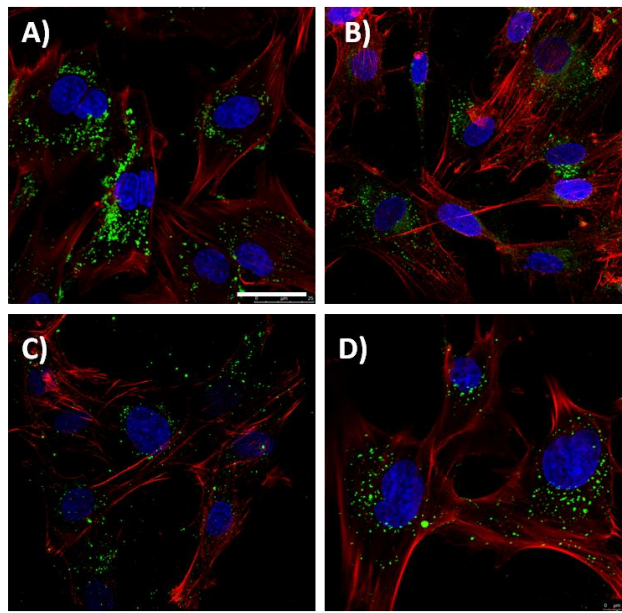
Figure 4. *Confocal image of HDF cells incubated for 24 h with 44-NPs (a), 100-NPs (b), COOH-NPs (c) and NH$_2$-NPs. Different colors are applied to improve visualization: nuclei (DAPI) are shown in blue; actin filaments (phalloidin) in red; nanoparticles in green. Scale bar: 10 μm.*

Moreover, apparently the amount of PS-NPs internalized by cells seems to be higher for HT1080 compared to healthy cells, probably due to a different cytoskeletal organization between cancer and non cancer cells (**Fig. 5**). Indeed, Swartz *et al* demonstrated that a malignant phenotype of HT1080 cells induced profound change in cytoskeleton structure, including rounding shape and diffuse myosin expression [40].
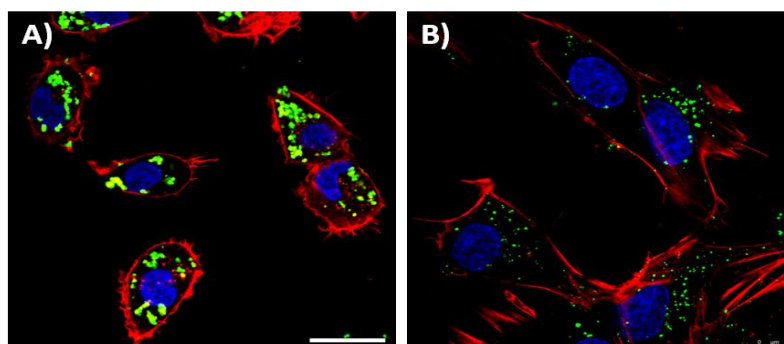
Figure 5. *Confocal images of HT180 cells (a) and HDF cells (b) after 24 hours of incubation with 100-NPs. Different colors are applied to improve visualization: nuclei (DAPI) are shown in blue; actin filaments (phalloidin) in red; nanoparticles in green. Scale bar: 10 μm.*

Noteworthy, in both cell types the NPs were distributed in the cytoplasm, mainly localized around the nucleus. Also, the confocal z-sectioning of HT1080 cells embedded in 3D collagen matrix confirmed the NP distribution observed for confocal images acquired in 2D cell culture conditions (**Fig. 6**). Apparently, uptaken NPs by cells were higher for 2D compared to 3D matrix, as shown in **Fig. 6** with the compressed z-stack as the central image and projection through the z-plane along the red line in the x- and y- directions given as the sidebars.

These qualitative results were confirmed by quantification of uptaken NPs, exploiting dye-loaded inside the particles, through spectrophotometric analysis. The amount of internalized NPs was quantified on a number of NPs *per* cell basis. In the framework of this work, NP uptake is considered to be governed by the balance between NP adhesion to the external cell membrane and NP actual internalization [34]. In particular, during the initial transient state, NPs adhere to the cells, but the process of internalization is still slow. At the pseudo-steady state, the number of NPs bound to the cell surface equals the number of NPs being internalised, which is consistent with a linear uptake. This view suggests that NP uptake is predominantly determined by NP binding/adsorption to the external cell membrane. The adhesion properties of NPs to the cell membrane are difficult to distinguish when internalisation events are simultaneously occurring. Indeed, NP binding to cell membrane is normally quantified by incubating the cells with NP at 4 °C, so as to inhibit internalisation phenomena and estimate the number of particles adsorbed [34, 41-43]. However, this is cumbersome to carry out in a 3D system. Furthermore, for prolonged times of incubation, in some papers desorption phenomena were observed, and this makes the distinction between adsorbed and internalised NPs unreliable and probably meaningless in the experimental conditions used in this work.
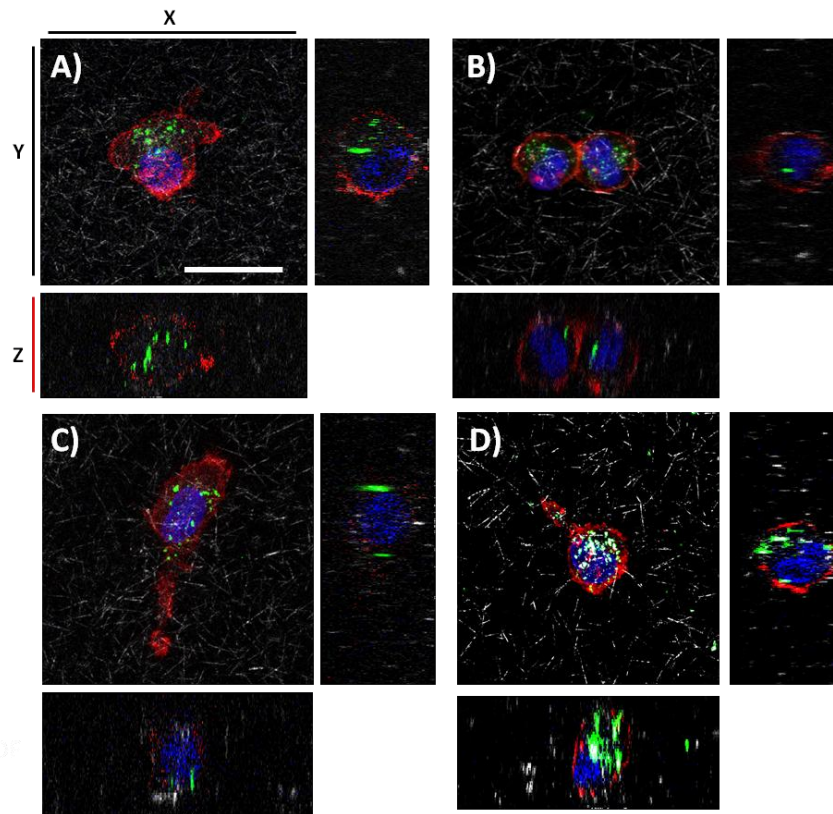
Figure 6. *Confocal z-sectioning images of HT1080 cells incubated with a) 44-NPs b) 100-NPs c) NH$_2$-NPs d) COOH-NPs in 3D collagen matrix for 24 hours. Nuclei: blue; TRITC: phalloidin; Green: NPs; Transmission: collagen. Obj 63 X oil. Magnification bar: 10 µm.*

Therefore, the uptake experiments were all performed at 37 °C without discriminating between bound and internalized NPs. The uptake kinetics of PS-NPs, COOH-NPs and NH$_2$-NPs by HDF and HT1080 cells, together with the results of numerical simulations, are shown in **Figs**. **7** and **8**. Under all culture conditions, and for each NP type and size, the uptake kinetics exhibited a qualitatively similar behaviour with an initial faster transient followed by a sort of quasi-linear uptake in the experimental time frame of this work (48 h). As for PS NPs, results showed that the uptake was higher in the case of HT1080 cells compared to HDF cells. The number of uptaken NPs was shown to depend on particle size, surface functionalization and culture model and, in all cases, was steadily increased with time and, specifically, higher for 44 nm NPs than for 100 nm. The uptake saturation was not reached within 48 h, and this was the most

evident in the case of HDF cells cultured with 44 nm NPs. Highest levels of uptake were observed for 44 nm, in 2D conditions and for HT1080 cells. In particular, size effect was found out to be mostly predominant for three dimensional collagen scaffolds in whose twisted network NPs with small diameter diffused much better than bigger ones. In fact, increasing NP size, a slight decrease of NPs internalized was observed.
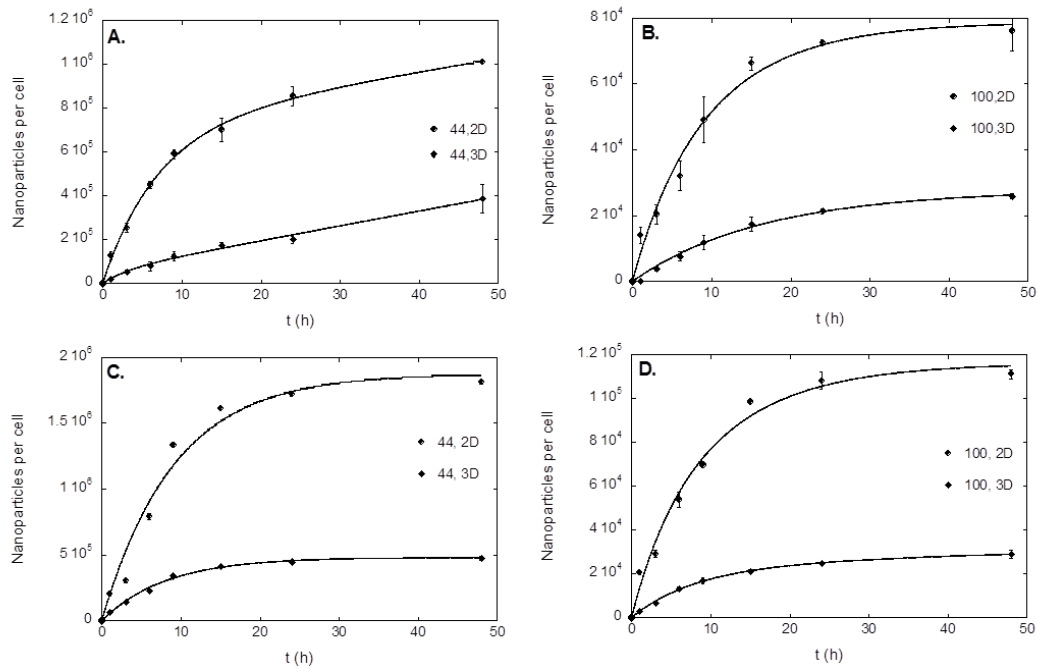
Figure 7. *Kinetics of uptake of fluorescently labeled 44 and 100 nm NPs by HDF (A, B) and HT1080 cells (C, D) during continuous exposure, as determined by spectrophotometric analysis Cells were exposed to NPs in both 2D [$2.1*10^{11}$ and $1.8*10^{10}$ for 44 and 100-NPs, respectively] and 3D conditions [$4.2*10^{11}$ and $3.6*10^{10}$ for 44 and 100-NPs, respectively]. The mean cell fluorescence of 4 x 10^4 cells was determined for each repeat. Data points and error bars represent the mean and standard deviation over three replicas. The solid lines represent results obtained by data fitting.*

Furthermore, for prolonged times of incubation, we have also observed desorption phenomena, which also contributes to the meaninglessness of the discrimination between adsorbed and internalised NPs. The lower uptake in 3D can be easily related to the tight contact established between NPs and collagen fibers, which occurs during diffusion in 3D complex, before NPs reach cells. Indeed, all other conditions being equal, the 48 h uptake of 44 nm NPs was 13-16 times higher compared to the uptake of 100 nm NPs. However, it should be taken

into account that the uptake of NPs did not reach a plateau in the timeframe of cell culture used in this work. The values of N_{MAX}, calculated by fitting uptake kinetics data to equations (1)-(4), suggest that the uptake of 44 nm PS NPs after an infinite time is from 6 to 166 times higher compared to N_{MAX} of 100 nm NPs (**Table 2**). Therefore, the number of uptaken NPs increased significantly with decreasing particle size for both cell lines on both culture conditions, i.e. the cells have a higher uptake capacity for the smaller particles. Overall, PS NP uptake was lower on 3D versus 2D substrates as shown in **Fig. 7** and **8**. For both NP sizes the uptake was 3- and 4- fold higher for HDF and HT1080 cells, respectively. A similar comparison on N_{MAX} shows that the decrease in uptake of NPs in 3D versus 2D culture conditions is mainly influenced smaller NP size and for HT1080 rather than HDF cells. The rate coefficients for binding (K_B), de-binding (K_D) and internalisation (K_i) versus size/cell line and culture conditions (2D and 3D) are summarised in **Table 2**.
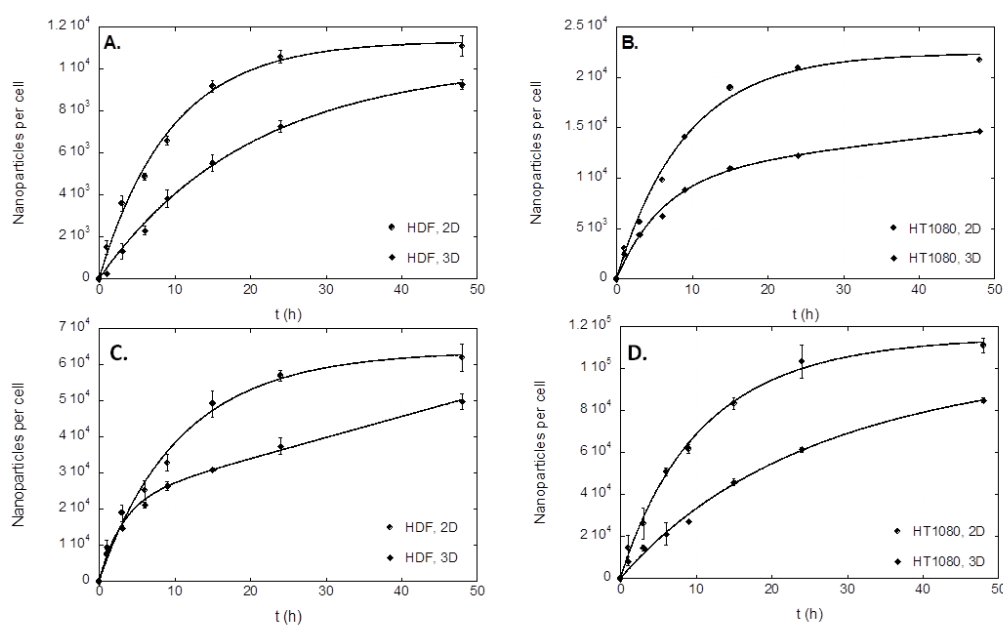
Figura 8. *Kinetics of uptake of fluorescently labeled 100 nm COOH-NPs and 100 nm NH$_2$-NPs by HDF (A-C) and HT1080 cells (B-C) during continuous exposure, as determined by spectrophotometric analysis. Cells were exposed to NPs in both 2D [$1.8*10^{10}$ and $1.83*10^{10}$ for COOH and NH$_2$-NPs, respectively] and 3D conditions [$3.6*10^{10}$ and $3.66*10^{10}$ for COOH and NH$_2$-NPs]. The mean cell fluorescence of 4×10^4 cells was determined for each repeat. Data points and error bars represent the mean and standard deviation over three replicas. The solid lines represent results obtained by data fitting.*

The adsorption rate coefficient, K_B is higher for the 2D culture system in the case of 100 nm NPs, while it is higher for the 3D culture for 44 nm diameter particles, which have a 2.1-4.8 fold change for 3D over 2D as for HDF and HT1080 cells, respectively. In the case of 100 nm NPs, K_B is 1.8 and 2.6-fold higher for 2D versus 3D-grown HDF/HT1080 cells. The other rate coefficients randomly vary with NP size, culture conditions and cell line. The COOH-NPs showed a drastically lower uptake compared to the PS-NP, in both cell culture conditions (**Fig. 8**). In particular, we found that the uptake in 2D was 5-6 fold less than in 2D and about 2-2.5 times lower in 3D. When passing from 2D to 3D, however, there was a slighter uptake reduction compared to what happened when using PS-NPs. Conversely, NH_2-NPs displayed a peculiar behavior: indeed, in 2D the uptake was only slightly lower in the case of HDF cells, while being basically the same for HT1080 cells. Surprisingly, in 3D a strong increase in uptake was found out. In particular, depending on the cells population, NP increase of NH_2-NPs was 2-4 fold higher compared to bare PS-NPs (**Fig. 8**).

A)

Cell line	Size [nm]		k_B [mg·mL⁻¹·h⁻¹]	N_{max}	k_D [h⁻¹]	k_i [h⁻¹]
HDF	44	2D	7.52	1.48×10^6	5.20×10^{-2}	8.71×10^{-3}
		3D	16.1	1.50×10^5	5.01×10^{-2}	8.55×10^{-2}
	100	2D	11.3	7.88×10^4	-5.04×10^{-10}	3.52×10^{-7}
		3D	6.33	2.69×10^6	-2.19×10^{-3}	2.67×10^{-8}
HT1080	44	2D	0.968	2.14×10^7	6.53×10^{-2}	1.02×10^{-5}
		3D	4.69	1.28×10^6	7.05×10^{-2}	3.00×10^{-7}
	100	2D	10.9	1.28×10^5	8.46×10^{-3}	1.21×10^{-9}
		3D	4.17	7.09×10^4	6.96×10^{-2}	4.78×10^{-3}

B)

Cell line		K_B [mg·mL⁻¹·h⁻¹]	N_{MAX}	K_D [h⁻¹]	K_i [h⁻¹]
HDF	2D	10.6	1.13×10^4	2.60×10^{-10}	2.29×10^{-9}
	3D	4.98	1.03×10^4	7.77×10^{-10}	2.86×10^{-10}
HT1080	2D	11.1	2.24×10^4	3.53×10^{-10}	3.69×10^{-10}
	3D	15.2	1.15×10^4	6.79×10^{-9}	8.01×10^{-3}

C)

Cell line		K_B [mg·mL⁻¹·h⁻¹]	N_{MAX}	K_D [h⁻¹]	K_i [h⁻¹]
HDF	2D	9.55	6.41×10^4	5.72×10^{-4}	1.31×10^{-8}
	3D	30.5	2.61×10^4	2.83×10^{-8}	2.44×10^{-2}
HT1080	2D	9.91	1.15×10^5	1.07×10^{-12}	3.28×10^{-9}
	3D	4.05	1.03×10^5	6.26×10^{-10}	7.27×10^{-4}

Table 2. *Model parameters of 44-NPs and 100 NPs (a); COOH-NPs (b); NH_2-NPs.*

2.4.4. PS-NPs diffusion in collagen matrix and scanning electron microscopy

The cellular uptake results obtained regarding anionic particles in 3D matrix suggested the existence of possible interactions among several collagen components and carboxyl groups upon the surface of the negative NPs. Indeed, images acquired by scanning electron microscopy showed that COOH-NPs interacted with collagen fibers, generating cluster structures as shown in **Fig. 9E**. Conversely, NH_2-NPs slipped among the network of fibers without absorbing on their surfaces (**Fig. 9D**). Furthermore, only few nanoparticles of 44 and 100 nm interacted with fibers (**Fig. 9B-C**).
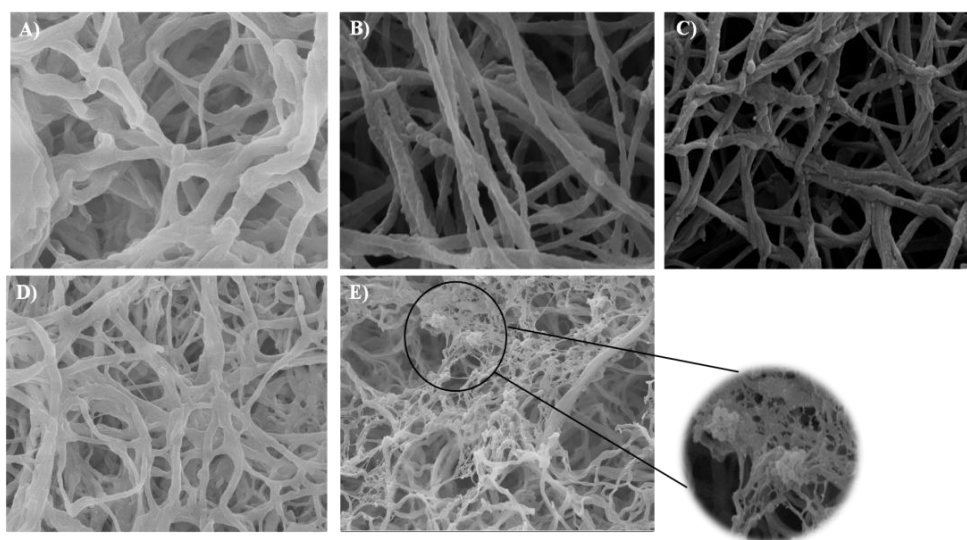
Figure 9. *Scanning electron microscopy images of all PS-NPs in 3D collagen matrix after 24 hours of incubation. A) Collagen without PS-NPs, used as control; B) with 44 nm PS-NPs; C) with 100 nm PS-NPs; D) with 100 nm NH_2-NPs; E) with 100 nm COOH-NPs. Bare scale: 0.2 μm.*

Hence, for better understanding NP behaviour in collagen matrices, permeability experiments using transwell permeable insert were performed. This system is composed by a donor and acceptor chamber separated by a membrane pore filter and has allowed to study NP diffusion crossing collagen gel. The same experiments are followed in transwell without collagen scaffold to rule out that membrane pore filter could hinder NP diffusion (data not shown). Results were expressed as percentage of NP transported in function of time. Data showed that the smaller particles diffused without any apparent hindrance in the collagen

matrix, as shown also in **Fig**. **10**, where reached a plateau already to 6 hours. The same results were registered for cationic NPs in which the total amount of NPs crossed the scaffold in few hours. Conversely, the percentage of COOH-NPs that passed through the 3D matrix in 24 hours was very low, since just the 27 % was measured in the acceptor chamber. These results suggested the possibility of interactions between negative NPs and collagen fibers that could hinder the NP ability to diffuse within matrix (**Fig**. 7). As regarding, the neutral 100-NPs showed an intermediate behaviour, where the total amount of NPs that crossing the matrix run out within 15 hours.
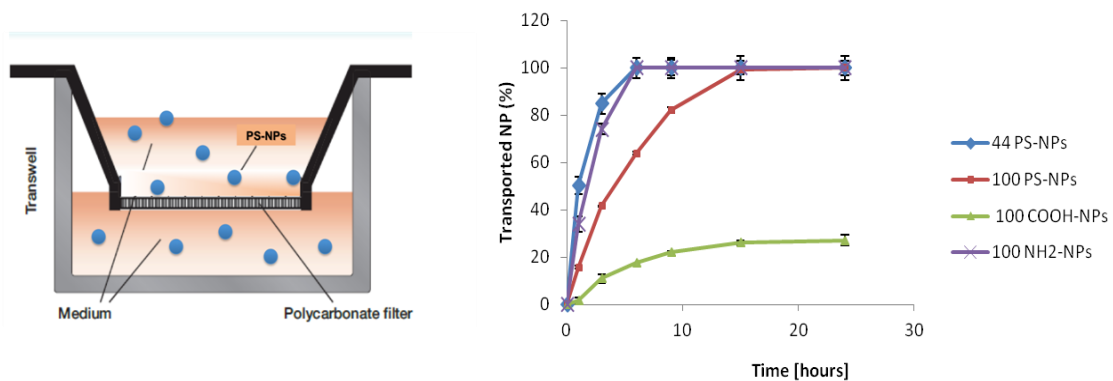
Figure 10. *Diffusion study of PS-NPs using transwell permeable inserts until 24 hours.*

Taken all together, these results demonstrated that surface features, due to the charge of NPs in contact with ECM components, play a crucial role on their diffusion in 3D matrix and consequently in cellular uptake. Indeed, we showed that a large amount of anionic NPs interacted with ECM components and remained attached on the surface of collagen fibers. This effect could suggest that, in our experimental conditions, collagen gel could take a slight positive charge, generating attractive electrostatic interactions with the COOH-NPs. Nevertheless, further investigations are necessary to clarify which relationships are established among ECM molecules and surface of charged NPs.

2.5. CONCLUSIONS

Three-dimensional gel matrices provide the opportunity to reproduce natural microenvironments that mimic the native tissues where essential cell activities are regulated, such as proliferation, adhesion and differentiation. In this more complex framework, also cellular responses to particles, in term of NP uptake could drastically change. This point is of extreme relevance, in particular for biomedical fields, since also NP properties can influence their diffusion in 3D environment and to generate cellular response quite different from that expected. In this work, we demonstrated that all NP properties are crucial to crossing the matrix. First, NP diameter showed to be a crucial parameter in fact 44-NPs diffused better in 3D matrix and consequently their cellular uptake was massive. Importantly, the amount of NPs observed within cancer cells was higher compared to healthy cells. This effect can be attributed to a different cytoskeleton organization between cancer and non-cancer cells. Swartz *et al* demonstrated that a malignant phenotype of HT1080 cells induces profound change in cytoskeleton structure, including pronounced rounding and diffuse myosin expression also in 3D system [40]. Moreover, recent data suggested that myosin VI plays a role in clathrin-coated vesicle formation and the trafficking of uncoated nascent vesicles. It is likely that in both processes, myosin VI plays an accessory role, perhaps increasing the efficiency of endocytosis [44]. In agreement with our results, these data could explain the greater NP uptake in tumor cells. In addition, increasing NP size a decrement of uptaken NPs was detected in both 2D and 3D conditions. The results can be attributed not only at the bigger size, but mainly to the surface charge of NPs. Indeed, the surface functionalization of nanoparticles is crucial for the durability, suspensibility in biological media, biocompability and biodistribution [45, 46]. We demonstrated that positive charge on surface of NPs allowed them to be internalized into cells in greater numbers compared to negative one, in both 2D and 3D systems. This effect was mainly due to the positive charge that improves their diffusion in collagen matrix and increases the cell surface affinity and uptake in both cell lines. This phenomenon may be

caused by electrostatic interactions with the net negative surface charge of plasma membrane that favour NH_2-NP uptake [47, 48]. In addition, independently from NP size or surface charge, their uptake in both cell lines was lower in 3D collagen matrix compared to 2D cell culture systems. The reasons to explain this behaviour can be manifolds. First, the path that particles must follow to reach cells in a three-dimensional matrix is longer compared to that observed in 2D systems. Indeed, the cell arrangement on monolayers makes them most available for NP uptake. Second, cell morphology in 3D condition was drastically changed compared to 2D system, in particular way for HT1080 cell line that adopted a shape relatively more rounded in collagen matrix [40]. Furthermore, the difference in cell morphology reflected the different cytoskeletal organization within cells, as observed in previous works with other cells grown in 3D matrix. Indeed, some studies demonstrated that the organization of actin' microfilaments and stability of microtubules was drastically different compared to 2D system [49, 50]. These distinct organizations could influence not only cellular activity, such as mobility and migration, but also the amount of NPs that cells are able to internalize. In this view, further investigations are necessary to define if the molecular expression of several proteins involved in active endocytosis mechanisms could be altered when moving to three-dimensional systems.

2.6. REFERENCES

1. Froehlich, E., *The role of surface charge in cellular uptake and cytotoxicity of medical nanoparticles.* International Journal of Nanomedicine, 2012. **7**: p. 5577-5591.
2. Reix, N., et al., *In vitro uptake evaluation in Caco-2 cells and in vivo results in diabetic rats of insulin-loaded PLGA nanoparticles.* International Journal of Pharmaceutics, 2012. **437**(1-2): p. 213-220.
3. Sethi, M., et al., *Effect of drug release kinetics on nanoparticle therapeutic efficacy and toxicity.* Nanoscale, 2014. **6**(4): p. 2321-2327.
4. Pan, J., Y. Liu, and S.-S. Feng, *Multifunctional nanoparticles of biodegradable copolymer blend for cancer diagnosis and treatment.* Nanomedicine, 2010. **5**(3): p. 347-360.
5. Noguera, R., et al., *Extracellular matrix, biotensegrity and tumor microenvironment. An update and overview.* Histology and Histopathology, 2012. **27**(6): p. 693-705.
6. Bosman, F.T. and I. Stamenkovic, *Functional structure and composition of the extracellular matrix.* Journal of Pathology, 2003. **200**(4): p. 423-428.
7. Maquart, F.X. and J.C. Monboisse, *Extracellular matrix and wound healing.* Pathologie Biologie, (0).
8. Owen, S.C. and M.S. Shoichet, *Design of three-dimensional biomimetic scaffolds.* Journal of Biomedical Materials Research Part A, 2010. **94A**(4): p. 1321-1331.
9. Harjanto, D. and M.H. Zaman, *Modeling Extracellular Matrix Reorganization in 3D Environments.* Plos One, 2013. **8**(1).
10. Stylianopoulos, T., et al., *Diffusion Anisotropy in Collagen Gels and Tumors: The Effect of Fiber Network Orientation.* Biophysical Journal, 2010. **99**(10): p. 3119-3128.
11. Stylianopoulos, T., et al., *Diffusion of Particles in the Extracellular Matrix: The Effect of Repulsive Electrostatic Interactions.* Biophysical Journal, 2010. **99**(5): p. 1342-1349.
12. Chithrani, B.D., A.A. Ghazani, and W.C.W. Chan, *Determining the size and shape dependence of gold nanoparticle uptake into mammalian cells.* Nano Letters, 2006. **6**(4): p. 662-668.
13. Jiang, W., et al., *Nanoparticle-mediated cellular response is size-dependent.* Nature Nanotechnology, 2008. **3**(3): p. 145-150.
14. Cartiera, M.S., et al., *The uptake and intracellular fate of PLGA nanoparticles in epithelial cells.* Biomaterials, 2009. **30**(14): p. 2790-2798.
15. Lunov, O., et al., *Differential Uptake of Functionalized Polystyrene Nanoparticles by Human Macrophages and a Monocytic Cell Line.* Acs Nano, 2011. **5**(3): p. 1657-1669.
16. Rancan, F., et al., *Skin Penetration and Cellular Uptake of Amorphous Silica Nanoparticles with Variable Size, Surface Functionalization, and Colloidal Stability.* Acs Nano, 2012. **6**(8): p. 6829-6842.
17. Jain, R.K., *TRANSPORT OF MOLECULES IN THE TUMOR INTERSTITIUM - A REVIEW.* Cancer Research, 1987. **47**(12): p. 3039-3051.
18. Ramanujan, S., et al., *Diffusion and convection in collagen gels: Implications for transport in the tumor interstitium.* Biophysical Journal, 2002. **83**(3): p. 1650-1660.

19. Verma, A. and F. Stellacci, *Effect of Surface Properties on Nanoparticle-Cell Interactions.* Small, 2010. **6**(1): p. 12-21.

20. Kettler, K., et al., *Cellular uptake of nanoparticles as determined by particle properties, experimental conditions, and cell type.* Environmental Toxicology and Chemistry, 2014. **33**(3): p. 481-492.

21. Albanese, A., P.S. Tang, and W.C.W. Chan, *The Effect of Nanoparticle Size, Shape, and Surface Chemistry on Biological Systems.* Annual Review of Biomedical Engineering, Vol 14, 2012. **14**: p. 1-16.

22. Biondi, M., et al., *Sub-100 nm biodegradable nanoparticles: in vitro release features and toxicity testing in 2D and 3D cell cultures.* Nanotechnology, 2013. **24**(4).

23. Hu, Q., et al., *Glioma therapy using tumor homing and penetrating peptide-functionalized PEG-PLA nanoparticles loaded with paclitaxel.* Biomaterials, 2013. **34**(22): p. 5640-5650.

24. El-Dakdouki, M.H., E. Pure, and X. Huang, *Development of drug loaded nanoparticles for tumor targeting. Part 2: Enhancement of tumor penetration through receptor mediated transcytosis in 3D tumor models.* Nanoscale, 2013. **5**(9): p. 3904-3911.

25. Sagnella, S.M., et al., *Dextran-Based Doxorubicin Nanocarriers with Improved Tumor Penetration.* Biomacromolecules, 2014. **15**(1): p. 262-275.

26. Goodman, T.T., P.L. Olive, and S.H. Pun, *Increased nanoparticle penetration in collagenase-treated multicellullar spheroids.* International Journal of Nanomedicine, 2007. **2**(2): p. 265-274.

27. Dormann, S. and A. Deutsch, *Modeling of self-organized avascular tumor growth with a hybrid cellular automaton.* In silico biology, 2002. **2**(3): p. 393-406.

28. Chevallay, B. and D. Herbage, *Collagen-based biomaterials as 3D scaffold for cell cultures: applications for tissue engineering and gene therapy.* Medical & Biological Engineering & Computing, 2000. **38**(2): p. 211-218.

29. Guarnieri, D., et al., *Effects of fibronectin and laminin on structural, mechanical and transport properties of 3D collageneous network.* Journal of Materials Science-Materials in Medicine, 2007. **18**(2): p. 245-253.

30. Tibbitt, M.W. and K.S. Anseth, *Hydrogels as Extracellular Matrix Mimics for 3D Cell Culture.* Biotechnology and Bioengineering, 2009. **103**(4): p. 655-663.

31. Carletti, E., A. Motta, and C. Migliaresi, *Scaffolds for Tissue Engineering and 3D Cell Culture*, in *3d Cell Culture: Methods and Protocols*, J.W. Haycock, Editor. 2011. p. 17-39.

32. Grinnell, F. and W.M. Petroll, *Cell Motility and Mechanics in Three-Dimensional Collagen Matrices*, in *Annual Review of Cell and Developmental Biology, Vol 26*, R. Schekman, L. Goldstein, and R. Lehmann, Editors. 2010. p. 335-361.

33. Biondi, M., et al., *Investigation of the mechanisms governing doxorubicin and irinotecan release from drug-eluting beads: mathematical modeling and experimental verification.* Journal of Materials Science-Materials in Medicine, 2013. **24**(10): p. 2359-2370.

34. Wilhelm, C., et al., *Interaction of anionic superparamagnetic nanoparticles with cells: Kinetic analyses of membrane adsorption and subsequent internalization.* Langmuir, 2002. **18**(21): p. 8148-8155.

35. Doiron, A.L., B. Clark, and K.D. Rinker, *Endothelial Nanoparticle Binding Kinetics are Matrix and Size Dependent.* Biotechnology and Bioengineering, 2011. **108**(12): p. 2988-2998.

36. Lesniak, A., et al., *Nanoparticle Adhesion to the Cell Membrane and Its Effect on Nanoparticle Uptake Efficiency.* Journal of the American Chemical Society, 2013. **135**(4): p. 1438-1444.

37. Box, C., et al., *Tumour-microenvironmental interactions: paths to progression and targets for treatment.* Seminars in Cancer Biology, 2010. **20**(3): p. 128-138.

38. Friedl, P. and S. Alexander, *Cancer Invasion and the Microenvironment: Plasticity and Reciprocity.* Cell, 2011. **147**(5): p. 992-1009.

39. Geraldo, S., A. Simon, and D.M. Vignjevic, *Revealing the Cytoskeletal Organization of Invasive Cancer Cells in 3D.* Journal of visualized experiments : JoVE, 2013(80).

40. Schwartz, M.P., et al., *A Quantitative Comparison of Human HT-1080 Fibrosarcoma Cells and Primary Human Dermal Fibroblasts Identifies a 3D Migration Mechanism with Properties Unique to the Transformed Phenotype.* Plos One, 2013. **8**(12).

41. Salvati, A., et al., *Experimental and theoretical comparison of intracellular import of polymeric nanoparticles and small molecules: toward models of uptake kinetics.* Nanomedicine-Nanotechnology Biology and Medicine, 2011. **7**(6): p. 818-826.

42. Shapero, K., et al., *Time and space resolved uptake study of silica nanoparticles by human cells.* Molecular Biosystems, 2011. **7**(2): p. 371-378.

43. Safi, M., et al., *The effects of aggregation and protein corona on the cellular internalization of iron oxide nanoparticles.* Biomaterials, 2011. **32**(35): p. 9353-9363.

44. Hasson, T., *Myosin VI: two distinct roles in endocytosis.* Journal of Cell Science, 2003. **116**(17): p. 3453-3461.

45. Nel, A.E., et al., *Understanding biophysicochemical interactions at the nano-bio interface.* Nature Materials, 2009. **8**(7): p. 543-557.

46. Monopoli, M.P., et al., *Biomolecular coronas provide the biological identity of nanosized materials.* Nature Nanotechnology, 2012. **7**(12): p. 779-786.

47. Lorenz, M.R., et al., *Uptake of functionalized, fluorescent-labeled polymeric particles in different cell lines and stem cells.* Biomaterials, 2006. **27**(14): p. 2820-2828.

48. Shin, E.H., et al., *Membrane potential mediates the cellular binding of nanoparticles.* Nanoscale, 2013. **5**(13): p. 5879-5886.

49. Martins, G.G. and J. Kolega, *A role for microtubules in endothelial cell protrusion in three-dimensional matrices.* Biology of the Cell, 2012. **104**(5): p. 271-286.

50. Belletti, B., et al., *p27(kip1) Controls Cell Morphology and Motility by Regulating Microtubule-Dependent Lipid Raft Recycling.* Molecular and Cellular Biology, 2010. **30**(9): p. 2229-2240.

CHAPTER 3

In vitro release features and cytotoxicity assays in 2D and 3D cell culture of sub-100 nm PELGA nanoparticles loaded with doxorubicin

3.1. ABSTRACT

A big challenge in tumor targeting by nanoparticles (NPs), taking advantage of the enhanced permeability and retention effect, is the fabrication of small size carriers for enhanced diffusion and penetration in tumor, which is considered fundamental to improve chemotherapy efficacy. The purposes of this study are (i) to prepare the formulation of doxorubicin-loaded poly(D,L-lactic-co-glycolic acid) (PLGA)–block–poly(ethylene glycol) (PEG) NPs to obtain <100 nm carriers, and (ii) to translate standard 2D cytotoxicity studies to 3D collagen systems in which an initial step gradient of the NPs is present. Indeed, the study of NP mediated drug delivery in a 3D *in vitro* model would resemble a more realistic estimate of drug efficiency before the *in vivo* tests. The release of doxorubicin can be prolonged for days to weeks depending on the NP formulation and the pH of the release medium. Moreover, Dox-loaded PELGA NPs were characterized for size distribution, ζ –potential and release kinetics at the pH physiological milieu, of the tumor ECM and lysosomes. The effect of the formulation on the uptake and cytotoxicity was investigated in HeLa and IGROV-1 cells, which are used as *in vitro* models of human cervix carcinoma and ovarian adenocarcinoma, respectively. The results showed that smaller NPs than 100 nm are effectively internalized by HeLa cells in 2D and are less cytotoxic compared to free doxorubicin. In 3D, < 100 nm NPs are significantly more toxic than larger ones towards HeLa cells, and the cell death rate is affected by the contributions of drug release and device transport through collagen. Thus, the reduction of NP size is a fundamental feature from both a technological and a

biological point of view and must be properly engineered to optimize the tumor response to the NPs.

3.2. INTRODUCTION

Nanoparticles (NPs) have received great attention as carriers in cancer therapy since nanocarrier-mediated drug delivery (i) enhances the antitumor efficacy of many chemotherapeutic drugs, (ii) helps to reduce unwanted drug-related side effects, and (iii) limits the effects of multi-drug resistance (MDR) by evading drug efflux pumps, whereas intracellular drug concentration can be increased [1-3]. Furthermore, NPs can guide the drug preferentially to tumor cells and tissues by taking advantage of NP active and/or passive targeting [4-7]. Passive targeting generally refers to the well-known enhanced permeability and retention (EPR) effect [8-11], which is promoted when NPs possess a hydrophilic surface, a quasi-neutral ζ-potential [12] and a controlled size of approximately 70–200 nm [13-16]. In particular, size reduction positively affects carrier extravasation, penetration depth and cell uptake [17, 18], depending on the properties of both the biological environment (density, distribution, aggregation and size of vascular fenestrae) and the NPs (shape and surface charge) [10, 17-22].

The efficacy of anticancer drugs and NPs is often tested in 2D cell cultures, but drug efficacy *in vivo* is generally lower, and this difference is partly due to the 3D nature of tumor tissue. In fact, cells grown in 3D have totally different behaviors, in terms of cell surface receptor expression and proliferation [23, 24], extracellular matrix (ECM) synthesis [25] and metabolic functions [26]. This discrepancy has been suggested to depend on the loss of key regulators and tissue phenotypes in 2D cell cultures [27]. Indeed, the study of NP-mediated drug delivery in a 3D *in vitro* model would simulate a more realistic estimate of drug efficacy before *in vivo* tests. To date, systematic studies dealing with the effect of NP size on cell uptake and cytotoxicity have been carried out basically with model NPs with diameters ranging from tens to several hundreds of nm [28, 29]. Few attempts have been made to develop *in vitro* 3D models to evaluate the efficacy of anticancer drugs [30, 31], which are particularly relevant because in 3D cells 'sense' the ECM all around, thus producing phenotypic differences and modifying their behavior accordingly [32-34].

In this framework, the aim of this study was to produce small sized (sub-100 nm) NPs made up of a biodegradable poly(D,L-lactic-co-glycolic acid) (PLGA)–block–poly(ethylene glycol) (PEG) copolymer (namely PELGA), which holds promise for accumulation in hypervascular tumors [15], and compare the effect of the formulation on cell uptake and cytotoxicity. PELGA copolymer was synthesized in our laboratories and chosen as the NP-constituting amphiphilic copolymer since both PEG and PLGA meet FDA approval criteria for clinical use as drug adjuvants. As a proof-of concept study, we report on the production and technological characterization of PELGA NPs, loaded with a chemotherapeutic agent called doxorubicin (Dox), in terms of technological features, cell uptake and cytotoxicity behavior as a function of the formulation.

Dox is an anthracycline which exerts its cytotoxic effect by intercalating the planar aromatic chromophore portion between two base pairs of DNA [35, 36], thus inhibiting the progression of the enzyme topoisomerase II and hence the synthesis of nucleic acids within cells [37, 38]. When intravenously administered, Dox lacks specificity towards tumor tissues [39] and causes severe side effects such as myelosuppression, irreversible cardiotoxicity [40] and nephrotoxicity [41]. Thus, many studies have focused on the development of drug delivery systems and administration routes for Dox to increase tissue selectivity and improve its toxicity profile [42-44]. Indeed, free and polymer-conjugated Dox has been successfully loaded into many nanometric devices, including NPs [45] and liposomes [46]. Dox release from nanodevices can reduce drug-associated toxic side effects and metastasis generation in murine models [47, 48], possibly due to drug transfer to the malignant tissues from hepatic tissue, acting as a drug reservoir [49]. Some clinical success has also been attained by nanocarrier-mediated Dox release. Indeed, drug toxicity towards the heart and liver could be reduced, probably due to a lower cumulative dose (around 180 mg m^{-2}), with a degree of success depending on tumor localization with respect to the liver, which probably governs the attainment of therapeutic drug concentrations in target tissues [50]. Dox is widely used in cancer

chemotherapy, either as a single agent or in combination with other chemotherapeutics [51, 52], and in this work was chosen as a model molecule for NP loading [35, 53]. PELGA NPs were prepared by the double emulsion–solvent diffusion technique, which allows the encapsulation of hydrophilic molecules within a compartmentalized structure together with a controlled drug release kinetics [54, 55]. Dox-loaded PELGA NPs were characterized for size distribution, ζ-potential and release kinetics at the pH of the physiological environment, of the tumor ECM and of lysosomes (7.4, 6.8 and 5.0, respectively). The effect of the formulation on the uptake and cytotoxicity was investigated in standard two-dimensional (2D) cell cultures on HeLa and IGROV-1 cells, which were used as *in vitro* models of human cervix carcinoma and ovarian adenocarcinoma, respectively. The cytotoxicity of Dox-loaded PELGA NPs towards HeLa cells was also assessed in three-dimensional (3D) collagen matrices, in which the NPs were confined in a region separated from the cells by a porous membrane, thus creating an initial step gradient of the Dox. The cytotoxicity of the Dox/NPs was quantified by time-lapse monitoring of Dox accumulation in cell nuclei at different distances from the deposition site and as a function of NP formulation/size.

3.3. MATERIALS AND METHODS

3.3.1. Materials

Equimolar uncapped Poly (D,L-lactide-co-glycolide) (PLGA) (Resomer RG502H, Mw 12 000 Da, inherent viscosity 0:16–0:24 dl g^{-1} in chloroform at 25° C) was purchased from Boehringer Ingelheim (Ingelheim, Germany). Doxorubicin hydrochloride (Dox; purity >99%) was obtained from Discovery Fine Chemicals (Wimborne, UK). Type one collagen solution from bovine skin, potassium bromide, pluronic F68, dicyclohexylcarbodiimide (DCC), 4-(dimethylamino)pyridine (DMAP), dichloromethane (DCM), ethyl acetate (EA), sodium dihydrogen phosphate, disodium hydrogen phosphate, trehalose dihydrate and polyethylene glycol (PEG, Mw 1500 Da), rhodamine B (Rhod), 1-ethyl-3-(3-dimethylaminopropyl) carbodiimide hydrochloride (EDC-HCl), ethyldiisopropylamine (EDPA) and dimethylformamide (DMF) were obtained from Sigma-Aldrich (USA). Analytical grade dimethyl sulfoxide (DMSO) was purchased from J T Baker (The Netherlands). Bidistilled water was pretreated with a Milli-Q R Plus System (Millipore Corporation, Bedford, USA). Phosphate buffer saline (PBS) tablets without calcium and magnesium were obtained from MP Biomedicals Inc. (France). Dulbecco's modified Eagle's Medium (DMEM) and 10X Dulbecco's phosphate saline buffer from Gibco R, Life Technologies and containing 1 g^{-1} glucose were purchased from Invitrogen. Fetal bovine serum (FBS), penicillin and streptomycin from HyClone (UK) and RPMI 1640 medium (Lonza, Switzerland) were used.

3.3.2. Synthesis of PLGA–PEG copolymer

PLGA–PEG (PELGA) copolymer was synthesized via a coupling reaction between PLGA and PEG similarly to a previously reported procedure [57]. The reaction scheme is reported in **Fig. 1(A)**. Briefly, 2.4 g of PLGA 502H, 1.2 g of PEG, 0.165 g of DCC (0.8 mmol) and 0.049 g of DMAP (0.8 mmol) were dissolved in 20 ml of anhydrous DCM. The reaction was carried out at room temperature for 2 days under an inert nitrogen atmosphere. Afterwards, the

residual DCC was changed into dicyclohexylcarbodiurea (DCU) by adding 10 μl of bidistilled water and the DCU was removed by filtration as a reaction byproduct. Unreacted PEG was separated by precipitation five times in methanol, while unreacted PLGA was removed by precipitation in ethyl ether. Both protocols were performed five times at 4 °C. Finally, the residue was dried overnight under vacuum at room temperature.
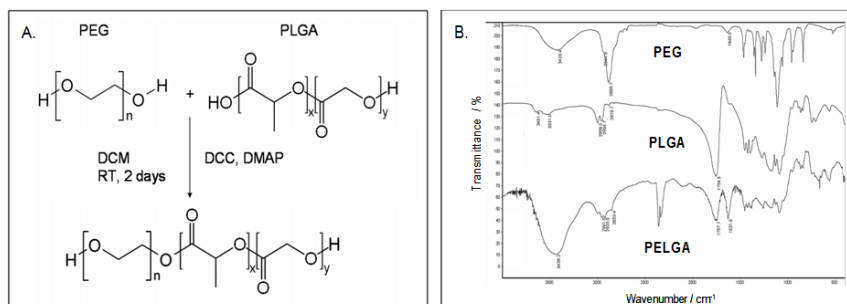
Figure 1. *Synthesis and characterization of the poly(d,l-lactic-co-glycolic acid) (PLGA) – block – poly(ethylene glycol) (PEG) (PELGA) copolymer. A: Synthetic reaction scheme of the PLGA-PEG reaction. FITR spectra of the reactants (PEG, PLGA) and of the product (PELGA).*

3.3.3. Synthesis of PLGA–rhodamine copolymer

For uptake and colocalization experiments, fluorescent NPs were prepared by conjugating Rhod to PLGA. The polymer (3 g) was reacted with Rhod in the presence of EDC-HCl and EDPA in 5 ml anhydrous DCM under nitrogen atmosphere. The reacting mixture was stirred at room temperature for one day. Afterwards, aminated PLGA (0.2 g) was conjugated to Rhod (38.4 mg) with EDC-HCl (15.5 mg) and EDPA (10.4 mg) in 1 ml anhydrous DMF. The reacting mixture was stirred for 24 h at room temperature, protected from light, under nitrogen atmosphere. The polymer was precipitated in water solution and filtered. The resulting solid material was dissolved with DCM, and the polymeric solution was washed with water three times. Afterwards, DCM solution was poured into anhydrous sodium sulfate, set under agitation overnight, and finally precipitated and washed with methanol as described in section 2.2. Rhod-PLGA was used to prepare fluorescent NPs for uptake and colocalization studies, and unreacted Rhod was removed by dialysis against water.

3.3.4. Fourier transform infrared (FTIR) analysis

Fourier transform infrared spectroscopy (FTIR) spectra of the PELGA copolymer were recorded using a Nicolet 6700, Thermo Fisher Scientific Inc. (USA) spectrometer with an average of 50 scans. The samples were crushed with potassium bromide and the spectra of PLGA, PEG and PELGA were scanned in the 4000–400 cm^{-1} range.

3.3.5. Nanoparticle preparation and characterization

Blank and Dox-loaded NPs were prepared by a modified double emulsion–solvent diffusion technique. Briefly, the internal aqueous phase, composed of 0.5 ml of ultrapure water or of a 4 mg ml^{-1} Dox aqueous solution, was emulsified by vortexing for 5 min with 5 ml of 10 or 20 mg ml^{-1} PEG–PLGA solution in EA. The NP formulations were named PELGA10 and PELGA 20, respectively, and the drug:polymer mass ratios were 1:25 and 1:50. The resulting emulsion was sonicated for 30 s (output power: 50 W) over an ice bath with a probe sonifier (Branson S250-D, USA). The primary nanoemulsion was immediately poured into 15 ml of 1% (w/v) aqueous Pluronic F68 and further sonicated (120 s, 75 W). The resulting double emulsion was then poured into 35 ml of water and stirred overnight for complete diffusion and evaporation of EA. Furthermore, to examine the effect of device size on cell internalization, NPs with larger diameters (>100 nm) were produced using a 40 mg ml^{-1} solution of PELGA in EA as the organic phase; the second sonication was carried out at 50 W for 30 s. This formulation was named PELGA40. The NP suspensions were centrifuged (AvantiTM J-25, Beckman, USA) for 30 min (4 C, 24 000 rpm) and ultrafiltered twice using an ultrafiltration concentrator (MWCO 10 000 Da, Corning) for 15 min (4, 5000 rpm) for washing. Subsequently, the NPs were resuspended in 1.5 ml of aqueous 5% w/v trehalose as a cryoprotectant, and lyophilized (Heto PowerDry PL6000 Freeze Dryer, Thermo Electron Corp., USA; -50 °C, 0.73 hPa) for 24 h. NP morphology was investigated through a transmission electron microscope (TEM EM208S, Philips, The Netherlands) by spraying 5 ml of ultradiluted NP suspension in ultrapure water onto a copper TEM grid (300

meshes, 3 mm diameter). NP mean size, size distribution and ζ-potential were determined by laser light scattering (ZetaSizer Nano ZS, Malvern Instruments, Malvern, UK) on a 0.1 mg ml^{-1} suspension of NPs in water (12 runs each sample). NP size and size distribution were also determined after 24 h incubation in cell culture medium to assess device stability during the time frame of the cell uptake/cytotoxicity experiments. Results were averaged on at least five measurements. Prior to the cell experiments, NP stability in cell culture medium was investigated to assess whether the NPs aggregated in the time frame of the cell uptake tests. Stability tests were performed by incubating 100 µl of NP suspension in 1 ml of cell culture medium at 37 °C for 24 h, and by determining size distributions at time zero and after 24 h. Size measurements were also performed on cell culture medium at time zero and after 24 h to verify its possible self-aggregation. Dox entrapment efficiency was calculated by dissolving freeze-dried NPs (1 mg) in 1 ml of DCM. The solvent was evaporated at room temperature for 6 h and, subsequently, 1 ml of dimethyl sulfoxide (DMSO) was added to dissolve the Dox. The resulting solution was sonicated (FALC, Italy) for 1 h in a water bath at 59 kHz, 100 % power and filtered by a 0.45 µm polyvinylidene fluoride (PVDF) membrane filter (Millipore Filter Corporation, Bedford, MA). Dox content was quantified by spectrofluorimetric assay (Wallac 1420 Victor2TM, Perkin-Elmer, USA) at 488 nm, performed in 96-well black flat-bottom plates (Corning, USA). The linearity of the spectrofluorimeter response was verified on Dox solutions in DMSO (0.1–10 µg ml^{-1} concentration range; $r^2 > 0.99$). Entrapped Dox percentage was calculated as η 100 * Dox $_{entrapped}$/Dox $_{total}$. Results were averaged on three batches. For uptake/colocalization experiments, Dox-free fluorescent NPs were produced by dissolving Rhod–PLGA and PELGA (1:1 weight ratio) in the organic phase of the emulsion (10% w/v). The produced formulation was named Rhod–PELGA10, correspondingly.

3.3.6. Thermal analyses

To assess the influence of the synthesis and the formulation parameter on the thermal properties of both materials and devices, thermograms reporting glass transition temperatures (T_g) and/or melting point temperatures (T_m) of the raw polymers (PEG, PLGA, PELGA), as well as Dox, placebo and PELGA10/PELGA20 Dox-loaded NPs were acquired by a differential scanning calorimeter (DSC Q20, TA Instruments) calibrated with a pure indium standard and operating under an inert nitrogen atmosphere (flow rate: 50 ml min^{-1}). Desiccated samples (mass: 2–5 mg) were placed in aluminium pans, and an empty one was used as a reference. The determination was made by cooling the sample from room temperature to -40 °C and then heating to 250 °C (0 and 200 °C for PLGA) at a heating rate of 5 °C min^{-1} for all runs. In the case of Dox, the samples were heated from room temperature to 250 °C. The thermograms were obtained after the second heating of the samples. Results were averaged on at least three repeats.

3.3.7. In vitro release kinetics of doxorubicin

Dox release kinetics from PELGA10 and PELGA20 NPs were evaluated by a standard sampling-separation method in PBS at pH 7.4, or in phosphate buffers (PBS) at pH 6.8 and pH 5.0. The buffers were prepared by mixing 0.5 M sodium dihydrogen phosphate and 0.5 M disodium hydrogen phosphate aqueous solutions. For release experiments, dialysis bags (MWCO 10 000 Da, Spectra) were loaded with 1 ml of NP suspensions (1 mg ml^{-1}) and incubated in the release medium (25 ml) at 37 °C in an orbital incubator (SI50, Stuart R, UK) operating at 100 rpm. At scheduled time intervals, 1 ml of the release medium was withdrawn and replaced with the same volume of fresh medium. Dox content in the supernatant was quantified by spectrofluorimetric assay. The instrument response was linear over the concentration range 0.1–2 μg ml^{-1} ($r^2 >$ 0.99). The experiments were run in triplicate. The release data were fitted by the simple Korsmeyer–Peppas equation [56], which helps in determining whether the drug release deviates from Fick's law and is described by the following equation:

$$F = k\mathrm{t}^{\mathrm{n}}, \tag{1}$$

where k is a kinetic constant comprising the geometric NP features, and n is the release exponent characterizing the release mechanism. For a spherical geometry, $n \leq 0.43$ corresponds to a Fickian, while $0.43 \leq n \leq 0.85$ indicates an anomalous diffusion regime.

3.3.8. Cell culture

To test the biological effects of the NPs, human epithelial cervix carcinoma (HeLa) and human ovarian adenocarcinoma (IGROV-1) cell lines were used. In particular, the latter were chosen as a control drug-resistant system. HeLa cells were cultured with a complete medium, composed of DMEM with 1 g l^{-1} glucose, containing 10% (v/v) FBS, 100 U ml^{-1} penicillin and 0.1 mg ml^{-1} streptomycin, while IGROV-1 cells were grown in RPMI 1640 with 10 % FBS and antibiotics. The cells were maintained in 100 mm diameter cell culture dishes in a humidified atmosphere at 37 °C and 5 % CO2.

3.3.9. Nanoparticle uptake and cytotoxicity in 2D

The cell uptake of the Dox-loaded NPs was investigated by a confocal laser scanning microscope (CLSM), taking advantage of the intrinsic fluorescence of Dox. For CLSM observations, PELGA10, PELGA20 and PELGA40 NPs were dispersed in cell culture medium at a final Dox concentration of 2 μg ml^{-1}. A subconfluent layer of cells was incubated with NP suspension at 37 °C for 24 h. Afterwards, the cells were rinsed twice with PBS to remove non internalized NPs and fixed with 4 % paraformaldehyde for 20 min. The cell nuclei were stained by using 40, 6-diamidino-2-phenylindole (DAPI) (Sigma). The samples were observed at 488 nm with a water-immersion 63X objective by a CLSM (LSM510, Zeiss) equipped with an argon laser line. Image resolution was set to 1024 x 1024 square pixels. The cytotoxic activity of Dox-loaded PELGA10, PELGA20 and PELGA40 NPs against HeLa and IGROV-1 cells was compared to non-treated cells, free drug and blank NPs, which were used as a control. Cell

survival was quantified by Alamar Blue Assay. 5 x 10^4 cells were added to 200 µl of cell culture medium in each well of a 96-well plate and allowed to recover for 24 h. After recovery, free drug, blank or drug-loaded NPs were added to the wells in 100 µl of medium and non-treated cells received 100 µl of medium. The cells were treated for 24 h, and afterwards Alamar Blue Assay was performed. The absorbance of Alamar Blue reagent solution was read at 570 nm and 600 nm by a plate reader (Wallac Victor 1420, Perkinelemer). Data were reported as percentage of viable cells normalized to non-treated cells.

3.3.10. Nanoparticle uptake and cytotoxicity in 3D collagen matrices

For the uptake and cytotoxicity of the NPs in a 3D matrix, we set up a home-made experimental system in order to mimic a tumor ECM network *in vitro*. As shown in Fig. 2, a porous membrane was used to separate two silicon chambers, filled with collagen gel prepared by diluting collagen solution with 10 X Dulbecco's phosphate saline buffer (D-PBS, Gibco, Life Technologies) (8:1 volume ratio) and adjusting the pH to 7.4 by dropwise addition of NaOH and HCl. 1 * 10^5 HeLa cells were suspended in 370 µl of 2.4 mg ml^{-1} collagen solution and poured into the larger chamber. The system was then incubated at 37 °C for 1 h to allow collagen fibrillogenesis and, afterwards, fresh cell culture medium was added to the gel. After 24 h, 330 µl of 2.4 mg ml^{-1} collagen solution containing Dox-loaded NPs at a final Dox concentration of 2 µg ml^{-1} was poured into the smaller chamber at 37 °C for fibrillogenesis for about 1 h.

For cytotoxicity experiments, membranes with 0.05 μm or 0.65 μm pore diameters were used (IsoporeTM membrane filters, Millipore). In the first case,
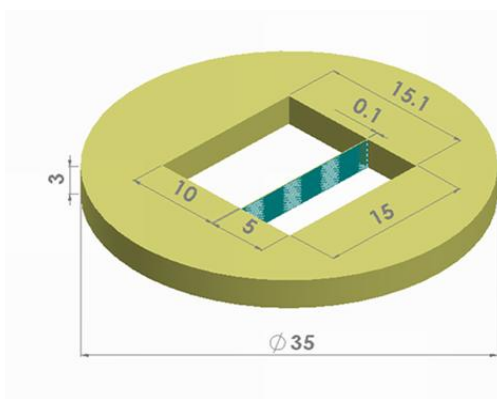
Figure 2. *Schematic drawing of the two-compartment experimental system used for experiments. Cells were embedded in collagen and placed in the bigger chamber, with free Dox or Dox-loaded NPs in collagen in the smaller one. The membrane*

the pore diameter was smaller than the NP size, thus the devices were confined in the small chamber and could not diffuse through the collagen gel. In the second case, the NPs could freely diffuse within the collagen matrix, and cytotoxicity was contributed also by NP diffusion. Cell cytotoxicity in 3D matrices was evaluated by a time-lapse experiment by using a CellR microscope (Olympus) equipped with a mini-incubator to control temperature and CO_2 percentage. Images were acquired every 10 min for 24 h. In order to test the capability of the NPs to release Dox in 3D matrices, the cytotoxic effect in 3D was analyzed at 1, 2 and 4 mm from the porous membrane. The changes in cell morphology (from stretched to round) and the increment of cell fluorescence, due to intracellular Dox accumulation during the time-lapse experiments, indicated cell death. NP cytotoxicity in 3D was expressed as the percentage of dead cells after 24 h as a function of the distance from the porous membrane.

Prior to the cytotoxicity tests in 3D, the diffusion coefficients of the Dox and the NPs were determined by single-channel fluorescence correlation spectroscopy (FCS) in combination with CLSM. A confocal fluorescence correlation spectroscope, ConfoCorII (Carl Zeiss, Jena, Germany) was used. For the FCS studies, non-gelled collagen (200 μl) or water was poured into each chamber of an eight-well borosilicate coverglass (Lab-Tek, Germany) and fibrilled at 37 °C. The Dox or NPs were loaded into the collagen gel by overnight contacting of a drug solution/NP suspension in water with the fibrilled gel. The final drug and NP concentrations in the gel were optimized to 20 ng ml^{-1} and 0.042 mg ml^{-1},

respectively. The gel or NP suspension was excited by laser light at 488 nm, and the laser beam was focused by a Zeiss 40 Apochromat water-immersion objective (Carl Zeiss, Germany). The fluorescent emission beam was mapped onto a pinhole in the image plane of the objective (70 μm), sent to a 530 nm LP filter, and then acquired on an avalanche photodiode (APD) in single-photon counting mode. The diffusion coefficients were derived from the normalized autocorrelation function [57]

$$G(\tau) = \frac{[F(t)F(t+\tau)]}{[F(t)]^2} = \frac{[\delta F(t)\delta F(t+\tau)]}{[F(t)]^2} + 1 \,, \tag{2}$$

which describes the fluctuations of fluorescence intensity at time t, $\delta F(t) = F(t) - [F(t)]$, and at time $t + \tau$, $\delta F(t + \tau) = F(t + \tau) - [F(t + \tau)]$, around the corresponding mean values $[F(t)]$ and $[F(t + \tau)]$. The autocorrelation function gives information on τ_D, the dwell time in the confocal volume [58], which ia s prolate spheroid having axes ω_{xy} and ω_z. The structure parameter $S = \omega_z / \omega_{xy}$ was variable. The diffusion coefficients were calculated assuming that the confocal volume (which was estimated to be <0.04 fl) depends only on the confocal parameters (pinhole aperture, laser power) and the nature of the fluorescent molecule. Based on the previously determined diffusion coefficient of Dox in water at 37 °C (2.12 * 10^{-6} cm2 s^{-1} [59]), the confocal volume was calculated taking into account that

$$\omega_{xy} = \sqrt{4D^{\tau_D}} \,, \tag{3}$$

where D is the diffusion coefficient of Dox and τ_D is the dwell time in the confocal volume. The confocal volume is easily derived as

$$V_{C=\frac{4\pi}{3}S\omega_{xy}^3}. \tag{4}$$

Hence,

$$D = \frac{\omega_{xy}^2}{4\tau_D}. \tag{5}$$

FCS experiments were run at least five times at 37 °C.

3.3.11. Nanoparticle uptake quantification

To evaluate the cell uptake of Rhod–PELGA10 NPs, $5 * 10^4$ cells were seeded in a 24-well plate for 2D culture conditions and the same amount of cells was grown in 250 µl of 2.4 mg ml^{-1} collagen gel for 24 h at 37 °C for 3D culture conditions. Afterwards, the cells were incubated with Rhod–PELGA10 NPs dispersed in cell culture medium. The total amount of NPs was kept constant for the 2D and 3D experiments. More precisely, the Rhod–PELGA10 NP final concentrations were 50 µg ml^{-1} for 2D and 100 µg ml^{-1} for 3D, i.e. 500 µl and 250 µl of NP suspension were added to the cells for the 2D and 3D experiments, respectively. The cells were incubated with NP suspensions for 24 h at 37 °C.

After incubation, the cells in 2D were rinsed with PBS and lysed with 1 % Triton X100 in PBS. For the 3D experiments, after rinsing with PBS, the collagen gel was digested with 2.5 mg ml^{-1} collagenase A solution, centrifuged and the pellet of cells was suspended in 1 % Triton X 100 in PBS. Finally, the cell lysates were analyzed by a spectrofluorometer (Wallac 1420 Victor2TM, Perkin-Elmer, USA) by measuring the NP fluorescence intensity at $\lambda = 543$ nm. The amount of internalized NPs was quantified by interpolating the fluorescence intensity data with a calibration curve.

3.3.12. Colocalization with LAMP2, clathrin and caveolin 1

For indirect immunofluorescence, after NP incubation, the cells were first rinsed twice with PBS to remove noninternalized NPs and fixed with paraformaldehyde 4 % for 20 min. Then, the cells were incubated with Triton X 100 0.1 % in PBS for 10 min and with PBS-BSA 0.5 % for 15 min at room temperature (RT). Caveolae were localized by first incubating samples with rabbit anti-caveolin 1 (Abcam) primary antibodies. For lysosomes, rabbit polyclonal anti-LAMP2 (Abcam) primary antibodies were used. Clathrin coated vesicles were localized

with mouse anti-clathrin monoclonal (ABR). After primary antibody incubation, Alexa-fluor 488 goat anti-rabbit secondary antibodies (Molecular Probes, Invitrogen) and Alexa-fluor 488 goat anti-mouse secondary antibodies (Molecular Probes, Invitrogen) were used. Afterwards, the samples were rinsed three times with PBS. The cell nuclei were stained with DAPI. Immunofluorescence analyses were performed by a confocal and multiphoton microscope system (Leica TCS SP5 MP). Images were acquired with a resolution of 1024 X 1024 pixels. Colocalization was estimated by an ImageJ software plugin.

3.3.13. Statistical analysis

In all cases, quantitative data were reported as mean value standard deviation (SD). The results were analyzed by one-way analysis of variance (ANOVA). A value of $p < 0.05$ was considered statistically significant.

3.4. RESULTS AND DISCUSSION

3.4.1. FTIR characterization

PLGA–PEG copolymer (namely PELGA) was synthesized and used to produce NPs, and the reaction scheme is reported in **Fig. 1(A)**. FTIR spectra of PEG, PLGA and PELGA copolymer are presented in **Fig. 1(B)**. The peak at 1631 cm^{-1} of the PELGA spectrum was associated with the bending vibration of the absorption water in the materials. The peaks at 3423.4 and 2885.7 cm^{-1} in the PEG spectrum were assigned to the terminal –OH group and C–H stretching of CH$_2$ groups, respectively. The peaks at 2999.0 and 2954.7 cm^{-1} in the PLGA spectrum are related to C–H stretching of CH$_3$ groups, while the peaks at 2878.7 cm^{-1} and 1754.5 cm^{-1} correlate to C–H stretching of CH$_2$ and CDO stretching in PLGA, respectively. For the PELGA, the peak at 3439.2 cm^{-1} was assigned to –OH stretching, the ones at 2961.0 and 2923.0 cm^{-1} to C–H stretch of CH$_3$, and the one at 2853.4 cm^{-1} was C–H stretching of CH$_2$. The strong peak at 1757.7 cm^{-1} was related to CDO stretching of PELGA, indicating the formation of ester groups, and of the copolymer.

3.4.2. Differential scanning calorimetry (DSC)

The thermal properties of drug-loaded carriers are of importance in pharmaceutical technology since information such as melting and crystallization is useful to assess the physico-chemical status of the loaded drug and hence drug–material interactions, which are relevant for the *in vitro* release properties. DSC experiments were performed on a drug (Dox), polymers (PLGA, PEG and PELGA) and NPs (unloaded and Dox-loaded PELGA10 and PELGA20). **Fig. 3** depicts the corresponding DSC spectra. Native Dox exhibited a sharp endothermic peak at 231.5 ± 1.5 °C (**Fig. 3(A)**). For the polymers, PLGA showed a glass transition temperature (Tg) at 36.8 ± 1.2 °C, while PEG displayed a clear endothermic melting peak at 49.3 ± 0.3 °C. The PELGA copolymer did not exhibit the PEG melting temperature (Tm) and underwent a glass transition at 24.4 ± 2.5 °C, lower compared to PLGA. This strongly suggests that short PEG segments plasticize the adjacent PLGA chain and the molecular weight is low,

thus hampering the formation of any crystalline structure. A broad and not relevant exothermic peak was detected around 200 °C (**Fig. 3(B)–(D)**).

DSC tests were also performed on placebo and Dox loaded NPs. As shown in Fig. 3(E), the Tg of unloaded NPs was 23.6 ± 1.8 °C, very close to that of PELGA, and basically behaved as the synthesized copolymer. Likewise, the DSC thermogram of Dox-loaded PELGA20 NPs was basically superimposable on the PELGA thermogram, and no endothermic melting peak could be detected (**Fig. 3(G)**), which indicates that Dox is present in the non-crystalline state in these NPs, and therefore that the undesired phenomenon of Ostwald ripening is inhibited [60].
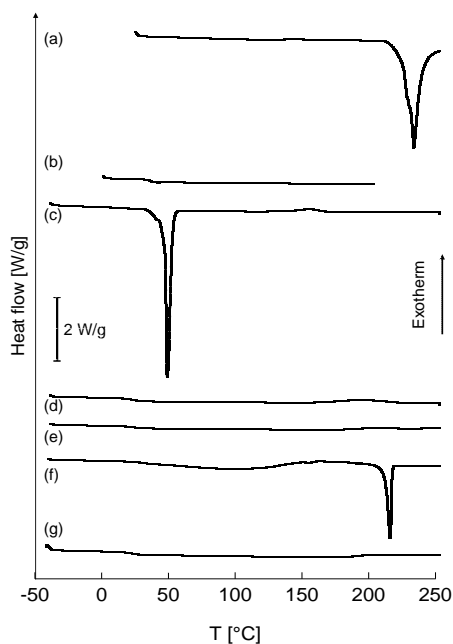
Figure 3. *DSC thermograms of plain Dox (A); PLGA (B); PEG (C); PELGA (D); blank NPs (E); Dox-loaded PELGA10 NPs (F); Dox-loaded PELGA20 NPs (G). Heating rate was 5°C min^{-1}.*

Interestingly, the thermogram of the Dox-loaded PELGA10 NPs showed the endothermic melting peak of Dox at 222.3 ± 7.8 °C, but strongly attenuated. This suggested a partial interaction between the PELGA and the Dox, which allowed the presence of some drug in the crystalline state. The discrepancy in the DSC

results relative to the PELGA20 formulation can be reasonably ascribed to the higher drug:polymer mass ratio in the case of PELGA10 compared to PELGA20 NPs (1:25 versus 1:50). In the latter case, the DSC results suggest that the Dox could be efficiently dispersed within the PELGA and could not organize into crystalline structures. The amorphous drug phase results in a higher solubility, which in turn influences both the *in vitro* and *in vivo* dissolution features [61].

3.4.3. Nanoparticle characterization

Like other amphiphilic copolymers, the PELGA emulsion formed core–shell NPs [62]. As shown in **Fig. 4(A)** and summarized in table 1, the PELGA10 and PELGA20 NPs were spherical and possessed <100 nm diameters and polydispersity indices ranging from 0.13 to 0.16, indicating a narrow overall size distribution. The NP size increased with PELGA concentration in the organic phase of the emulsion due to a poorer dispersibility of the organic phase, while the ζ -potentials were mildly negative and decreased slightly with increasing polymer concentration, which suggests that the hydrophilic PEG segments and non-ionic Pluronic partially mask the carboxylic groups of the PLGA chains. The Dox entrapment efficiency increased with increasing PELGA concentration due to the increasing viscosity of the organic phase which hampered drug leakage towards the external aqueous phase (**Table 1**).

Formulation	PELGA concentration in the organic solution [mg mL^{-1}]	Particle mean diameter [nm]	Polydispersity index (PDI)	Zeta potential [mV]	Entrapment efficiency (%)	Particle mean diameter after 24 h incubation in cell medium [nm]	Polydispersity index (PDI) after 24 h incubation in cell medium
PELGA10	10	77.2 ± 2.5	0.152 ± 0.033	-17.0 ± 1.3	32.4 ± 5.6	79.2 ± 5.7	0.162 ± 0.012
PELGA20	20	88.5 ± 5.1	0.131 ± 0.025	-20.4 ± 2.0	36.7 ± 4.1	90.5 ± 5.0	0.157 ± 0.032
PELGA40	40	174.9 ± 3.2	0.164 ± 0.012	-25.6 ± 2.2	55.4 ± 1.4	175.8 ± 4.3	0.174 ± 0.024

Table 1. *Size, polydispersity index (PDI), zeta potential and entrapment efficiency of Dox-loaded NPs.*

NP stability is important in view of NP use for cell experiments and pharmaceutical applications. The stability of the devices was assessed by incubation for 24 h in cell culture medium and size measurements of the NPs after incubation in PBS. The NP diameters were basically constant in all cases (the mean diameters after incubation were 79.2 ± 5.7, 90.5 ± 5.0 and 175.8 ± 4.3 nm for PELGA10, PELGA20 and PELGA40 NPs, respectively), and no self-aggregation of the medium could be detected. Actually, due to the double emulsion preparation technique, PEG segments are exposed on the NP surface, thus contributing to reduction of the interfacial tension between the devices and the suspending adsorption and self-aggregation. These findings confirmed literature results on PEG-conjugated NPs, which were demonstrated to be stable in water at 4 °C for periods ranging from weeks to months [15, 63, 64]. Prior to the cell experiments, rhodamine release from the Rhod–PELGA10 NPs was assessed in the same conditions as the PELGA NPs.

As expected, due to the very stable amine bond between PLGA and the dye, no Rhod release was evidenced in the time frames of either the cellular experiments (24 h) or the drug release kinetics.

3.4.4. In vitro Dox release kinetics

In vitro Dox release profiles from the PELGA10 and PELGA20 NPs are shown in **Fig. 4(B)** and **(C)**. It was necessary to study the Dox release profiles at different pH values (7.4, 6.8 and 5.0) to simulate the conditions of normal ECM, tumor ECM and lysosomes. In all cases, a 24 h burst followed by a slower release phase was found. The PELGA20 NPs gave a one day burst fraction strongly dependent on the pH (18.1 % at pH 7.4 and 60.7 % at pH 5.0). In the case of the PELGA10 NPs the burst was less variable with the pH (30.2 % at pH 7.4 and 45.4 % at pH 5.0). In particular, the Dox release rate from the PELGA NPs decreased with increasing PELGA concentration in the organic phase of the emulsion and with increasing pH. To investigate the mechanisms of NP unloading, Dox release profiles were plotted as a function of $t^{1/2}$ (**Fig. 4(B)**).

In all cases, after a one day burst a second linear region followed, with a slope relatively constant with the pH and basically independent of the formulation, while the one day burst strongly depended on both the formulation and the pH. To envisage whether the Dox discharging from the PELGA NPs was driven by diffusion, the release data were fitted to equation (1). The estimated parameter values are listed in **Table 2**. The fitting results showed that *k* decreased slightly with the pH, with a strong dependence for the PELGA20 NPs, while n increased slightly/strongly with the pH for the PELGA10/PELGA20 NPs, respectively.
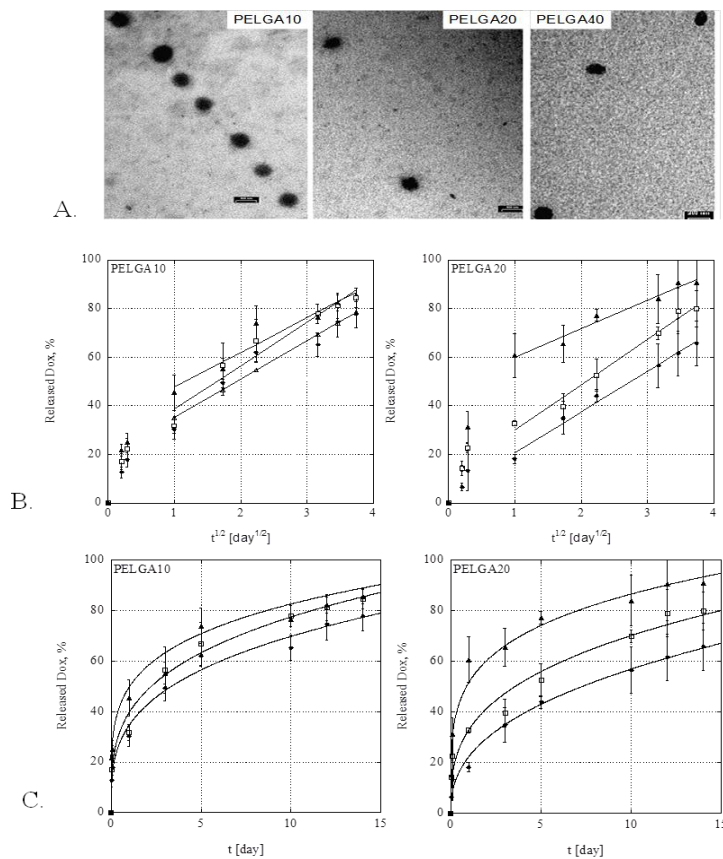
Figure 4. *Morphology and release features of PELGA nanoparticles. A: TEM micrographs of Dox loaded NPs. The bar: is 100 nm for PELGA10 and PELGA20 nanoparticles and 200 nm for PELGA40 nanoparticles. B: In vitro release profiles of Dox from PELGA10 and PELGA20 NPs as a function of square root of time. C: release data as a function of time. Solid lines represent curve fitting. Symbols: (▲) pH = 5.0; (□) pH = 6.8; (◆) pH = 7.4.*

In particular, the *n* values showed that the release was driven by diffusion in all cases, and the corresponding increase of the release rate in acidic conditions was

ascribed to an enhanced NP porosity during PELGA degradation, which further promoted a diffusion controlled release regime.

Indeed, drug desorption/diffusion and PELGA degradation occurred simultaneously and, in all cases, n ranged from 0.223 to 0.404 ($n < 0:43$), indicating that drug desorption/diffusion is faster than polymer degradation/erosion. In the case of the PELGA20 NPs (at pH 7.4), a threshold value of n is approached, suggesting that the PELGA degradation rate is less negligible compared to Dox transport at physiological pH and at a higher polymer concentration.

	pH					
	5.0		6.8		7.4	
	PELGA10	PELGA20	PELGA10	PELGA20	PELGA10	PELGA20
k	0.457 ± 0.029	0.518 ± 0.051	0.396 ± 0.033	0.331 ± 0.026	0.346 ± 0.124	0.225 ± 0.025
n	0.238 ± 0.018	0.223 ± 0.012	0.292 ± 0.034	0.326 ± 0.005	0.305 ± 0.016	0.404 ± 0.032

Table 2 – *Peppas-Korsmeyer parameter estimates for Dox release from PELGA NPs.*

Thus, Dox release from PELGA NPs primarily depends on drug diffusion and is secondarily affected by PELGA degradation. Indeed, in a previous work [65], we demonstrated that the autocatalytic degradation of PLGA microspheres produced by double emulsion was not affected by the polymer concentration in the organic phase of the emulsion, even at much higher polymer concentrations in the organic phase of the emulsion (10 %–20 % w/v versus 1 %–2 %–4 % w/v in this work). Thus, at the nanoscale level and with lower PLGA concentration in the organic phase of the emulsion, the formulation is not expected to affect the degradation pattern, and the weak dependence on pH of the Dox release rate from the PELGA10 NPs could be ascribed to their higher nanoporosity. In

contrast, the strong dependence of the Dox release kinetics from the PELGA20 NPs on the pH of the release medium strongly suggests a nonnegligible role of PELGA degradation, ascribed to a more efficacious Dox entrapment within the NP matrix. The PELGA20 NPs showed a more desirable release behavior as it was more sensitive to pH and more sustained at physiological pH.

3.4.5. Nanoparticle uptake

The uptake of the Dox-loaded PELGA10, PELGA20 and PELGA40 NPs in HeLa and IGROV-1 cell lines was systematically studied and compared to the internalization of free, non-encapsulated Dox. After 24 h incubation with a Dox-loaded NP suspension, a cytoplasmic distribution of fluorescence due to Dox was observed in HeLa cells. In particular, CLSM images showed that the NP uptake by HeLa cells was slightly more extensive in the case of the smaller, Dox-loaded PELGA10 NPs (**Figs. 5(D)–(F)**) compared to the PELGA20 NPs (**Figs. 5(G)– (I)**), which had a higher mean diameter (88.5 versus 77.2 nm). Moreover, the fluorescence appeared to be non-homogeneously diffused within the cells, but rather organized in discrete spots, mainly located in a perinuclear region, which strongly suggests Dox confinement within the NPs. Conversely, free Dox was preferentially localized within the cell nuclei, as evidenced by colocalization with DAPI staining (**Figs. 5(A)–(C)**). Upon Dox release in the endosomal or lysosomal lumen, the cell nuclei were expected to turn green. In our case, however, the PELGA NPs displayed prolonged release features and, therefore, in the first 24 h of delivery, only the burst fraction could be released and reach the intracellular space. These findings are consistent with previous results, which showed that nuclear penetration may take place in the case of free drug or of NPs with a diameter of around 4 nm [66], much smaller than the NPs prepared in this work. It must also be underlined that an increase in NP size leads to a drastic decrease of the cellular uptake amount. Indeed, after 24 h incubation with PELGA40 NPs (mean diameter: 174.9 nm), very few or no NP aggregates could be detected within the cytoplasm of the HeLa cells, while a weak cell nucleus

green staining was observed (**Figs. 5(J)–(L)**), probably due to the released Dox in the time frame of the cell experiments.
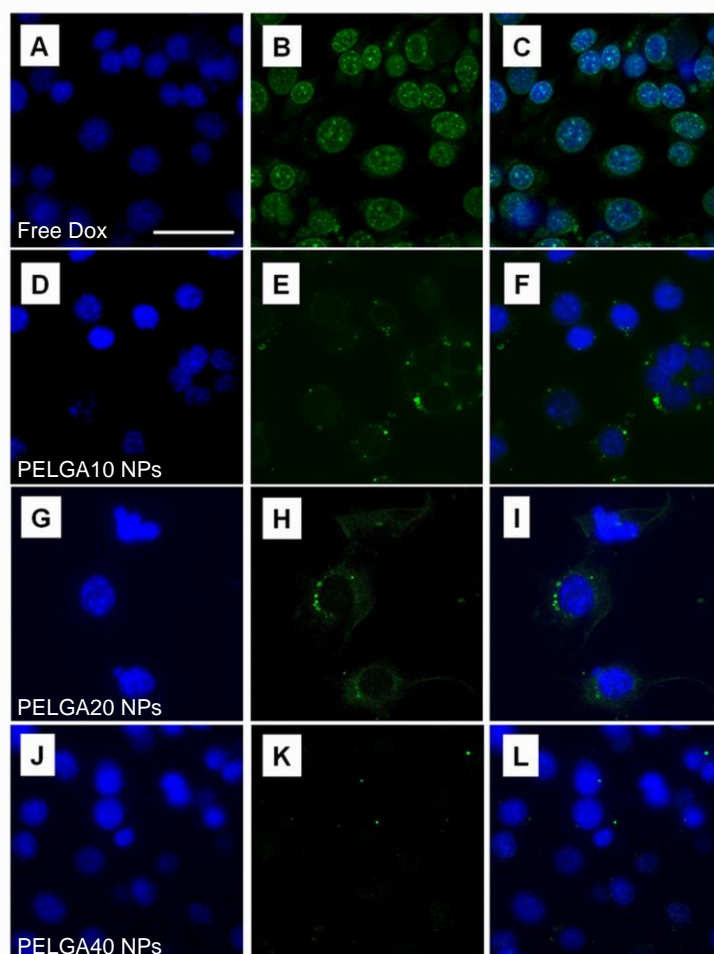
Figure 5. *Confocal laser scanning microscope images of HeLa cells incubated for 24 hours with 2 μg mL^{-1} free Dox (A-C); Dox-loaded PELGA10 NPs (D-F); Dox-loaded PELGA20 NPs (G-I); Dox-loaded PELGA40 NPs (J-L). A, D, G, J: DAPI staining of cell nuclei. B, E, H, K: intracellular localization of Dox; C, F, I, L: merge. Magnification bar: 50 μm.*

In the case of the IGROV1 cells, a negligible NP internalization was observed for the PELGA10 and PELGA20 formulations (**Figs. 6(D)–(L)**), and also the free Dox uptake was lower than for the HeLa cells, as shown in **Figs. 5(A)–(C)** and **6(A)–(C)**. Actually, it has been reported that IGROV1 cells show a very low doubling time and are more resistant to drug treatments [67]. Thus, our results confirm the resistance to treatment of IGROV1 cells and, more importantly, a specific localization of NPs within HeLa cells, which was mainly attributed to the size of the devices.
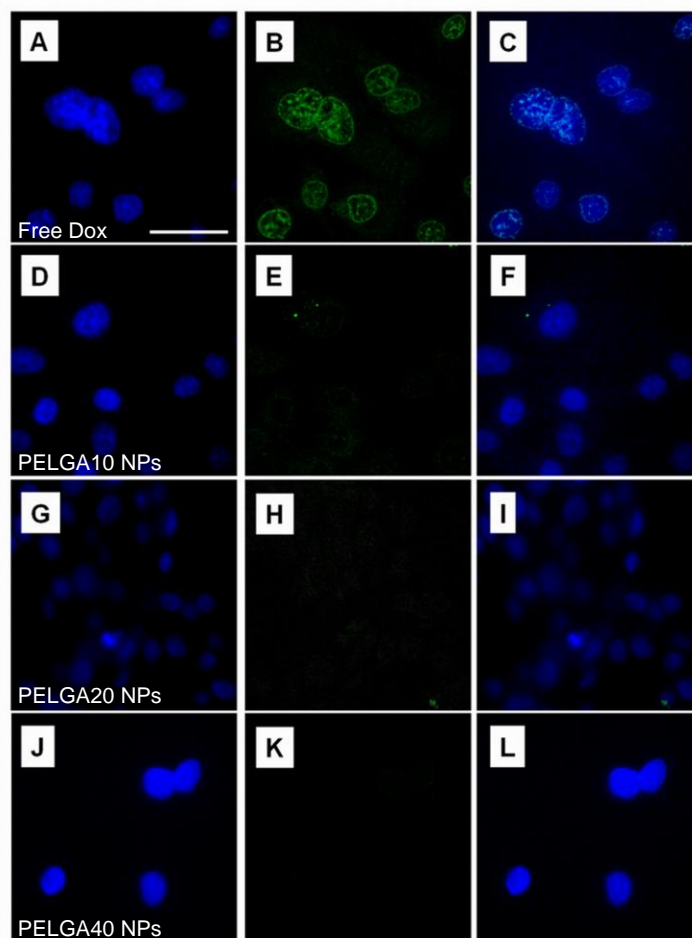
Figure 6. *Confocal laser scanning microscope images of IGROV1 cells incubated for 24 hours with 2 µg mL^{-1} free Dox (A-C); Dox-loaded PELGA10 NPs (D-F); Dox-loaded PELGA20 NPs (G-I); Dox-loaded PELGA40 NPs (J-L). A, D, G, J: DAPI staining of cell nuclei. B, E, H, K: intracellular localization of Dox; C, F, I, L: merge. Magnification bar: 50 µm.*

To the best of our knowledge, NP uptake mostly occurs by endocytosis or potentially pinocytosis. In this latter case, the NPs experience lysosomal pH (around 5), which strongly accelerates the Dox release from the PELGA20 NPs (**Fig. 4(B)**), while having a weaker influence on the release kinetics from the PELGA10 NPs. Taken all together, these results suggest that the PELGA20 formulation is more promising in the perspective of intracellular drug delivery due to the drug delivery being more strongly dependent on the pH.

Many works report on mechanisms underlying PLGA NP internalization. Depending on the cell type and the NPs' technological and physico-chemical features (such as NP size, surface charge, etc), several authors have demonstrated

that PLGA NPs can follow different uptake pathways [68-71]. Thus, to elucidate PELGA NP uptake by cells, we performed indirect immunofluorescence analyses of specific endocytic markers. As shown in **Fig. 7**, Rhod–PELGA10 NPs do not use caveolae-mediated endocytosis (**Fig. 7(A)**), though they partially colocalize with clathrin (**Fig. 7(B)**) and LAMP2 (**Fig. 7(C)**), thus indicating that Rhod–PELGA10 NPs enter by clathrin coated pits and reach lysosomes. In particular, by using ImageJ analysis software, we found 0.51 % colocalization between clathrin 1 and NPs and 1.72 % colocalization between LAMP2 and NPs.
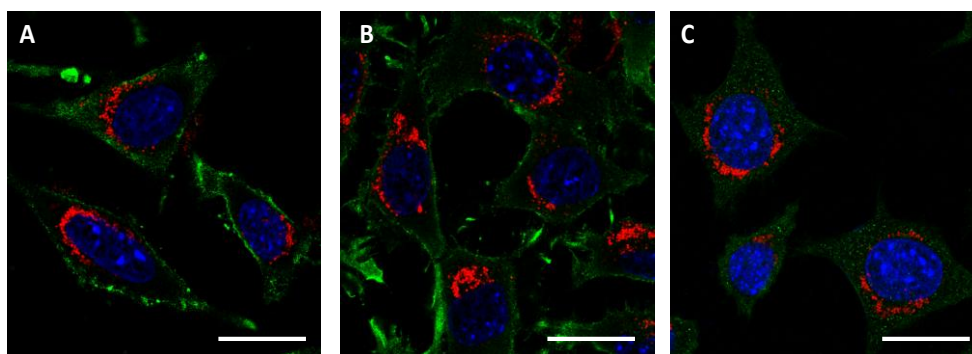
Figure 7. *Colocalization between Rhod PELGA 10 NPs and endocytic markers. A. Caveolin 1 (green), NPs (red) and DAPI (blue); B. Clathrin (green), NPs (red) and DAPI (blue); C. LAMP2 (green), NPs (red) and DAPI (blue). Magnification bar: 20 μm.*

3.4.6. Nanoparticle cytotoxicity

To demonstrate how the formulation and sub-100 nm size affect NP uptake, we tested the *in vitro* cytotoxic response of HeLa and IGROV1 cell lines elicited by Dox-loaded PELGA NPs. The biological activity was quantified using the Alamar Blue cytotoxicity assay. **Fig. 8** shows the cell viability percentage of treated cells normalized to non-treated cells. The results indicate a significant cytotoxic effect after 24 h of incubation when free Dox at 2 μg ml^{-1} is used. In particular, after 24 h of incubation with free drug, HeLa and IGROV1 cells were 50 % and 90 % viable, respectively, in agreement with previous literature results [67]. In the case of incubation with drug-loaded PELGA10 and PELGA20 NPs, the cytotoxic response was less significant and basically the same for both NP

formulations. In particular, a slight reduction (around 20 %) of HeLa cell viability was observed after exposure to Dox-loaded NPs, thus demonstrating that NPs able to sustain Dox release induce a lower cytotoxicity compared to the free drug at the same concentration. In the case of IGROV1 cells, no cytotoxic effects were observed.
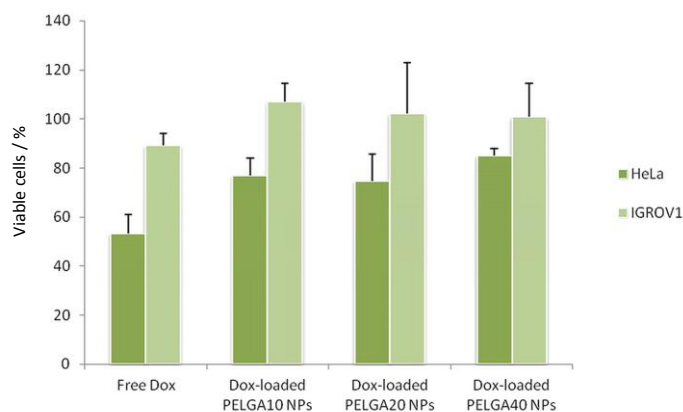
Figure 8. *Cytotoxicity assay in 2D cell culture conditions. Percentage of viable HeLa and IGROV1 cells treated with 2 μg mL^{-1} free Dox and with Dox-loaded PELGA10, PELGA20 and PELGA40 NPs for 24 hours. p < 0.05.*

Dox-loaded PELGA40 NPs elicited a weaker cytotoxic response compared to the smaller PELGA10 and PELGA20 NPs. This effect was immediately related to a higher diameter and subsequent inability to enter cells. Control experiments were carried out using placebo NPs, which were non-cytotoxic in all formulations (data not shown), suggesting that the low cytotoxicity could be ascribed to the low percentage of Dox released. The results of the 2D cytotoxicity assays were consistent with the drug release kinetics and NP uptake observations. Indeed, after 24 h in buffer medium at pH 7.4, the percentage of released Dox was 30.3 $\pm$ 4.0 %, 18.8 $\pm$ 1.8 % and 0.55 $\pm$ 0.3 % for the PELGA10, PELGA20 and PELGA40 NPs, respectively. These values approximately correspond to Dox concentrations of 0.60, 0.35 and 0.01 μg ml^{-1} in the cell culture medium, much lower than the concentration of free Dox (2 μg ml^{-1}) used to incubate the cells. Moreover, CLSM observations revealed that the NPs tend to localize within the

cell cytoplasm, and this contributes to make them less cytotoxic than free Dox, which tends to accumulate into the nucleus. Actually, the intracellular location is expected to play an important role, as it directly correlates with the cytotoxicity response and pharmacological effect of internalized NPs. In fact, it has recently been suggested that PLGA–PEG NPs are translocated via a lysosomal pathway after uptake [72]. Lysosomes contain varying concentrations of hydrolases, which promote NP degradation and therefore Dox release and transport towards the cell nucleus and, ultimately, the cytotoxic effect. The latter is more significant in the case of PELGA10 and PELGA20 NPs compared to PELGA40 NPs, and this can be reasonably ascribed to the decrease of device nanoporosity with increasing PELGA concentration in the organic phase of the emulsion. All considered, the results of the cytotoxicity assays confirmed that HeLa cells are much more vulnerable than IGROV1 to both non-encapsulated and encapsulated Dox. Furthermore, the data clearly show that the cytotoxic response is promoted by the size-dependent possibility of NP internalization, and is more significant in the case of the PELGA20 devices, which showed a 24 h burst release that strongly increased when the NPs experienced low lysosomal pH, which is related to a higher concentration of intracellular free Dox diffusing to the nucleus.

To study the effect of NP size on cell toxicity in 3D, we incubated cells with PELGA NPs in matrices made up of collagen, which is the major constituent of the ECM in malignant tumors [73]. Experiments were performed on HeLa cells, which were more susceptible to Dox compared to the IGROV1 cell line. In particular, the internalization and cytotoxicity of PELGA10 and PELGA20 NPs in 2D were not significantly different and, for this reason, the cytotoxic effect of only PELGA10 and PELGA40 NPs was assessed, to highlight the importance of NP size in cell viability. The cytotoxic response was quantified after 24 h of culture and expressed in terms of percentage of dead cells in 3D collagen matrices upon contact with free Dox or Dox-loaded NPs. HeLa cells were grown in 2.4 mg ml^{-1} collagen in the presence of free Dox and Dox-loaded PELGA10 or PELGA40 NPs, confined in the smaller chamber of the experimental system

(schematically drawn in **Fig. 2**), separated from the cell containing chamber by a porous membrane whose pore diameter (0.65 µm) was higher than the mean size of the NPs, thus allowing particle diffusion through the collagen. After 24 h of culture in the presence of free Dox or Dox-loaded particles, the cell morphology changed from stretched to round and an increment in cell fluorescence, indicating an intracellular accumulation of Dox, was observed (**Fig. 9(A2)**). In particular, the cytotoxic response was lower with PELGA40 compared to PELGA10 NPs, and this can be immediately correlated with the lower 24 h burst release observed with the PELGA40 formulation, as shown in **Fig. 4(B)** and discussed in this section.

The percentage of dead cells after 24 h of culture in collagen matrices indicated a cytotoxic effect of both free Dox and Dox-loaded PELGA NPs. As expected, the cytotoxicity decreased with increasing distance from the porous membrane (**Fig. 9(B)**). However, a contribution of particle transport in the collagen to the cytotoxic response cannot be excluded. Indeed, we observed the uptake of placebo fluorescent rhodamine-conjugated PELGA10 NPs in HT1080 cells seeded for 24 h within 2.4 mg ml^{-1} collagen gel (data not shown), indicating NP diffusion through the 3D matrix. Likewise, the transport of smaller PELGA10 NPs within the collagen gel is obviously enhanced compared to larger PELGA40 NPs, and therefore the cytotoxic effect in 3D is dependent on both particle diffusion within the matrix and Dox release. Furthermore, the amount of Dox released at neutral pH after 24 h must be considered; this is higher from PELGA10 than from PELGA40 NPs. Thus, to discriminate the contributions of particle diffusion and drug release to toxicity, the same experiments were carried out under NP confinement, using a membrane pore size of 0.05 µm, smaller than the particle size. Compared to standard 2D cell cultures, these conditions better resemble the *in vivo* tumor environment since, in most cases, device penetration through tumor interstitium is hampered after extravasation [74].
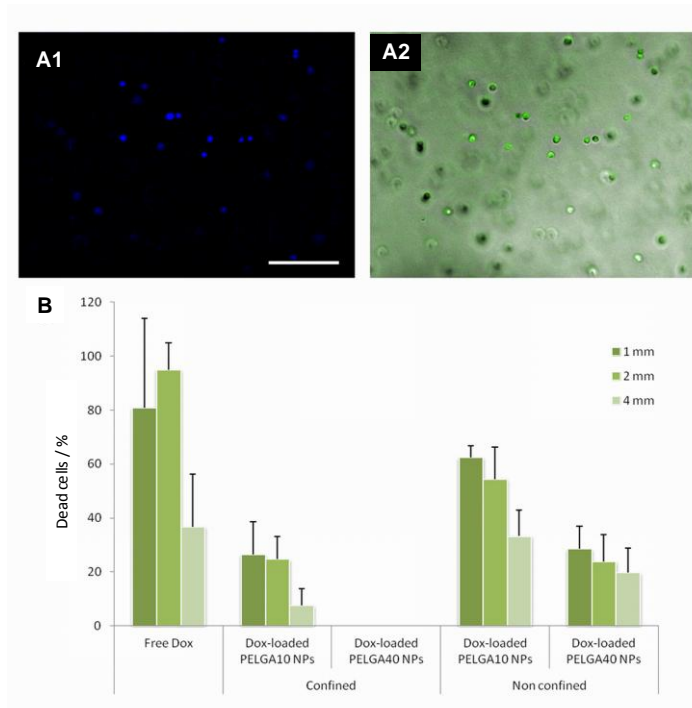
Figure 9. *Cytotoxicity against HeLa cells in 3D collagen gel. A. Results of cytotoxicity assay in 3D collagen matrices in presence of free Dox and Dox-loaded NPs. A1: Microscope images of HeLa cells in 3D culture conditions obtained by CellR after 24h of incubation with Dox-loaded PELGA10 NPs. DAPI staining of cell nuclei. A2: brightfield and fluorescence image overlapping. Green fluorescence indicates Dox intracellular accumulation. Magnification bar: 200 μm. B: Percentage of dead cells in presence of free Dox, PELGA10 and PELGA40 NPs with membranes having 0.05 μm (Confined) and 0.65 μm (Non confined) pore diameters, calculated at 1, 2 and 4 mm from the porous membranes. $p < 0.05$.*

In our experiments, the PELGA10 NPs elicited a cytotoxic effect which was lower and decreased with increasing distance from the porous membrane, while the PELGA40 particles did not induce any cytotoxicity (**Fig. 9(B)**). These results can be related to hampered transport of the devices through the gel matrix. Actually, a fraction of the PELGA10 NPs can cross the membrane pores, thus contributing to the cytotoxicity with their cargo features and burst release. In contrast, the larger PELGA40 NPs are expected to be mostly confined in the small chamber. Therefore, the lack of cytotoxicity of the PELGA40 NPs can be mainly attributed to a sublethal released amount of Dox at any distance from the porous membrane. These data show that, also in 3D matrices, Dox delivery from NPs is effective and, in particular, the cytotoxicity strongly depends upon the distance from the deposition site of the NPs (i.e., the porous membrane). On the other hand, with both 0.05 and 0.65 μm pore sizes, and at any distance from the

membrane, the cytotoxicity due to the free Dox was higher compared to the NPs, and basically independent of the size of the membrane pores. This is consistent with the FCS results, which showed that the diffusion coefficients (D) of Dox at 37 °C in water and collagen are quite similar, i.e. 2.12 ± 0.37 [59] and $1.80 \pm 0.09 \ 10^{-6} \ cm^2 \ s^{-1}$, respectively. On the other hand, the diffusion coefficient of Rhod–PELGA10 NPs decreases drastically in collagen gel. In particular, the D values are $4.58 \pm 0.41 \ 10^{-8} \ cm^2 \ s^{-1}$ in water and $8.50 \pm 5.44 \ 10^{-9} \ cm^2 \ s^{-1}$ in collagen. To further demonstrate the effect of the 3D collagen matrix on NP diffusion and cellular internalization, we quantified the Dox-free Rhod–PELGA10 NP uptake in HeLa cells cultured in 2D and 3D conditions. As shown in **Fig. 10**, the results demonstrate a higher nanoparticle uptake in 2D than in 3D after 24 h of incubation, in agreement with FCS measurements, indicating that collagen gel strongly hampers NP transport compared to water, thus limiting NP uptake in 3D.
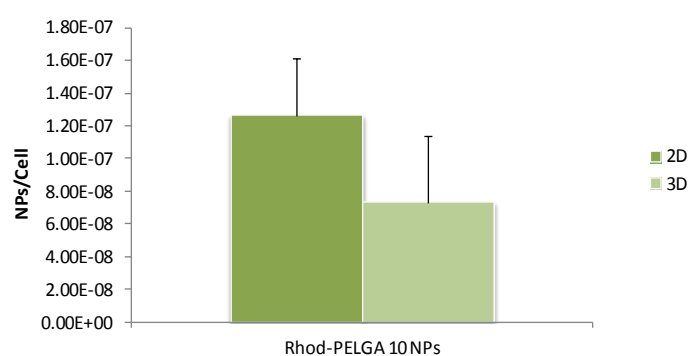
Figure 10. *Rhod-PELGA10 NP uptake by HeLa cells in 2D versus 3D culture conditions. p < 0.05.*

To summarize, our findings clearly demonstrate that the cytotoxic effect of NPs decreases with increasing device size, drug release kinetics and distance from the porous membrane. Indeed, 3D *in vitro* tumor models have been previously developed with the aim of studying the effect of anticancer drugs in tissue analogs, demonstrating that cell responses in 2D and 3D matrices are drastically different [31, 73, 75]. In this study, the cytotoxicity was much lower when the

NPs were confined in a compartment separated from the cells while, when the NPs were not confined, the cell cytotoxicity in 3D was promoted also in the case of the PELGA40 NPs, which released a much smaller amount of Dox in 24 h. This indicates that larger devices can also diffuse within the collagen matrix. Taken all together, the results show that, assuming the EPR effect and subsequent NP accumulation in the interstitial area, Dox is less cytotoxic when encapsulated in NPs also in 3D matrices. In particular, when 0.05 μm pore size is used, only small NPs are cytotoxic, due to the fraction travelling across the collagen gel, therefore highlighting the importance of NP transport through the matrix. This clearly demonstrates the importance of the combination of sub-100 nm NP size and controlled release features as key parameters governing NP diffusion and Dox release within 3D matrices. Interestingly, the produced NPs could elicit, in the 3D culture conditions employed in this work, a cytotoxic response at distances of the order of some mm from the deposition site, due to both drug release and device transport through the collagen matrix. It must be underlined that the collagen concentrations used in this work do not resemble the actual *in vivo* conditions of a tumor matrix, which is intrinsically unsteady and fibrotic, and contains many dead end capillaries. However, <100 nm devices with controlled release features are potentially promising as they may travel through tumor interstitium and exert their cytotoxic effect. In particular, **Fig. 9(B)** indicates that by matching proper NP size and controlled release features (i.e. optimizing the polymer concentration in the organic phase of the emulsion), a cytotoxic response can be elicited by a device traveling through collagen, which is strongly favored by size reduction. In addition, we showed that PELGA40 NPs, even if they possess a diameter suitable for EPR, are basically unable to induce cell death when in confinement conditions, which further underlines the importance of NP diffusion to carry the drug in the proximity of target cells.

3.5. CONCLUSIONS

In this work, PEG was covalently bound to PLGA and the resulting PELGA copolymer was used to fabricate biodegradable NPs by a modified double emulsion technique to obtain sub-100 nm cargos for pH-dependent drug delivery to tumors. PELGA10 NPs could not provide a relevant response to pH, but Dox release was sustained at neutral pH and with high PELGA concentration in the organic phase of the emulsion; at acidic pH, drug release was much faster (around 75 % in 5 days for PELGA20 NPs). Cellular studies showed that, depending on the NP formulation and size, smaller PELGA NPs were effectively internalized by HeLa cells, while only a small amount of NPs could enter IGROV1 cells. In contrast, NPs with larger diameters (around 175 nm) could not be internalized by either cell population. In all cases, the NPs were less cytotoxic compared to free Dox, depending upon NP size and formulation and drug release kinetics. 3D experiments on HeLa cells showed a fundamental contribution of the NP size to the cell death rate, in that an increase in cytotoxicity at any distance was related to the diffusion of NPs within 3D constructs. More importantly, the smaller NPs could diffuse in collagen matrices for some mm, which is a relatively long diffusion path.

Overall, these findings underline that, even if NP uptake can promote cytotoxicity, the results obtained in 3D with PELGA40 NPs (which cannot enter cells) show that some cell death can be elicited even in the absence of NP internalization.

This suggests a new possible paradigm for controlled drug delivery in tumors, which is generally considered to be triggered by NP uptake by target cells. Particle size is a major feature from both a technological and a biological standpoint and must be properly taken into account to engineer the NP formulation and fabricate safe devices for the prolonged delivery of chemotherapeutic drugs and for reliable cell uptake/cytotoxicity studies. The results can be used as a basis to study NP applications for safe delivery of antitumor drugs.

3.6. REFERENCES

1. Cho, H.-J., et al., *Self-assembled nanoparticles based on hyaluronic acid-ceramide (HA-CE) and Pluronic (R) for tumor-targeted delivery of docetaxel.* Biomaterials, 2011. **32**(29): p. 7181-7190.
2. He, Q., et al., *A pH-responsive mesoporous silica nanoparticles-based multi-drug delivery system for overcoming multi-drug resistance.* Biomaterials, 2011. **32**(30): p. 7711-7720.
3. Vergara, D., et al., *Lapatinib/Paclitaxel polyelectrolyte nanocapsules for overcoming multidrug resistance in ovarian cancer.* Nanomedicine-Nanotechnology Biology and Medicine, 2012. **8**(6): p. 891-899.
4. Bae, K.H., H.J. Chung, and T.G. Park, *Nanomaterials for cancer therapy and imaging.* Molecules and Cells, 2011. **31**(4): p. 295-302.
5. Gao, Y., et al., *Targeted Nanoassembly Loaded with Docetaxel Improves Intracellular Drug Delivery and Efficacy in Murine Breast Cancer Model.* Molecular Pharmaceutics, 2008. **5**(6): p. 1044-1054.
6. Wang, J., D. Mongayt, and V.P. Torchilin, *Polymeric micelles for delivery of poorly soluble drugs: Preparation and anticancer activity in vitro of paclitaxel incorporated into mixed micelles based on poly(ethylene glycol)-lipid conjugate and positively charged lipids.* Journal of Drug Targeting, 2005. **13**(1): p. 73-80.
7. Tang, N., et al., *Improving penetration in tumors with nanoassemblies of phospholipids and doxorubicin.* Journal of the National Cancer Institute, 2007. **99**(13): p. 1004-1015.
8. Cho, K., et al., *Therapeutic nanoparticles for drug delivery in cancer.* Clinical Cancer Research, 2008. **14**(5): p. 1310-1316.
9. Davis, M.E., Z. Chen, and D.M. Shin, *Nanoparticle therapeutics: an emerging treatment modality for cancer.* Nature Reviews Drug Discovery, 2008. **7**(9): p. 771-782.
10. Ferrari, M., *Cancer nanotechnology: Opportunities and challenges.* Nature Reviews Cancer, 2005. **5**(3): p. 161-171.
11. Peer, D., et al., *Nanocarriers as an emerging platform for cancer therapy.* Nature Nanotechnology, 2007. **2**(12): p. 751-760.
12. Vonarbourg, A., et al., *Parameters influencing the stealthiness of colloidal drug delivery systems.* Biomaterials, 2006. **27**(24): p. 4356-4373.
13. Litzinger, D.C., et al., *EFFECT OF LIPOSOME SIZE ON THE CIRCULATION TIME AND INTRAORGAN DISTRIBUTION OF AMPHIPATHIC POLY(ETHYLENE GLYCOL)-CONTAINING LIPOSOMES.* Biochimica Et Biophysica Acta-Biomembranes, 1994. **1190**(1): p. 99-107.
14. Nomura, T., et al., *Effect of particle size and charge on the disposition of lipid carriers after intratumoral injection into tissue-isolated tumors.* Pharmaceutical Research, 1998. **15**(1): p. 128-132.
15. Schaedlich, A., et al., *Tumor Accumulation of NIR Fluorescent PEG PLA Nanoparticles: Impact of Particle Size and Human Xenograft Tumor Model.* Acs Nano, 2011. **5**(11): p. 8710-8720.
16. Schipper, M.L., et al., *Particle Size, Surface Coating, and PEGylation Influence the Biodistribution of Quantum Dots in Living Mice.* Small, 2009. **5**(1): p. 126-134.
17. Bae, Y.H. and K. Park, *Targeted drug delivery to tumors: Myths, reality and possibility.* Journal of Controlled Release, 2011. **153**(3): p. 198-205.

18. Toy, R., et al., *The effects of particle size, density and shape on margination of nanoparticles in microcirculation.* Nanotechnology, 2011. **22**(11).

19. Farokhzad, O.C. and R. Langer, *Impact of Nanotechnology on Drug Delivery.* Acs Nano, 2009. **3**(1): p. 16-20.

20. Moghimi, S.M., A.C. Hunter, and J.C. Murray, *Long-circulating and target-specific nanoparticles: Theory to practice.* Pharmacological Reviews, 2001. **53**(2): p. 283-318.

21. Nel, A.E., et al., *Understanding biophysicochemical interactions at the nano-bio interface.* Nature Materials, 2009. **8**(7): p. 543-557.

22. Verma, A. and F. Stellacci, *Effect of Surface Properties on Nanoparticle-Cell Interactions.* Small, 2010. **6**(1): p. 12-21.

23. Wang, F., et al., *Reciprocal interactions between beta 1-integrin and epidermal growth factor receptor in three-dimensional basement membrane breast cultures: A different perspective in epithelial biology.* Proceedings of the National Academy of Sciences of the United States of America, 1998. **95**(25): p. 14821-14826.

24. Anders, M., et al., *Disruption of 3D tissue integrity facilitates adenovirus infection by deregulating the coxsackievirus and adenovirus receptor.* Proceedings of the National Academy of Sciences of the United States of America, 2003. **100**(4): p. 1943-1948.

25. Beningo, K.A., M. Dembo, and Y.I. Wang, *Responses of fibroblasts to anchorage of dorsal extracellular matrix receptors.* Proceedings of the National Academy of Sciences of the United States of America, 2004. **101**(52): p. 18024-18029.

26. Rhodes, N.P., et al., *Metabolic and histological analysis of mesenchymal stem cells grown in 3-D hyaluronan-based scaffolds.* Journal of Materials Science-Materials in Medicine, 2004. **15**(4): p. 391-395.

27. Lee, G.Y., et al., *Three-dimensional culture models of normal and malignant breast epithelial cells.* Nature Methods, 2007. **4**(4): p. 359-365.

28. Clift, M.J.D., et al., *The impact of different nanoparticle surface chemistry and size on uptake and toxicity in a murine macrophage cell line.* Toxicology and Applied Pharmacology, 2008. **232**(3): p. 418-427.

29. Zhang, M., et al., *Variation in the internalization of differently sized nanoparticles induces different DNA-damaging effects on a macrophage cell line.* Archives of Toxicology, 2011. **85**(12): p. 1575-1588.

30. Dhiman, H.K., A.R. Ray, and A.K. Panda, *Three-dimensional chitosan scaffold-based MCF-7 cell culture for the determination of the cytotoxicity of tamoxifen.* Biomaterials, 2005. **26**(9): p. 979-986.

31. Horning, J.L., et al., *3-D tumor model for in vitro evaluation of anticancer drugs.* Molecular Pharmaceutics, 2008. **5**(5): p. 849-862.

32. Child, H.W., et al., *Working Together: The Combined Application of a Magnetic Field and Penetratin for the Delivery of Magnetic Nanoparticles to Cells in 3D.* Acs Nano, 2011. **5**(10): p. 7910-7919.

33. Sivaraman, A., et al., *A microscale in vitro physiological model of the liver: Predictive screens for drug metabolism and enzyme induction.* Current Drug Metabolism, 2005. **6**(6): p. 569-591.

34. Yamada, K.M. and K. Clark, *Cell biology - Survival in three dimensions.* Nature, 2002. **419**(6909): p. 790-791.

35. Frederick, C.A., et al., *STRUCTURAL COMPARISON OF ANTICANCER DRUG DNA COMPLEXES - ADRIAMYCIN AND DAUNOMYCIN.* Biochemistry, 1990. **29**(10): p. 2538-2549.

36. Pigram, W.J., W. Fuller, and L.D. Hamilton, *Stereochemistry of intercalation: interaction of daunomycin with DNA.* Nature: New biology, 1972. **235**(53): p. 17-9.

37. Fornari, F.A., et al., *INTERFERENCE BY DOXORUBICIN WITH DNA UNWINDING IN MCF-7 BREAST-TUMOR CELLS.* Molecular Pharmacology, 1994. **45**(4): p. 649-656.

38. Momparler, R.L., et al., *Effect of adriamycin on DNA, RNA, and protein synthesis in cell-free systems and intact cells.* Cancer Research, 1976. **36**(8): p. 2891-5.

39. Barry, E., et al., *Anthracycline-induced cardiotoxicity: course, pathophysiology, prevention and management.* Expert Opinion on Pharmacotherapy, 2007. **8**(8): p. 1039-1058.

40. Ferreira, A.L.A., L.S. Matsubara, and B.B. Matsubara, *Anthracycline-induced cardiotoxicity.* Cardiovascular & hematological agents in medicinal chemistry, 2008. **6**(4): p. 278-81.

41. Injac, R., et al., *Acute doxorubicin nephrotoxicity in rats with malignant neoplasm can be successfully treated with fullerenol C-60(OH)(24) Via suppression of oxidative stress.* Pharmacological Reports, 2008. **60**(5): p. 742-749.

42. Gao, Z.G., et al., *Doxorubicin loaded pH-sensitive micelle targeting acidic extracellular pH of human ovarian A2780 tumor in mice.* Journal of Drug Targeting, 2005. **13**(7): p. 391-397.

43. Weinberg, B.D., et al., *Antitumor efficacy and local distribution of doxorubicin via intratumoral delivery from polymer millirods.* Journal of Biomedical Materials Research Part A, 2007. **81A**(1): p. 161-170.

44. Chen, Y., et al., *Anticancer efficacy enhancement and attenuation of side effects of doxorubicin with titanium dioxide nanoparticles.* International Journal of Nanomedicine, 2011. **6**: p. 2321-2326.

45. Mitra, S., et al., *Tumour targeted delivery of encapsulated dextran-doxorubicin conjugate using chitosan nanoparticles as carrier.* Journal of Controlled Release, 2001. **74**(1-3): p. 317-323.

46. Nielsen, U.B., et al., *Therapeutic efficacy of anti-ErbB2 immunoliposomes targeted by a phage antibody selected for cellular endocytosis.* Biochimica Et Biophysica Acta-Molecular Cell Research, 2002. **1591**(1-3): p. 109-118.

47. Verdun, C., et al., *TISSUE DISTRIBUTION OF DOXORUBICIN ASSOCIATED WITH POLYISOHEXYLCYANOACRYLATE NANOPARTICLES.* Cancer Chemotherapy and Pharmacology, 1990. **26**(1): p. 13-18.

48. Chiannilkulchai, N., et al., *DOXORUBICIN-LOADED NANOPARTICLES - INCREASED EFFICIENCY IN MURINE HEPATIC METASTASES.* Selective Cancer Therapeutics, 1989. **5**(1): p. 1-11.

49. Chiannilkulachai, N., et al., *HEPATIC TISSUE DISTRIBUTION OF DOXORUBICIN-LOADED NANOPARTICLES AFTER IV ADMINISTRATION IN RETICULOSARCOMA M-5076 METASTASIS-BEARING MICE.* Cancer Chemotherapy and Pharmacology, 1990. **26**(2): p. 122-126.

50.   Kattan, J., et al., *PHASE-I CLINICAL-TRIAL AND PHARMACOKINETIC EVALUATION OF DOXORUBICIN CARRIED BY POLYISOHEXYLCYANOACRYLATE NANOPARTICLES.* Investigational New Drugs, 1992. **10**(3): p. 191-199.

51.   Gehl, J., et al., *Combined doxorubicin and paclitaxel in advanced breast cancer: Effective and cardiotoxic.* Annals of Oncology, 1996. **7**(7): p. 687-693.

52.   Yousefpour, P., et al., *Polyanionic carbohydrate doxorubicin-dextran nanocomplex as a delivery system for anticancer drugs: in vitro analysis and evaluations.* International Journal of Nanomedicine, 2011. **6**: p. 1487-1496.

53.   Barry, M.A., C.A. Behnke, and A. Eastman, *ACTIVATION OF PROGRAMMED CELL-DEATH (APOPTOSIS) BY CISPLATIN, OTHER ANTICANCER DRUGS, TOXINS AND HYPERTHERMIA.* Biochemical Pharmacology, 1990. **40**(10): p. 2353-2362.

54.   Tewes, F., et al., *Comparative study of doxorubicin-loaded poly(lactide-co-glycolide) nanoparticles prepared by single and double emulsion methods.* European Journal of Pharmaceutics and Biopharmaceutics, 2007. **66**(3): p. 488-492.

55.   Pays, K., et al., *Double emulsions: how does release occur?* Journal of Controlled Release, 2002. **79**(1-3): p. 193-205.

56.   Korsmeyer, R.W., et al., *Mechanisms of potassium chloride release from compressed, hydrophilic, polymeric matrices: effect of entrapped air.* Journal of Pharmaceutical Sciences, 1983. **72**(10): p. 1189-91.

57.   Haustein, E. and P. Schwille, *Fluorescence correlation spectroscopy: Novel variations of an established technique*, in *Annual Review of Biophysics and Biomolecular Structure.* 2007. p. 151-169.

58.   Gosch, M. and R. Rigler, *Fluorescence correlation spectroscopy of molecular motions and kinetics.* Advanced Drug Delivery Reviews, 2005. **57**(1): p. 169-190.

59.   Biondi, M., et al., *New Insights into the Mechanisms of the Interactions Between Doxorubicin and the Ion-Exchange Hydrogel DC Bead T for Use in Transarterial Chemoembolization (TACE).* Journal of Biomaterials Science-Polymer Edition, 2012. **23**(1-4): p. 333-354.

60.   Lindfors, L., et al., *Amorphous drug nanosuspensions. 1. Inhibition of Ostwald ripening.* Langmuir, 2006. **22**(3): p. 906-910.

61.   Hancock, B.C. and M. Parks, *What is the true solubility advantage for amorphous pharmaceuticals?* Pharmaceutical Research, 2000. **17**(4): p. 397-404.

62.   Wang, Y., et al., *Co-delivery of drugs and DNA from cationic core-shell nanoparticles self-assembled from a biodegradable copolymer.* Nature Materials, 2006. **5**(10): p. 791-796.

63.   Coffin, M.D. and J.W. McGinity, *BIODEGRADABLE PSEUDOLATEXES - THE CHEMICAL-STABILITY OF POLY(D,L-LACTIDE) AND POLY (EPSILON-CAPROLACTONE) NANOPARTICLES IN AQUEOUS-MEDIA.* Pharmaceutical Research, 1992. **9**(2): p. 200-205.

64.   Schaedlich, A., et al., *How Stealthy are PEG-PLA Nanoparticles? An NIR In Vivo Study Combined with Detailed Size Measurements.* Pharmaceutical Research, 2011. **28**(8): p. 1995-2007.

65. Biondi, M., et al., *Bioactivated collagen-based scaffolds embedding protein-releasing biodegradable microspheres: tuning of protein release kinetics.* Journal of Materials Science-Materials in Medicine, 2009. **20**(10): p. 2117-2128.

66. Nabiev, I., et al., *Nonfunctionalized nanocrystals can exploit a cell's active transport machinery delivering them to specific nuclear and cytoplasmic compartments.* Nano Letters, 2007. **7**(11): p. 3452-3461.

67. Bénard, J., et al., *Characterization of a Human Ovarian Adenocarcinoma Line, IGROV1, in Tissue Culture and in Nude Mice.* Cancer Research, 1985. **45**(10): p. 4970-4979.

68. Harush-Frenkel, O., et al., *Targeting of nanoparticles to the clathrin-mediated endocytic pathway.* Biochemical and Biophysical Research Communications, 2007. **353**(1): p. 26-32.

69. Panyam, J., et al., *Rapid endo-lysosomal escape of poly(DL-lactide-co-glycolide) nanoparticles: implications for drug and gene delivery.* Faseb Journal, 2002. **16**(10).

70. Sahay, G., D.Y. Alakhova, and A.V. Kabanov, *Endocytosis of nanomedicines.* Journal of Controlled Release, 2010. **145**(3): p. 182-195.

71. Qaddoumi, M.G., et al., *Clathrin and caveolin-1 expression in primary pigmented rabbit conjunctival epithelial cells: Role in PLGA nanoparticle endocytosis.* Molecular Vision, 2003. **9**(68-69): p. 559-568.

72. Wang, H., et al., *Enhanced anti-tumor efficacy by co-delivery of doxorubicin and paclitaxel with amphiphilic methoxy PEG-PLGA copolymer nanoparticles.* Biomaterials, 2011. **32**(32): p. 8281-8290.

73. De Wever, O. and M. Mareel, *Role of tissue stroma in cancer cell invasion.* Journal of Pathology, 2003. **200**(4): p. 429-447.

74. Jain, R.K. and T. Stylianopoulos, *Delivering nanomedicine to solid tumors.* Nature Reviews Clinical Oncology, 2010. **7**(11): p. 653-664.

75. Doillon, C.J., et al., *Three-dimensional culture system as a model for studying cancer cell invasion capacity and anticancer drug sensitivity.* Anticancer Research, 2004. **24**(4): p. 2169-2177.

CHAPTER 4

Engineered nanoparticles with cleavable domains for safe delivery of doxorubicin

4.1. ABSTRACT

The incorporation of stimuli-responsive cassettes in engineered NPs is promising in achieving controlled and localized release of drugs, offering the chance to improve their therapeutic effects. Indeed, the localized delivery of anticancer drugs is mandatory to avoid or reduce the unwanted side effects to healthy cells, organs and tissue elicited by the cytotoxic drugs, and to increase the drug bioavailability and fraction accumulated in tumor. Although, a number of strategies to deliver drugs to target sites have been developed, physical obstacles to NP penetration within tumors due to aberrant vasculature and extracellular matrix (ECM) still remain to overcome. In the light of these considerations, the preparation of NPs able to safely carry a chemotherapic drug and release it specifically within tumor sites, possibly at extracellular level, is particularly attractive in the field of controlled drug delivery.

In this view, we report on the design of a novel nanocarrier, able to safely carry doxorubicin (Dox) in tumor tissues, and to respond to matrix metalloprotease-2 (MMP2) enzyme, which is over-expressed in ECM of tumors. Specifically, two MMP2 sensitive peptides were used as cleavable linkers between Dox and polyethylene glycol (PEG) to form a polymer-peptide-drug conjugate, working as a tumor-activated prodrug (TAP). The obtained TAP was then attached to the surface of 200 nm carboxyl-modified polystyrene model nanoparticles (NPs). The resulting TAP conjugated NPs were characterized *in vitro* for their release features at different MMP2 concentrations, in order to identify the minimum bioactive enzyme dose-response, and for their cytotoxic effect on three different human cell types, namely fibrosarcoma cell line (HT1080), primary dermal

fibroblasts (HDF) and umbilical vein endothelial cells (HUVECs), as models of tumor and healthy tissues. Results showed that Dox release from TAP NPs was specifically triggered by MMP2 cleavage and it was also dependent on MMP2 enzyme concentration. Furthermore, the produced NPs were cytotoxic against all cell lines in presence of MMP2 enzyme. On the contrary, no cytotoxic effect was observed for TAP NPs in absence of MMP2 pre-treatment, even if these systems could be internalized by cells. Taken all together, these data demonstrated the potentiality of TAP NP systems in the light of translating the same TAP production technology to biodegradable systems intended for the "on-demand" delivery of cytotoxic anticancer drugs.

4.2. INTRODUCTION

The use of nanoparticles (NPs) for the controlled release of anticancer drugs has been well studied in recent years [1-3] and is considered promising to increase the *in vivo* efficacy of the delivered drugs. The localized delivery of anticancer drugs is mandatory to avoid or reduce the unwanted side effects to healthy cells, organs and tissues elicited by the cytotoxic drugs, and to increase the drug bioavailability and fraction accumulated in tumor [4]. Actually, passive targeting obtained by the enhanced permeability and retention (EPR) effect is often insufficient to ensure an effective drug dose to the tumor site [5]. On the contrary, active targeting can allow a higher drug selectivity towards tumors by using suitable moieties so as to target the receptors overexpressed at the tumor site [6, 7] and enhance specific cellular uptake/internalization through receptor-mediated endocytosis [8-10]. For example, monoclonal antibodies (mAbs) [11-14] and small molecules such as folate [15] and galactose [16, 17], are commonly used as targeting ligands for NP formulations. Besides that, it must also be considered that *in vivo*, a number of biochemical and physical obstacles hamper NP and/or drug cellular internalization, and this generally results into a drastically lowered efficacy of the treatment. Indeed, even if a number of strategies to deliver drugs to tumor sites have been developed, physical obstacles to NP penetration within tumors due to aberrant vasculature and extracellular matrix (ECM) still remain to overcome [18]. In the light of this consideration, the preparation of NPs able to safely carry a chemotherapic drug and release it specifically within tumor sites, possibly at the extracellular level, is particularly attractive in the field of controlled drug delivery. In this context, physiological variations naturally occurring within tumors are interesting for the preparation of stimuli-responsive prodrugs or nanocarriers reacting to specific endogenous stimuli, such as pH and enzymes [19, 20]. This challenging goal can be attained by conjugating the drug(s) to specific bioactive molecules cleavable by the physiological stimulus. Actually, many anticancer drugs, such as methotrexate, paclitaxel, cisplatin and doxorubicin (Dox), have been specifically delivered to

tumor tissues after conjugation to polymers through bioactive molecules [21-24]. In tumors, many proteolytic enzymes, involved in a number of biological mechanisms and catalytic activities related with tumor progression, are overexpressed [25, 26]. In particular, matrix metalloproteinase-2 (MMP2, also known as gelatinase A) is a 72 kDa enzyme belonging to the matrix metalloproteinase family, [27] present in high concentrations at active tumor sites [28]. MMP2 hydrolyzes type IV collagen, which is a major constituent of tumor extracellular matrix (ECM), thus resulting in enhanced tumor progression [29], invasion and angiogenesis [30]. Thus, in this work MMP2 was chosen as the biological signal to be exploited to induce the release of drugs in those tissues in which the enzyme is overexpressed.

In literature, previous studies were mainly centered on the development of nanoparticles (NPs) inhibiting MMP2 action and therefore tumor progression. For example, iron-oxide NPs conjugated to chlorotoxin via poly(ethylene glycol) (PEG) silane functionalized with amine, were able to deactivate MMP2 on tumor surface, thus inhibiting cell invasion more efficiently compared to the peptide alone [31]. In another study, 50 nm magnetite NPs, functionalized with a specific protein (biotin or neutravidin) and conjugated to polyethylene glycol (PEG) by means of an MMP-sensitive substrate, were produced. The presence of high MMP concentrations caused the loss of PEG and therefore the self-assembly of NPs, which remained as aggregates in tumor sites [32].

Here we report on the design of a model NP, responding to MMP2 and releasing Dox only after enzyme exposure [33]. Two MMP2 cleavable peptides NH$_2$-Pro-Leu-Gly-Ser-Tyr-Leu-COOH (Mw = 648.76 Da; namely: pep A) and NH$_2$-Gly-Pro-Leu-Gly-Ile-Ala-Gly-Gln-COOH (Mw = 711.82 Da; namely: pep B) were used as sensitive linkers between Dox and PEG linker (Mw = 3500 Da), to form a polymer-peptide-drug conjugate, working as a tumor-activated prodrug (TAP). In both peptides the MMP-driven cleavage occurs near Gly unit. The obtained TAP was then attached to the surface of 200 nm carboxyl-modified polystyrene (PS) model NPs. PEG is a steric shield for NPs, and, when in tumor

microenvironment, the peptide is expected to be cleaved by the overexpressed extracellular MMP2, thus triggering Dox release. The resulting TAP-conjugated PS NPs were characterized for their *in vitro* release features at different MMP2 concentrations in order to identify the minimum bioactive enzyme dose-response. NP cytotoxicity was tested *in vitro* against three different human cell types, namely fibrosarcoma HT1080 cell line, primary dermal fibroblasts HDF and umbilical vein endothelial cells HUVECs, as models of tumor and healthy tissues.

4.3. MATERIALS AND METHODS

4.3.1. Chemicals

Doxorubicin Hydrochloride (purity > 99%) was purchased from Discovery Fine Chemicals (UK). N,N-diisopropylethylamine (DIEA, or Hünig's base), O-benzotriazole-N,N,N',N'-tetramethyluronium–hexafluoro-phosphate (HBTU), anhydrous N,N-dimethylformamide (DMF), piperidine, 1,1′-Carbonyldiimidazole (CDI), Trifluoroacetic acid (TFA), 2-(N-Morpholino) ethanesulfonic acid (MES) sodium salt, p-aminophenylmercuric acetate (APMA), acetonitrile (ACN) and water (HPLC grade) and buffer solutions were obtained from Sigma-Aldrich (USA). Fmoc-NH-PEG-COOH (Mw = 3500 Da) was obtained from JenKem Technology Inc. (USA). 200 nm polystyrene (PS) nanoparticles (NPs) modified on the surface with carboxyl groups (1% solid content), were obtained from Phosphorex (PolyspherexTM PS-COOH, Phosphorex Inc., USA). Recombinant Human Matrix metalloproteinase-2 (MMP2) from Peprotech Inc. (Peprotech, USA) was used. Milli-RO 10 Plus distilled and deionized water (Millipore, USA; 18MΩ resistance) was used.

4.3.2. Synthesis of MMP2-sensitive peptides

MMP2 sensitive peptides (NH_2-Pro-Leu-Gly-Ser-Tyr-Leu-COOH, namely peptide A; NH_2-Gly-Pro-Leu-Gly-Ile-Ala-Gly-Gln-COOH, namely peptide B) were synthesized manually using the standard solid-phase 9-fluorenylmethoxycarbonyl (Fmoc) method [34]. A Wang resin carrying a free C-terminus for the selective binding of Dox in solution was used. The identity of the purified peptides was confirmed by electron spray ionization liquid chromatography-mass spectrometry (ESI LC-MS) using a Phenomenex (Torrance, CA) C18 column (4.6x250 mm size, 5 μm particle size) eluted with a 0.1 % v/v TFA solution in water (solvent A) and acetonitrile (solvent B) solvent mixture. A linear gradient from 15 to 95 % solvent B over 20 min at a flow rate of 1 ml/min was used on a Thermo electron MSQ surveyor ESI-LC MS spectrometer.

4.3.3. Synthesis of Fmoc-Peg 3500-MMP2 peptide conjugates

The coupling reaction of Fmoc-PEG-COOH with MMP2 sensitive peptides linked on resin was performed manually using Fmoc-PEG-COOH/HBTU/DIPEA (1.2 eq). To verify the reaction progress, the presence of the Fmoc group on the peptides was followed spectrophotometrically by analytic RP-HPLC on a 1220 Infinity LC System (Agilent Technologies Inc. US), analyzing crude conjugates from test cleavage. The peptides were then purified to homogeneity by preparative reverse-phase high-pressure liquid chromatography (RP-HPLC) using a Shimadzu class LC10 equipped with a diode array detector (SPD-M10AV). The samples were injected in a Phenomenex (Torrance, CA) C18 column (22x250 mm size, 5 µm particle size) eluted with a 0.1 % v/v TFA solution in water (solvent A) and acetonitrile (solvent B) solvent mixture. A linear gradient from 15 to 95% solvent B over 20 min at a flow rate of 20 mL/min was used. The collected fractions were lyophilized for 48 h at -54.6°C (Heto powerDry PL6000, Thermo electron Corp., USA) and analyzed by analytical RP-HPLC as perviously resorted.

4.3.4. Synthesis of the MMP2 sensitive tumor activated prodrug (TAP)

Fmoc-PEG-peptide-Dox conjugates were synthesized using HATU as a coupling reagent. One equivalent of PEG-peptides sequences and doxorubicin hydrochloride (1.5 Eq) were dissolved in anhydrous DMF, and DIEA (2 Eq) was added. The resulting solution was stirred 15 min at 4°C in dark. Afterwards, HATU (1.5 Eq) solution in DMF was added and the reacting mixture was stirred overnight at room temperature. Reaction was monitored by analytical RP-HPLC as reported previously. The synthesis of the conjugate was verified by assessing of the absorption spectra of Fmoc and Dox on the peptide. Afterwards, to remove the protective Fmoc group from the conjugate, piperidine was added into the reactor to a final 40 % v/v solution in DMF. The reaction mixture was then precipitated from DMF solution with cold ethyl ether. The crude mixture was dissolved in ACN/water containing 0.1 % v/v TFA, purified by preparative RP-HPLC and lyophilized as described in the previous section.

4.3.5. Preparation and characterization of TAP- conjugated nanoparticles

TAP-conjugated NPs were prepared by superficially binding the obtained TAPs on PS-COOH NPs, which were washed three times with 50mM MES buffer (pH = 6.0) solution prior to use. Then, 10 mg of TAP were added to 1 mL NP suspension (1 % w/v) in MES buffer solution; the resulting suspension was stirred 15 minutes at room temperature and 2 mg CDI were added. The pH of the suspension was adjusted to 6.5 by dropwise addition of 0.05 M HCl, and continuously stirred for further 2 h to allow reaction completion. Afterwards, the suspension was washed three times with distilled water using a concentrator membrane (Spin-X UF 500, Corning Corp., UK, 100 kDa molecular weight cutoff). The washing solutions were collected to measure unreacted prodrug concentration by spectrofluorimetric analysis (Wallac 1420 Victor2TM, Pekin-Elmer, USA; λ = 488nm). TAP binding efficiency was easily calculated as follows:

$$\eta(\%) = 100 \cdot \frac{m_0 - C_w \cdot V_w}{m_0}$$

Where η is the binding efficiency, m_0 the total TAP mass, C_w the concentration of the washed TAP and V_w the washed volume.

4.3.6. Characterization of TAP NPs

Mean size, size distribution and zeta-potential of NPs were determined by triplicate laser light scattering measurements (Zetasizer Nano ZS, Malvern Instruments, UK) on 1 % w/v NP suspensions. NP morphology was analyzed by transmission electron microscopy (TEM EM208S, Philips, The Netherlands) by placing 10 µL of NP suspensions sample on a TEM grid, which was then allowed to air dry for 5 minutes.

4.3.7. In vitro cleavage assay of TAP-conjugated nanoparticles

In vitro release of Dox from 200 nm NPs was evaluated in MMP2 buffer solution; the enzyme was activated with p-aminophenylmercuric acetate (APMA) as described in the following: 10 mM solution of APMA, (3.9 mg) in

0.1 M NaOH (1 mL) was diluted with 50 mM Tris•HCl buffer (99 mL, pH 7.5). The pH of the obtained solution was adjusted to pH 7.2. MMP2 solutions in buffer (2 mL; 50 mM HEPES, 200 mM NaCl, 10 mM $CaCl_2$, 1 mM $ZnCl_2$, pH 7.4) were activated for 3 h at 37°C to obtain final enzyme concentrations of 0.1, 0.5, 1, 5, 10, 20 and 40 nM. For release tests, 100 μl of NP suspension (200 nm size) were first centrifuged at 13,000 rpm for 30 min. Then, the supernatant was carefully removed, and finally 200 μL of blank buffer or activated MMP2 buffer (at the given enzyme concentrations) were added. NPs were resuspended by vortexing for 5 min and all the tubes were placed in a thermostatic bath at 37°C under agitation at 100 rpm (HT TR-225, INFORS HT Corp., Switzerland). At scheduled time intervals, the samples were centrifuged at 13,000 rpm for 30 min and the supernatant was analyzed for Dox content by spectrofluorimetric assay. Experiments were run in triplicate. The linearity of the response was verified over the 0 – 2 μg/mL concentration range ($r^2 > 0.99$).

4.3.8. Cell culture

To test the biological effect of the NPs, human fibrosarcoma cells (HT1080), primary human dermal fibroblasts (HDF) and primary human umbilical vein endothelial cells (HUVECs) were used. The latter were isolated by collagenase treatment of human umbilical veins and cultured in human endothelial-SFM basal growth medium (Gibco) supplemented with 20 % fetal bovine serum (FBS, Gibco), 100 U/mL penicillin, 100 mg/mL streptomycin and 1 X endothelial cell growth factor (ECGF, Sigma). The HT1080 cells were cultured with complete medium, composed of Eagle's minimal essential medium (EMEM) supplemented with 10 % FBS, 100 U/mL penicillin, 100 mg/mL streptomycin. The HDF cells were cultured with EMEM supplemented with 20 % FBS, 100 U/mL penicillin, 100 mg/mL streptomycin and 2 X non essential amino-acids. Cells were incubated in a humidified controlled atmosphere with 95 % to 5 % ratio of air/CO_2, at 37°C. Medium was changed every 2-3 days. All experiments were performed in triplicate.

4.3.9. Cytotoxicity assay

Adherent cells were seeded in 96 well microplates at a density of $1 * 10^4$ cells/well at a final volume of 100 μL and incubated for 24 h in a humidified atmosphere at 37 °C and 5 % CO_2 to obtain a subconfluent monolayer. Cells were treated with Dox free at final concentration of 4 μg mL^{-1} in cell culture medium and placebo polystyrene NPs as positive and negative controls, respectively. In particular, cells were incubated with TAP NPs at a concentration that allowed a final Dox release of 4 μg mL^{-1} after 24h incubation with MMP2 enzyme, according to the release kinetic curve (**Fig. 4B**). TAP NPs were simply added to cell culture medium or pre-treated with 40 nM MMP2 activated enzyme as described above. All samples were in a final volume of 100 μl. The metabolic activity of all cell cultures was determined after 1, 2, 5 and 7 days of exposure by using standard Alamar Blue assay (Invitrogen). Briefly, after incubation time, cells were washed with PBS and 150 μl of Dulbecco's modified Eagle's medium without phenol red (Gibco), containing 10 vol % Alamar Blue reagent, was added to each well and samples were incubated for 4 hours at 37 °C. The solution was subsequently removed from the wells and analyzed with a spectrophotometer (1420 Victor, Perkin Elmer) at wavelengths of 570 and 600 nm. Data represent the cell viability percentage of treated cells normalized to non treated cells.

4.3.10. Confocal microscopy for nanoparticle uptake

HT1080 cells were incubated with pre-treated and non pre-treated TAP NPs at the same concentrations used for cytotoxicity assay for 24 hours at 37 °C in 5 % CO2. Then, samples were washed two times with PBS to remove non internalized NPs and fixed with paraformaldehyde 4 % for 20 min. Finally, cell nuclei were stained with DAPI. Samples were observed by confocal multiphoton microscope system (Leica TCS SP5 MP) with a 63 X oil immersion objective. Images were acquired with a resolution of 1024x1024 pixels.

4.4. RESULTS

4.4.1. TAP NP synthesis

Purified peptides were obtained with yields > 90 %. Figure 1 reports the results of the synthesis of the MMP2 sensitive peptides, of the Fmoc-PEG-MMP2 adduct and of the TAP. Figure 1A shows, the HPLC chromatogram of Peptide A (**Fig. 1B**). Subsequently, the binding of Fmoc-PEG-COOH on NH_2 terminus of peptide on resin was confirmed by RP-HPLC analysis of the crude conjugate, following the specific Fmoc absorbance appearance at 301 nm into second peak (panel C) (containing conjugate Fmoc-PEG-Peptide). The yield of PEG coupling on resin-peptides was about 20-25 %. The purified Fmoc-conjugate was then bound to Dox (**Figs. 1E and 1F**). Fmoc-TAP synthesis was verified by the absorbance appearing at 301 nm (Fmoc) and at 485 nm (Dox) in the third peak at 17 min (panel E).
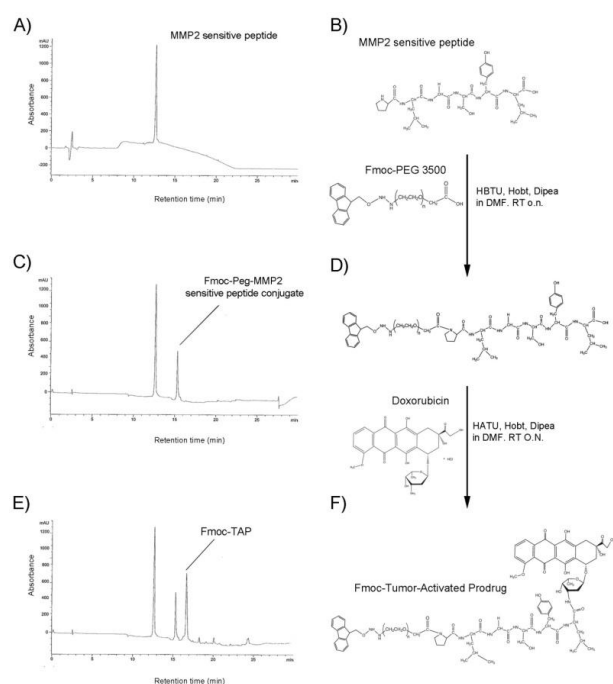
Figure 1. *Step synthesis and characterization of TAP. A) HPLC profile of MMP2 sensitive peptide; B) chemical structure of MMP 2A sensitive peptide; C) HPLC profile of reaction mix from Fmoc-PEG linked to MMP 2A peptide; the formation of the conjugate is highlighted by peak appearance at 15 min, that show Fmoc absorbance at 301 nm; D) chemical structure of Fmoc-PEG-MMP 2A sensitive peptide conjugate; E) HPLC profile of reaction mixture after ligation of Doxorubicin on conjugate added with MMP 2A sensitive peptide; F) Chemical structure of Fmoc-TAP product synthesized.*

PEG amine group was then de-blocked from Fmoc moiety through piperidine treatment and purified. Finally, TAP was conjugated on NPs with a 20-30% binding efficiency (**Table 1**).

	NP	TAP NPs (Peptide A)	TAP NPs (Peptide B)
size (nm)*	177 ± 1	179 ± 2	180 ± 1
ζ-potential (mV)	-50.5 ± 0.6	-20.5 ± 2.6	-19.5 ± 1.5
η	-	25 ± 5	23 ± 4

Table 1 - *Size and ζ-potential of Dox-conjugated PS-NPs. * PDI < 0.2*

4.4.2. NP characterization

Fig. 2 shows the transmission electron microscope (TEM) images of the as-prepared, randomly distributed, blank (**Fig. 2A**) and TAP-conjugated PS-NPs with A and B peptides (**Figs. 2B and 2C**, respectively). The insets show single representative NPs.
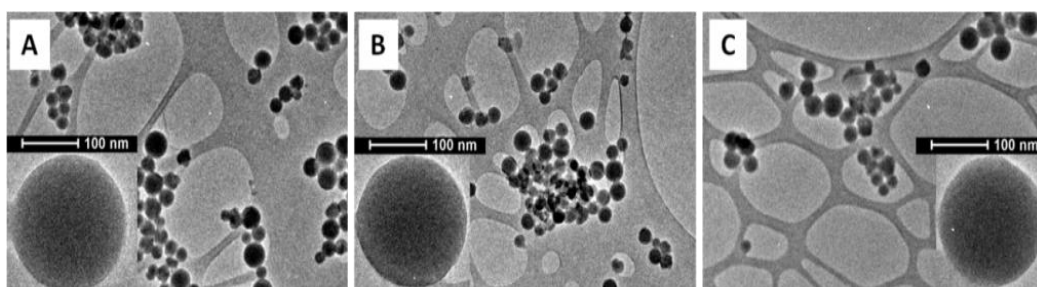

Figure 2. *TEM images of: A) unmodified PS-NPs; B) TAP-conjugated NPs by peptide A; C) and TAP- conjugated NPs by peptide B.*

As shown in **Fig. 3** and summarized in **Table 1**, the conjugation of the TAP to PS-NPs causes negligible changes in diameter of the NPs (from about 177 to about 180 nm) compared to the blank PS NPs. In contrast, the conjugation with TAP entailed considerable variations of the ζ-potential of the NPs, which changed from about -50 mV to about -20 mV when the conjugation was carried

out with both A and B peptides. This suggests that the addition of the hydrophilic segments of the PEG can partially mask the terminal carboxyl group of PS-NPs and does not affect NP colloidal stability.

4.4.3. Doxorubicin release kinetics from TAP NPs

In vitro release profiles of Dox from TAP MMP-sensitive NPs were evaluated by a standard sampling-separation method as described in the *Materials and Methods* section. Dox release was investigated in MMP-free medium (**Fig. 3A**) as well as at three different MMP2 concentrations (10, 20 and 40 nM), (**Figs. 3B and 3C**). In the absence of the enzyme, Dox was released very slowly and, after 5 days of incubation in enzyme-free buffer, the percentage of the released drug was 1.5 % (peptide A) and 7.3 % (peptide B). On the contrary, the MMP2 presence within the release medium induced a much faster rapid Dox release, which reached a plateau after approximately 10 h at 37 °C. The increment of Dox released percentage was 40-50 fold higher in the case of TAP-A NPs, and 70-80 fold higher for TAP-B NPs compared to the case of MMP2-free releae medium. In particular, when the TAP was conjugated to the NPs through the peptide A, the released percentage of Dox after 24 h of incubation was approximately between 19 % (concentration 10 nM) and 49 % (concentration 40 nM). In the case of the TAP conjugated to NPs by peptide B, the release after 24 h was between about 88 % (concentration 10 nM) and 95 % (20 and 40 nM), thus showing that peptide B is more active than peptide A in inducing faster Dox release. It must be also noticed that in both TAP NP formulations, the enzyme effect reaches a saturation above 20 nM, while, below 20 nM MMP2 concentration, a reduction in drug release rate was observed.
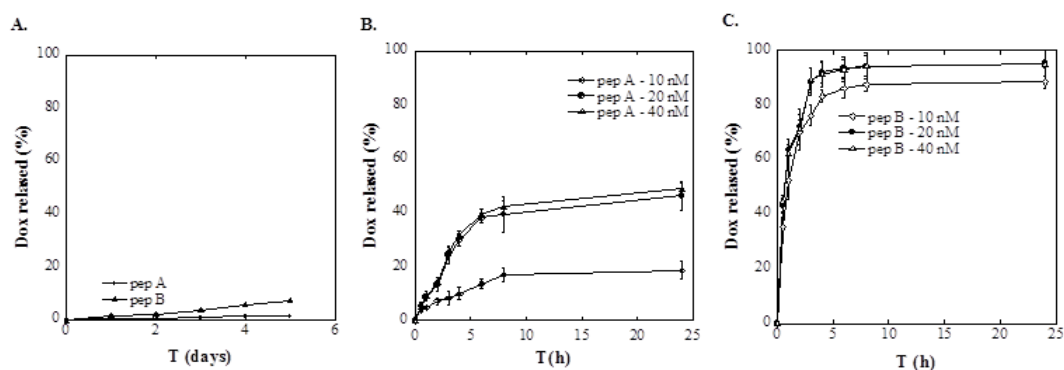
Figure 3. *In vitro release profiles of Dox release from TAP-conjugate PS-NPs in: A) PBS; B) MMP-activated buffer, peptide A; C) MMP-activated buffer, peptide B.*

In particular, analyzing dose-dependent release, as shown in **Fig. 4**, below 1 nM enzyme concentration a drastic decrease in drug release profile was observed after 2h incubation, while above 1 nM a slight increase of Dox release until 20 nM was obtained, and this effect was more evident in the case of TAP-B NPs.
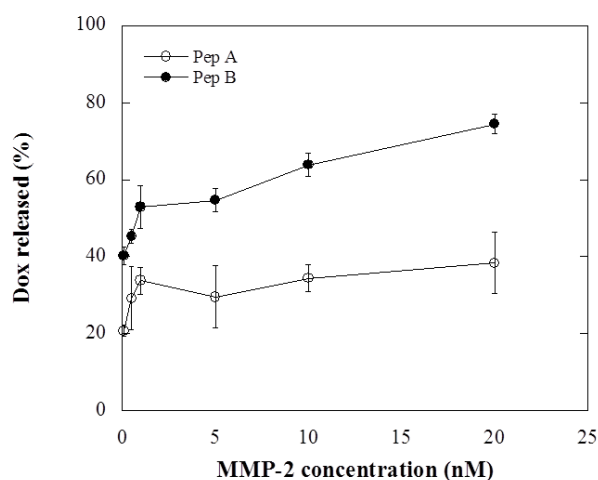
Figure 4. *In vitro release profiles of Dox released from TAP-conjugate PS-NPs after 2h incubation with different MMP2 enzyme concentrations.*

4.4.4. TAP NP cytotoxicity and uptake

The cytotoxic effect of TAP NP delivery systems was evaluated by an *in vitro* Alamar Blue assay on HT1080, HDF and HUVEC cells. **Fig. 5** shows the cell viability percentage of treated cells normalized to non-treated cells. As expected, a significant cytotoxic effect between 1 day and 7 days was observed for free

Dox at 4 μg mL^{-1}. The cytotoxic effect was higher for tumor than healthy and primary cells. In particular, HT1080 cell viability drastically decreased already after 24 hours of incubation with the free drug up to 36 %. On the other hand, a slighter reduction of cell viability percentages was detected for HDF and HUVECs (66 % and 73 %, respectively). Furthermore, this gap continued along the incubation time. Also TAP NPs, pre-treated for 24h with MMP2 activated enzyme, showed a cytotoxic effect on all the cell types. In particular, in agreement with Dox release kinetics, the cytotoxic effect was more evident for NPs functionalized with peptide B compared to peptide A. Moreover, the cytotoxic response increases by increasing incubation time. However, the decrease of cell viability was less evident than free Dox, probably due to the presence of aminoacidic residues bound to drug molecule after the enzyme cleavage that reduced Dox effects. On the other hand, no cytotoxic effects until 48 hours were observed when TAP NPs, without enzyme pre-treatment, were used. Increasing incubation time, a very slight reduction in cell viability, in particular for HT1080 cells, was detected.
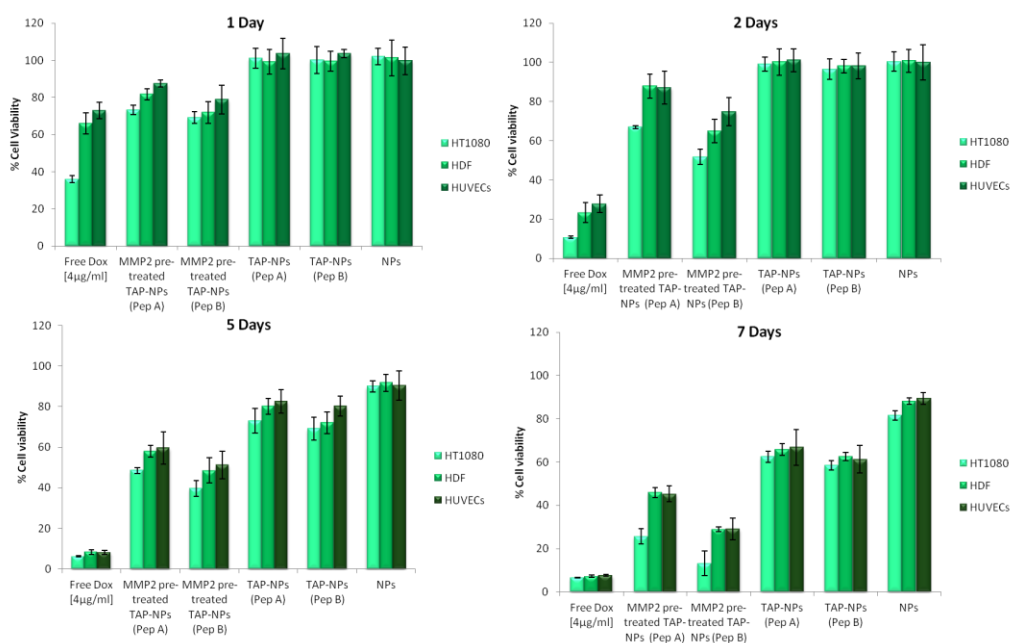
Figure 5. *Cytotoxicity assay of TAP NPs and MMP2 pre-treated TAP NPs in HT1080, HDF and HUVECs cells follow until one week of incubation. Cell viability was expressed as percentage respect to the non-treated control cells.*

These results probably suggested that NPs could be entrapped in the lysosome where the acid pH (5.0) could cut the link between NPs and peptide with consequent drug release. Finally, control experiments, carried out by using placebo NPs, showed no cytotoxic effects in all cell lines up to 7 days of culture. In order to verify the cellular uptake of Dox, HT1080 cells were observed by confocal microscope after 48 hours of incubation with TAP NPs and MMP2 pre-treated TAP NPs (**Fig. 6**). For cells incubated with MMP2 pre-treated TAP NPs, as expected, the images showed both a diffuse and spotted fluorescence signal within cell cytoplasm, indicating the partial release of free Dox (fig. 6 A and B). This Dox intracellular distribution was more evident for TAP-B NPs than TAP-A NPs. Interestingly, also for cells incubated with non pre-treated TAP NPs, an intracellular fluorescence was detected (fig. 6 C and D). However, Dox was distributed in discrete spots, mainly localized in perinuclear region, and no diffused free Dox was observed within the cytoplasm.
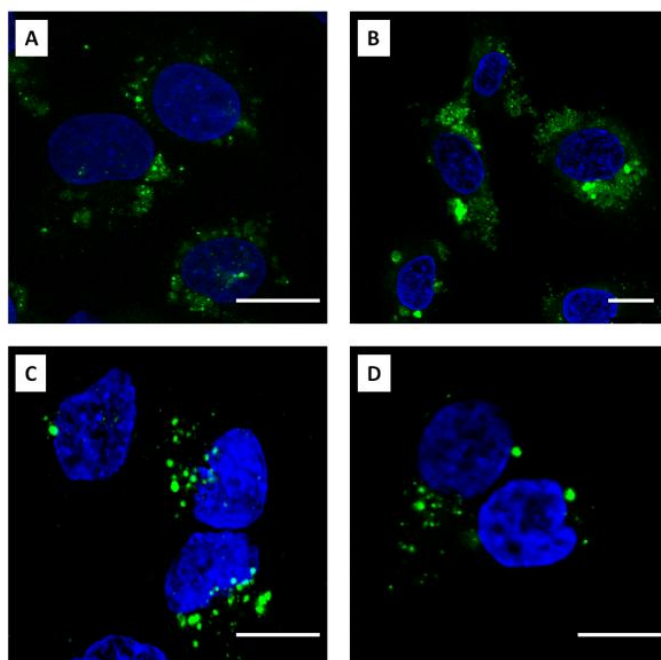
Figure 6. *Confocal images of HT1080 cells after 48 h incubation with MMP2 pre-treated TAP-A NPs and TAP-B NPs (A and B, respectively) and TAP-A NPs and TAP-B NPs (C and D, respectively). Blu: nuclei. Green: Dox. Magnification bar: 20 μm.*

4.5. DISCUSSION

The incorporation of stimuli-responsive portions in engineered NPs is promising in achieving controlled and localized release of drugs, offering the chance to improve their therapeutic profiles [16, 20, 33, 35]. In fact, in the tumor microenvironment, significant changes in the production of some specific extracellular proteins occur. Among these proteins, MMP2 and MMP9 play a major role in the degradation of tumor extracellular matrix (ECM), and are therefore involved in the invasion, progression and metastasis of manifold human tumors. In particular, MMP2 is overexpressed in many cancers such as breast, colorectal, lung, liver, prostate, pancreas and ovary [33].

In this context, the main focus of this study was the production of model NPs decorated on the surface with suitable tumor-activated prodrugs TAPs, and the key elements of these NPs were the enzyme-responsive polymers (PEG – Pep A and PEG – Pep B) which governed Dox release through sensitiveness to MMP2 upregulation [36, 37]. The produced nanodevices have been designed with the purpose of transporting cytotoxic drugs in safe manner through tissues that do not overexpress MMP2 enzyme and release the conjugated drug only in tissues overexpressing MMP2. The latter enzyme has been selected as the trigger for the release of the drug. It must also be underlined that specific and local drug release from NPs is a difficult task due to biochemical and physical obstacles present in tumor tissue architecture. Therefore, in this work we designed a tumor activated prodrug by using MMP2 sensitive peptide sequences, linked to Dox and conjugated to PS NPs, in order to have drug release triggered by specific enzymatic cleavage. Drug release from these is controlled by peptide enzymatic cleavage once the produced devices are in a MMP-overexpressing environment. The control of drug release rate after *in situ* cleavage of the drug-peptide bond may result in therapeutic levels of the drug, which is highly desirable for local drug delivery at tumor sites. In this study, MMP-sensitive NPs were tested for drug release triggered by enzymatic attack, which may be potentially useful in the achievement of effective local drug delivery for cancers. In particular, NPs

were placed in media simulating the elevated MMP2 concentrations associated with some cancers [38]. In the presence of nanomolar concentrations of MMP2, Dox was rapidly released, while in blank buffer solution the drug was released very slowly. The marked increase in drug release from the MMP-sensitive NPs suggests its potential as a bio responsive local drug delivery platform to be applied in cancer drug delivery.

Moreover, the TAP-activated PS NPs were expected to release the conjugated drug at a rate which is dependent on the enzyme concentration in the external medium until the drug is exhausted. In particular, in a very narrow range of enzyme concentration, Dox release rate is drastically changed, approaching a sort of on-off mechanism. Thus, the definition of the threshold enzyme concentration triggering Dox release is of vital importance. Furthermore, finding out the enzyme concentration within target tissue is another major task since it defines the usefulness of NPs themselves. Our results suggest the presence of an enzyme threshold dose, corresponding to approximately 1 nM (**Fig. 4**), and a linear dependence of Dox release on enzyme concentration in the range from 1 nM to 20 nM. This effect was more evident in the case of TAP-B NPs, thus showing that in the release experimental conditions peptide B is more sensitive to enzyme concentration compared to peptide A. Indeed, peptide B shows a steepest saturation curve, probably due to its major affinity constant, closely depending on substrate concentration, while Pep A is not very sensitive to enzyme amount into analysis range. Furthermore, we hypothesized that the TAP-B NP higher activity and more sensitivity to enzyme concentration than TAP-A NPs could be due to peptide B longer chain that results more available for proteolytic cleavage into the whole NP structure.

The specificity of TAP-conjugated NPs in Dox release was also observed by cytotoxicity experiments. Indeed, TAP NPs showed a cytotoxic effect on tumor cell line and primary cells only when pre-treated with activated MMP2 enzyme. In addition, the cytotoxic effect was more evident for NPs functionalized with peptide B compared to peptide A, in agreement with the observed drug release

kinetics. However, the decrease of cell viability was less evident than free Dox, probably due to the presence of an aminoacidic residue tail bound to drug molecule after the enzyme cleavage, which that partially reduced specific Dox effects. On the other hand, in the absence of MMP2, no cytotoxic effect was observed on all the three cell types used up to 2 days of incubation, even though the cells could internalize the Dox with and without MMP2 pre-treatment. This could be reasonably ascribed to a reduced cytotoxic effect of Dox when the drug is covalently bound to NPs. As well known, Dox can exert its cytotoxic activity by blocking topoisomerase II activity only when it enters cell nucleus [39, 40]. On the contrary when the drug is covalently bound to the NPs, it presents a reduced conformational freedom, and therefore an inferior ability to cross nuclear membrane and to inhibit the enzyme topoisomerase II.

Taken all together, our results clearly indicate that Dox, despite its high cytotoxicity when in the free state, can be safely transported through non-overexpressing MMP2 enzyme once it is bound to NPs through enzyme-sensitive TAPs. The release of the drug, and therefore its desired cytotoxic action towards tumor cells could be induced only in the presence of MMP2 at approximately nanomolar concentrations.

4.6. CONCLUSIONS

In this work, MMP-sensitive, TAP-conjugated NPs for enzyme-mediated release of cytotoxic drugs have been successfully synthesized by binding two MMP2-sensitive peptides to Dox and a PEG segment. The resulting adduct was in turn tethered to the surface of 200 nm model PS NPs. Results clearly indicate that Dox was not released in the absence of the enzyme and that, hence, drug release could be triggered only when MMP2 was present. Specifically, higher release rates were observed when NPs were functionalized with peptide B, and with an increasing MMP2 concentration in the release medium. The enzyme effect was basically saturated above 10 nM concentration, and basically similar Dox release rates were observed over this concentration.

The produced NPs were cytotoxic against all the cell lines used in this study, when are pre-treated with enzyme, with a stronger effect when NPs were functionalized with peptide B. However, the cytotoxicity of TAP NPs was in all cases lower compared to the free Dox. Interestingly, TAP NPs were not cytotoxic in the absence of MMP pre-treatment, even if the devices could be internalized within the cells. Our results showed that Dox was not released from TAP NPs in the absence of MMP2 and hence the cytotoxicity could be elicited by overexpressed enzyme. A critical issue is the definition of the actual enzyme concentrations *in vivo* which will determine the applicability of these MMP-sensitive NPs. The release of the drug, and therefore its desired cytotoxic action towards tumor cells, could be induced only in the presence of MMP2 at about 1 nM concentrations. Taken all together, our results are promising in the light of translating the same TAP production technology to biodegradable systems intended for the targeted delivery of cytotoxic anticancer drugs.

4.7. REFERENCES

1. Giustini, A.J., R. Ivkov, and P.J. Hoopes, *Magnetic nanoparticle biodistribution following intratumoral administration.* Nanotechnology, 2011. **22**(34).
2. Cho, K., et al., *Therapeutic nanoparticles for drug delivery in cancer.* Clinical Cancer Research, 2008. **14**(5): p. 1310-1316.
3. Biondi, M., et al., *Sub-100 nm biodegradable nanoparticles: in vitro release features and toxicity testing in 2D and 3D cell cultures.* Nanotechnology, 2013. **24**(4).
4. Torchilin, V.P., *Targeted pharmaceutical nanocarriers for cancer therapy and Imaging.* Aaps Journal, 2007. **9**(2): p. E128-E147.
5. Bae, Y.H. and K. Park, *Targeted drug delivery to tumors: Myths, reality and possibility.* Journal of Controlled Release, 2011. **153**(3): p. 198-205.
6. Holback, H. and Y. Yeo, *Intratumoral Drug Delivery with Nanoparticulate Carriers.* Pharmaceutical Research, 2011. **28**(8): p. 1819-1830.
7. Petros, R.A. and J.M. DeSimone, *Strategies in the design of nanoparticles for therapeutic applications.* Nature Reviews Drug Discovery, 2010. **9**(8): p. 615-627.
8. Allen, T.M., *Ligand-targeted therapeutics in anticancer therapy.* Nature Reviews Cancer, 2002. **2**(10): p. 750-763.
9. Danhier, F., O. Feron, and V. Preat, *To exploit the tumor microenvironment: Passive and active tumor targeting of nanocarriers for anti-cancer drug delivery.* Journal of Controlled Release, 2010. **148**(2): p. 135-146.
10. Lammers, T., et al., *Drug targeting to tumors: Principles, pitfalls and (pre-) clinical progress.* Journal of Controlled Release, 2012. **161**(2): p. 175-187.
11. Acharya, S., F. Dilnawaz, and S.K. Sahoo, *Targeted epidermal growth factor receptor nanoparticle bioconjugates for breast cancer therapy.* Biomaterials, 2009. **30**(29): p. 5737-5750.
12. Kocbek, P., et al., *Targeting cancer cells using PLGA nanoparticles surface modified with monoclonal antibody.* Journal of Controlled Release, 2007. **120**(1-2): p. 18-26.
13. Steinhauser, I.M., et al., *Effect of trastuzumab-modified antisense oligonucleotide-loaded human serum albumin nanoparticles prepared by heat denaturation.* Biomaterials, 2008. **29**(29): p. 4022-4028.
14. Wagner, S., et al., *Enhanced drug targeting by attachment of an anti alpha v integrin antibody to doxorubicin loaded human serum albumin nanoparticles.* Biomaterials, 2010. **31**(8): p. 2388-2398.
15. Gabizon, A., et al., *Targeting folate receptor with folate linked to extremities of poly(ethylene glycol)-grafted liposomes: In vitro studies.* Bioconjugate Chemistry, 1999. **10**(2): p. 289-298.
16. Zhu, L., et al., *Site-specific delivery of oligonucleotides to hepatocytes after systemic administration.* Bioconjugate Chemistry, 2008. **19**(1): p. 290-298.
17. Zhu, L. and R.I. Mahato, *Targeted Delivery of siRNA to Hepatocytes and Hepatic Stellate Cells by Bioconjugation.* Bioconjugate Chemistry, 2010. **21**(11): p. 2119-2127.
18. Jain, R.K. and T. Stylianopoulos, *Delivering nanomedicine to solid tumors.* Nature Reviews Clinical Oncology, 2010. **7**(11): p. 653-664.

19. Basel, M.T., et al., *Protease-Sensitive, Polymer-Caged Liposomes: A Method for Making Highly Targeted Liposomes Using Triggered Release.* Acs Nano, 2011. **5**(3): p. 2162-2175.

20. Sawant, R.M., et al., *"SMART" drug delivery systems: Double-targeted pH-responsive pharmaceutical nanocarriers.* Bioconjugate Chemistry, 2006. **17**(4): p. 943-949.

21. Chau, Y., et al., *Investigation of targeting mechanism of new dextran-peptide-methotrexate conjugates using biodistribution study in matrix-metalloproteinase-overexpressing tumor xenograft model.* Journal of Pharmaceutical Sciences, 2006. **95**(3): p. 542-551.

22. Huan, M., et al., *In Vitro and In Vivo Antitumor Activity of a Novel pH-Activated Polymeric Drug Delivery System for Doxorubicin.* Plos One, 2012. **7**(9).

23. Sugahara, S.-i., et al., *Complete regression of xenografted human carcinomas by a paclitaxel-carboxymethyl dextran conjugate (AZ10992).* Journal of Controlled Release, 2007. **117**(1): p. 40-50.

24. Tauro, J.R. and R.A. Gemeinhart, *Matrix metalloprotease triggered delivery of cancer chemotherapeutics from hydrogel matrixes.* Bioconjugate Chemistry, 2005. **16**(5): p. 1133-1139.

25. Koblinski, J.E., M. Ahram, and B.F. Sloane, *Unraveling the role of proteases in cancer.* Clinica Chimica Acta, 2000. **291**(2): p. 113-135.

26. Zucker, S., *A CRITICAL-APPRAISAL OF THE ROLE OF PROTEOLYTIC-ENZYMES IN CANCER INVASION - EMPHASIS ON TUMOR SURFACE PROTEINASES.* Cancer Investigation, 1988. **6**(2): p. 219-231.

27. Itoh, Y. and H. Nagase, *Matrix metalloproteinases in cancer.* Proteases in Biology and Medicine, 2002. **38**: p. 21-36.

28. Kugler, A., P. Thelen, and R.H. Ringert, *Matrix metalloproteinases and their inhibitors.* Renal Cancer, 2001. **53**: p. 139-150.

29. Klein, G., et al., *The possible role of matrix metalloproteinase (MMP)-2 and MMP-9 in cancer, e.g. acute leukemia.* Critical Reviews in Oncology Hematology, 2004. **50**(2): p. 87-100.

30. Holle, L., et al., *A matrix metalloproteinase 2 cleavable melittin/avidin conjugate specifically targets tumor cells in vitro and in vivo.* International Journal of Oncology, 2003. **22**(1): p. 93-98.

31. Veiseh, O., et al., *Inhibition of Tumor-Cell Invasion with Chlorotoxin-Bound Superparamagnetic Nanoparticles.* Small, 2009. **5**(2): p. 256-264.

32. Gould, P., *Size matters to cell uptake - but so does shape.* Nano Today, 2006. **1**(2): p. 15-15.

33. Mansour, A.M., et al., *A new approach for the treatment of malignant melanoma: Enhanced antitumor efficacy of an albumin-binding doxorubicin prodrug that is cleaved by matrix metalloproteinase 2.* Cancer Research, 2003. **63**(14): p. 4062-4066.

34. Cantisani, M., et al., *Peptides complementary to the active loop of porin P2 from Haemophilus influenzae modulate its activity.* International Journal of Nanomedicine, 2012. **7**: p. 2361-2371.

35. Zhu, L., et al., *Targeted delivery of methotrexate to skeletal muscular tissue by thermosensitive magnetoliposomes.* International Journal of Pharmaceutics, 2009. **370**(1-2): p. 136-143.

36. Kratz, F., et al., *Development and in vitro efficacy of novel MMP2 and MMP9 specific doxorubicin albumin conjugates.* Bioorganic & Medicinal Chemistry Letters, 2001. **11**(15): p. 2001-2006.

37. Torchilin, V.P., et al., *Cell transfection in vitro and in vivo with nontoxic TAT peptide-liposome-DNA complexes.* Proceedings of the National Academy of Sciences of the United States of America, 2003. **100**(4): p. 1972-1977.

38. Garripelli, V.K., et al., *Matrix metalloproteinase-sensitive thermogelling polymer for bioresponsive local drug delivery.* Acta Biomaterialia, 2011. **7**(5): p. 1984-1992.

39. Kik, K., et al., *Cytotoxicity and inhibitory properties against topoisomerase II of doxorubicin and its formamidine derivatives.* Acta Biochimica Polonica, 2009. **56**(1): p. 135-142.

40. Gruber, B.M., et al., *Effect of structural modification at the 4, 3 ', and 2 ' positions of doxorubicin on topoisomerase II poisoning, apoptosis, and cytotoxicity in human melanoma cells.* Archivum Immunologiae Et Therapiae Experimentalis, 2007. **55**(3): p. 193-198.

CHAPTER 5

5.1. CONCLUSIONS

The application of nanoparticles to drug delivery demonstrated to have significant impact on many areas of medicine. However, drugs delivered inappropriately to healthy tissues or organs can produce off-target and unwanted side effects that can impede to reach the most effective dose in the target sites. The overcoming of these limitations requires a precise control of NP interstitial diffusion and cellular uptake. In this context, this thesis highlighted the importance of defining the NP optimal physicochemical characteristics useful for a rational design finalized to a more specific drug delivery in tumor tissues.

For a best understanding of NPs behaviour and cellular uptake, a 3D culture model system that better mimics the native environment in which cells reside was reproduced. To this aim, matrices made up of collagen type I were prepared, and different cell lines were embedded in this network of fibers. The results obtained in this study demonstrated that not only size, but also surface charge influenced the NP diffusivity and consequently their cellular uptake in a 3D system. Depending on NP formulation and size, smaller NPs diffused better in a 3D collagen matrix and were more efficiently internalized by several cell types. Nevertheless, surface charge also influenced NP behaviour. In fact, cationic NPs not only are internalized by cells in an amount comparable to those of small carriers, but they also diffuse freely in a 3D matrix, without any apparent hindrance. On the contrary, increasing the negative charge at the NP surface drastically promotes their interaction with the matrix, lowering the efficiency by which they reach the cells. The same results, as regarding NP size, were observed for biodegradable NPs made up of PELGA polymers and loaded with DOX. Our data showed a fundamental contribution of sub < 100 nm nanoparticles on the cell death rate, particularly in a 3D collagen matrix.

I also developed a design of a novel carrier able to release DOX under the action of the MMP2 enzyme, which is over-expressed in tumor tissues. The results confirmed that NP cytotoxic effects can be specifically triggered by MMP2 cleavage, indicating that this type of nanocarriers could carry DOX more specifically in the target tumor tissues.

Collectively, the data obtained indicate that a better understanding of the interaction between NP and tumor microenvironment is necessary to optimize the control the side-adverse effects and increase both the therapeutic efficiency and specificity.